THE SINGLE FIBER PULL-OUT TEST: A STUDY OF FIBER/MATRIX INTERACTIONS

by

Célene DiFrancia

Dissertation submitted to the Faculty of the
Virginia Polytechnic Institute and State University
in partial fulfillment of the requirements for the degree of

DOCTOR OF PHILOSOPHY
in
Materials Engineering Science

APPROVED:

Richard O. Claus

R. O. Claus, Co-Chairperson

T. C. Ward, Co-Chairperson

D. A. Dillard

I. Jacobs

J.P. Wightman

August, 1992
Blacksburg, Virginia

c.2

LD
5655
V856
1992
D547
c.2

THE SINGLE FIBER PULL-OUT TEST: A STUDY OF FIBER/MATRIX INTERACTIONS

by
Célene DiFrancia

Committee Co-Chairs:
Richard O. Claus — Electrical Engineering
Thomas C. Ward — Chemistry

(ABSTRACT)

The single fiber pull-out test was employed to experimentally model the failure of an embedded optical fiber in neat resin. The objective was to evaluate load transfer between resin and fiber through the evaluation of the sensitivity of the single fiber pull-out test to the physical parameters of the polymer matrix. This was accomplished first by appropriately interpreting the load versus extension trace, second by determining the effect of fiber coating and embedding resin on the load carrying ability of the single fiber composite, third by characterizing the fiber/coating/resin system with respect to the physical parameters of the polymer and the failure mechanism of the composite as the cure temperature was varied, and fourth, by correlating the independent parameters of the polymer and fracture data.

For the first time, the load versus extension trace generated by such experiments was thoroughly interpreted and mathematically modeled. To this end, the embedding resin was physically characterized through the determination of the glass transition temperature, T_g, the relative change in volume with sample preparation and thus the resulting normal pressure exerted on the embedded fiber by the resin material. The experimental fracture data was quantified by determining the strain

energy release rate, SERR, for initiation of crack propagation and, with the consideration of friction, its continuation, as well as the interfacial shear stress, τ, of the bond, and τ associated with debonding and sliding.

Based on a series of experiments of varying material parameters, a model material system was chosen: a polyimide coated fiber embedded in uncatalyzed tetraglycidyl-4-4'-diaminodiphenylmethane with 4,4'-diaminodiphenylsulfone. Cure temperatures, T_{cure}, of 150, 177, 230 and 250°C were employed. The average critical strain energy release rates increased from the 150 to 177 to 230°C sample sets, then decreased for the 250°C sample set. Since the T_g of the fully cured resin is 260°C, these results support the hypothesis of increasing residual stress as a function of T_{cure} for cure in the vitreous state. In regards to the 250°C cure data set, since T_{cure} was within T_g - 30°C the internal pressures due to crosslinking were minimized due to cure in a rubber-like state.

The residual pressure, independently determined from both the resin characterization and fracture data, increased by a factor of 2.4 with a temperature increase from 150 to 230°C for the two hour cure period. The strain energy release rate and sliding interfacial shear stress of pull-out increased by a factor of 2.54 and 2.1, respectively. The coefficient of friction remained statistically constant at 0.6. Based on this work, it is concluded that the single fiber pull-out test is sensitive to fiber/matrix interactions via the physical parameters of the material system. Also, the failure response of the single fiber composite can be predicted for well characterized matrices.

With self-improvement we all benefit.

To

John,

Dominique & Jessica

Acknowledgements

I would like to thank my co-chairs for their support and guidance throughout my graduate tenure. To Dr. Claus for his patience and readiness to listen and to Dr. Ward for the many, many things taught in and out of the classroom, my sincere appreciation.

I would also like to thank my committee members, Dr. D.A. Dillard, Dr. I. Jacobs and Dr. J.P. Wightman for serving on my committee and for many helpful discussions. To Dr. Dillard, much appreciation for the many mechanics sessions in 120D Patton; to Dr. Jacobs, my gratitude for the broad perspective on research; and to Dr. Wightman, many thanks for the enthusiastic support and always open door.

Thanks are also extended to John Hellgeth for running the FTIR experiments, to Yeh-Hung Lai for fracture mechanics brainstorming and advice, to Paul Vail for thermal assistance and equipment use and to the members of PolyPChem for all the scientific and social activities that make a research group fun. Appreciation is extended to the organizers of CASS, CCMS, NSFS&TC-HPPAC and PMIL seminars from which so much is learned and so many ideas born. To the secretaries in NSFS&TC-HPPAC office and the neighbors in the CASS office - without your help and constant support, short courses, conferences on and off campus, as well as reports, papers and dissertations would not be possible. Thank you for the

stupendous efforts made toward the betterment of the graduate student experience.

To my friends from the classroom and the occasional lunch - Janis, Joannie, Mojee, Pamela, thanks for the encouragement and friendship. To my special friends Robin and Irene, the many sanity checks and unlimited emotional support were paramount in the success of completing my degree ... thank you both. To Karima, who has been the perfect caregiver for my children, inexpressible appreciation.

I would like to thank my sibs, Phyllis, Linda and Jimmy and Ron too, for the many conversations and helpful perspectives that kept me going. To Barbara, Mary, Matt & Elissa, Tom & Pam, and Cat & Keith, many thanks for the balance provided by all of you.

I cannot express the gratitude felt toward my parents who instilled the *"go-for-it, anything is possible"* attitude. Thank-you for your constant encouragement and love.

Finally, I would like to recognize and thank my spouse John and daughters Dominique Lucy and Jessica Lynn. To John who could not have been more supportive and was always ready to help, listen, push and have fun as needed, my love and gratitude to you for being you. To Dominique (Beena) and Jessica (Booby), your daily smiles and hugs were invaluable

... I Love you both!

Table of Contents

Abstract ii
Acknowledgments v
Table of Contents vii
List of Figures x
List of Tables xiii

Chapter 1 Implementation of the Single Fiber Pull-out Test to Model the Failure of Fiber Reinforced Materials 1

Chapter 2 Literature Review 7
2.1 The Single Fiber Pull-Out Test 11
2.1.1 Early Observations of the Single Fiber Pull-Out Test 11
2.1.2 Incorporation of Crack Propagation in the Evaluations of the Single Fiber Pull-Out Test 15
2.1.2.1 The Change of Fiber Diameter with Tensile Load 19
2.1.2.2 The Relationship Between Debonding Stress and Embedded Length 20
2.1.3 The Fracture Mechanics of the Single Fiber Pull-Out Test 22
2.1.3.1 The Approach of Morrison, Shah and Jeng 24
2.1.3.2 The Approach of Jiang and Penn 30
2.1.3.3 The Approach of Gao, Mai and Cotterell 35
2.2 The Effect of Cure Temperature on Tg, Density and Internal Stress 41
2.2.1 Extent of Reaction and Tg 43
2.2.2 The Density and Volume of the Epoxy Resin 44
2.2.3 Internal Stress in a Tetra-Functional Epoxy System 50
2.3 Residual Stress and the Single Fiber Pull-Out Test 53

2.3.1 Calculation of Residual Pressure Due to Cooling From Above T_g 54
2.3.2 Calculation of Residual Stress Due to Curing and Cooling 55
2.3.3 Calculation of the Residual Stress From Fracture Mechanics 58
2.4 Interfacial Shear Stress Between Fiber and Resin 79
2.4.1 Stress Transfer From Matrix to Fiber 60
2.4.2 Interfacial Bond Shear Stress 65
2.4.3 Interfacial Debond Shear Stress 67
2.4.4 Interfacial Sliding Shear Stress 67

Chapter 3 Experimental 69
3.1 Optical Fibers 71
3.1.1 Coupling Agent Coating 71
3.2 Resin Systems 72
3.3 Sample Preparation 73
3.4 Thermal Mechanical Experiments 74
3.4.1 Thermogravimetric Analysis 75
3.4.2 Differential Scanning Calorimetry 75
3.4.3 Thermal Mechanical Analysis 75
3.4.4 Dynamic Mechanical Thermal Analysis 75
3.5 Fourier Transform Infrared Spectroscopy 76

Chapter 4 The Effect of Fiber Coating and Embedding Resin on the Single Fiber Pull-Out Test 77
4.1 The Interpretation of the Single Fiber Pull-Out Test 78
4.2 The Effect of Fiber Coating on the Single Fiber Pull-Out Test 87
4.2.1 Bisphenol-A Based Epoxy Resin 88
4.2.2 Catalyzed TGDDM/DDS Epoxy Resin 90
4.3 The Effect of Fiber Manufacturer on the Single Fiber Pull-Out Test 92
4.4 The Effect of Resin Choice on the Single Fiber Pull-Out Test 96

4.5 Summation 101
Chapter 5 Cure Study: Variable Cure of Uncatalyzed TGDDM/DDS Epoxy and Its Effect on the Single Fiber Pull-Out Test 103
5.1 The Choice of Cure Temperature 105
5.2 Results and Interpretation of the Single Fiber Pull-Out Test as Cure Temperature is Increased 108
5.2.1 Experimental Results 108
5.2.2 Strain Energy Release Rate as a Function of Cure 112
5.2.2.1 Critical Strain Energy Release Rate 113
5.2.2.2 Debonding Strain Energy Release Rate 115
5.3 Polymer-Based Considerations Regarding the Single Fiber Pull-Out Test 117
5.3.1 Residual Stress Exerted on the Embedded Fiber 118
5.3.2 Determination of Residual Stresses 120
5.4 Interfacial Shear Stress and the Coefficient of Friction 122
5.4.1 Interfacial Shear Stress 123
5.4.2 The Coefficient of Friction 126
5.5 Summation 127

Chapter 6 Conclusions 131
Chapter 7 Future Work 137
References 139
Appendix A 151
Appendix B 169
Vita 170

List of Figures

1. Load versus extension curve for a phosphor bronze wire in an epoxy resin a) etched; b) PTFE coated -Kelly (8) 12

2. Load versus extension curve for a copper wire in an epoxy resin -Takaku and Arridge (11) 14

3. Schematic representation of debonding and pull-out of a ductile wire from a brittle matrix -Bowling and Groves (14) 16

4. Load versus displacement curve for a) copper/epoxy; b) copper/cement systems -Bowling and Groves (14) 17

5. Bimodal relationship between embedded length and stress of steady-state debonding -Bowling and Groves (14) 21

6. Schematic of load versus displacement when friction dominates: a) contribution of the debonded region; b) contribution of bonded region; c) total resistance to pull-out -Morrison et al. (35) 26

7. Load versus displacement curve for a steel fiber in cement -Morrison et al. (35) 29

8. Load versus displacement curve for ultra-high density polyethylene in an epoxy: a) catastrophic interfacial failure; b) crack initiation and propagation -Jiang and Penn (67) 34

9. The fiber-matrix pull-out problem -Gao et al. (33) 36

10. Density versus thermal history of a TGDDM/DDS epoxy system as a function of thermal history -Kong (78) 46

11. Schematic of specific volume (V) versus temperature (T) diagram for epoxies cured to different extents (1<2<3) -Pang and Gillham (81) 49

12. Internal stress during the curing and cooling processes for epoxide resins; top curve is TPGEE/DDM, Tg = 308°C; bottom curve is DGEBA, Tg = 165°C -Ochi (86) 52

13. Debonding load versus cure temperature; top curve is a polypropylene/epoxy system; bottom curve is PP/E with lubricant applied to fiber surface -Jang et al. (77) 57

14. Tensile stresses at the fiber/matrix interface for fiber length l. a) $l<l_c$; b) $l=l_c$ and c) $l>l_c$ 61

15. Load to debond versus embedded length a) as initially suggested by Piggott (28); b) revised version (69) 63

16. Hypothetical embedded length versus load required to debond 63

17. Sample configuration for the embedded optical fiber in a neat resin dogbone 70

18. Fiber debonding and pull-out sequence schematically showing the photoelastic birefringence patterns in time 79

19. Model load versus extension trace 82

20. Experimental load versus extension traces showing a) all described debonding and pull-out regions and stick-slip activity; b) no plateau regions 84

21. Fibers supporting various coatings embedded in the BGEBA resin system 88

22. SpecTran acrylate coated fiber embedded in catalyzed TGDDM/DDS 91

23. Typical load versus extension trace for coating/resin interface failure. Example from Fiberguide sample set 93

24. Typical load versus extension trace for glass/coating interface failure. Example from CeramOptec sample set 94

25. Results of different polyimide-coated fibers embedded in the uncatalyzed TGDDM/DDS epoxy resin 95

26. Bar chart of Polymicro polyimide coated fibers embedded in various resins: a) average stress at initiation; b) average interfacial shear stress for pull-out 98

27. a) TGA; b) DSC, and c) TMA of the uncatalyzed TGDDM/DDS epoxy resin 107

28. <SERR>c, bar chart using $G_{initiate}$ 114

29. Expansion versus temperature for T_{cure} a) 150; b) 177; c) 230 and d) 250°C 119

30. Load versus extension trace from the 230°C sample set. The debonding region of the trace is exploded to show the frictional effects on the debonding load 125

List of Tables

1. Values for the load on the fiber at various times during the single fiber pull-out test in N; P_{init}, $P_{friction}$, $P_{complete}$, P_{drop} are described in the text 29

2. Strain energy release rates for the initiation of crack propagation as reported in the literature 40

3. Effect of cure on the interfacial shear stress between resins systems -Biro et al. (56) 66

4. Experimentally determined values for the interfacial shear stress as reported in the literature 68

5. Results of different polyimide-coated fibers embedded in the uncatalyzed TGDDM/DDS epoxy resin 96

6. Experimental results of Polymicro polyimide coated fibers embedded in various resins 99

7. T_{cure}, T_g (DMTA), modulus (minimat), percent cure (FTIR relative to 130°C degassed samples) for the uncatalyzed TGDDM/DDS epoxy system 105

8. Stresses in MPa for interfacial crack initiation, σ_{init}, the end of the primary frictional zone, $\sigma_{friction}$, and steady state debond and fiber pull-out: σ_{drop} and σ_{chi} 110

9. Average critical strain energy release rate in N/m for the model pull-out experiments 113

10. Strain energy release rate calculated with the consideration of friction via Gao et al.'s model 116

11. T_{cure}, $(\Delta V)_{Chem}$, $(\Delta V)_{Temp}$, $(\Delta V)_{total}$ in percent decrease for the uncatalyzed TGDDM/DDS epoxy system 118

12. Residual pressure normal to the fiber surface via Gao et al.'s equation 120

13. Residual pressure normal to the fiber surface via TMA and Harris's equation 122

14. Various interfacial shear stresses in MPa and coefficients of friction for the same experimental values implemented in the determination of the critical strain energy release rates 126

15. Descriptors of the 150 and 230°C cure sets 129

Chapter 1

Implementation of the Single Fiber Pull-Out Test to Model the Failure of Fiber-Reinforced Materials

Fiber-reinforced composite materials have been developed for applications ranging from biomedical to aerospace. The combination of high modulus fibers with lower modulus polymeric resins has resulted in materials with enhanced mechanical performance. Due to the complexity of the composite material, mechanical characterization has been limited to overall performance assessment. Here, properties of the fiber and neat resin are readily determined as is the performance of the larger scale composite material. However, with the combination of fiber and resin, the interphase region between them is another component of the system that requires evaluation. This region appears to have both chemical and mechanical properties which differ from the bulk. With the understanding of how the fiber and matrix interact and the role of the interphase between them, reliable models can be developed for the prediction of material behavior at long times or with particular environmental exposures.

One approach for determining the behavior of a material under various conditions has evolved into what is now called smart or intelligent materials. A smart material is one which has various sensors and actuators with the related control system embedded in or attached to the structure of interest. The purpose of these components is to monitor and/or maintain the integrity of the structure. Through a complex series of component interactions, the material can be monitored for variables such as temperature, strain, impact, and chemical status. The appropriate conditional changes can be made to then optimize material status. To this end, fiber optic-based sensors have been developed. Of specific interest is the development of a fiber optic sensor to model composite performance and failure. Here, the sensor could be optimized to represent the reinforcing fiber. As the materials is then cycled through its use patterns, a greater understanding of the fiber/matrix interaction would result.

With the characterization of the fiber/matrix interface, the durability of the material may be better predicted. To this end, the evaluation of the performance of an embedded optical fiber along with the material parameters which effect it has been conducted.

Experimental techniques to remove a single fiber from neat resin are used extensively for the qualitative evaluation of interfacial adhesion between the fiber and resin (1-69). These tests examine the load transfer from fiber to resin; they are primarily used as a qualitative means for comparing different fiber/resin combinations and to evaluate aspects such as fiber

surface pretreatments. The research presented here addresses the sensitivity and dependencies of the single fiber pull-out test to the dynamics of the fiber/matrix interface by evaluating the load transfer between a polymer-coated optical fiber embedded in a neat polymer resin.

For the fiber/coating/resin combination of interest, the characterization of the single fiber pull-out experiment was accomplished in a variety of ways. Through the analysis of the loading, debonding and friction of a given fiber/resin combination, a mechanistic approach was used to describe the system via the strain energy release rate and interfacial shear stress. The same fiber/coating/resin combinations were also characterized via their chemistry. This was accomplished by determining the relative extent of cure, the degree of shrinkage with cure and the glass transition temperature of the resin. The objective of this work was to test the sensitivity of the single fiber pull-out test to the physical parameters of the polymer matrix. This was accomplished through the determination of the strain energy release rate and interfacial shear stress as a function of the relative shrinkage of the resin with cure cycle.

Extensive literature is available on this subject. Notable articles are reviewed in the Literature section, Chapter 2, and pertinent observations made to the current research. The evolution of the single fiber pull-out test is presented via the experimental observations and the characterization of these observations through models implementing fracture mechanics. These models provide information on the failure of the system through the

determination of the strain energy release rate. Parameters such as the residual pressure on the fiber due to densification during crosslinking and thermal contraction during cooling are then evaluated. This normal pressure effectively clamps the fiber within the resin. With loading of the system, this mechanical clamping results in interfacial shear stresses between the fiber and matrix. Thus, the interfacial shear stress as determined at the initiation of interfacial crack propagation, continued crack propagation and during frictional sliding with fiber removal is reviewed.

The preliminary efforts of this research were directed at the response differences between an array of fiber/coating/resin systems and are reported in Chapter 4. These initial experiments were conducted to determine the physical response of the embedded optical fiber to the pull-out experiment. The first model systems consisted of fibers supporting various coatings, i.e. acrylate, coupling agent and polyimide embedded in a butylglycidyl ether of bisphenol-A (BGEBA) with epichlorohydrin and catalyzed tetraglycidyl-4-4'-diaminodiphenylmethane, (TGDDM) with 4,4'-diaminodiphenylsulfone (DDS). Following this, polyimide-coated fibers from six different manufacturers were embedded in uncatalyzed TGDDM/DDS epoxy resin to determine the various loads and apparent locus of failure expected from the given fiber/polyimide/epoxy system. Finally, the effect of the resin chemistry and cure cycle on the single fiber pull-out test was evaluated. To accomplish this, polyimide coated optical fibers from one manufacturer were embedded in resins of different

chemistries and thermal cure cycles to evaluate the significance of the induced chemical and thermal stresses.

The final series of experiments were designed to evaluate the induced thermal stresses due to the cure cycle. This work is presented in Chapter 5. Here, single fiber composite specimens of the uncatalyzed TGDDM/DDS epoxy resin were brought to various temperatures with time of cure held constant. The polymeric parameters of these specimens were characterized by dynamic mechanical analysis, DMTA, thermal mechanical analysis, TMA, differential scanning calorimetry, DSC, and fourier transform infrared spectroscopy, FTIR; the failure of these specimens was evaluated with the determination of the strain energy release rate, various interfacial shear stress terms and the coefficient of friction.

Discussions of the experimental results as they relate to published work and regarding new insights is presented throughout the results chapters, Chapters 4 & 5. Particular emphasis was placed upon the results of the cure study. It was found that over small temperature increments between sample sets, a statistical difference between fracture values could not be demonstrated. However, the trend of the data supports the hypothesis that incremental changes in the polymer-based material parameters effect the mechanical failure of the single fiber composite. By evaluating sample sets with a larger difference in cure temperature, an excellent correlation

between the polymeric properties and the fracture mechanics of the single fiber pull-out test was made.

In conclusion, the single fiber pull-out test was found to be a viable means of modeling the interfacial failure of an embedded fiber loaded in tension. This test method can be used not only for the evaluation of fiber surface treatments as it has in the past, but also to relate the physical properties of the embedding resin to the failure mechanism of the single fiber composite.

Chapter 2

Literature Review

An extensive amount of work is published regarding the failure mechanisms of composite materials. One specific area addresses the debonding and bridging of fibers across a transverse crack. This type of failure describes some of the advantages of fiber reinforced resins, namely the dissipation of energy and thus the sometimes non-catastrophic nature of the event. Research in the area of fiber pull-out has considered the fracture mechanics and shear stresses of fiber/matrix failure (1-69). Various mechanistic models for the initiation of crack propagation between fiber and resin, as well as the continuation of this crack with the frictional dissipation of energy, have been presented. A fundamental assumption in the fracture mechanics based models is that an interfacial crack exists somewhere along the embedded length of the fiber due to fatigue, environment, et cetera. However, these models are not typically applied to a fiber debonding in the middle of the bonded length. Rather, they are applied to initial crack propagation between fiber and resin where the fiber emerges from the material. This, then, assumes that edge effects are negligible.

To date, the application of these models is limited to the onset of crack propagation. The partial reason for this is the difficulty in characterizing the failure process and the effect of the physical parameters of the fibers, resin, and interphase between them during propagation. In addressing the polymeric matrix of a composite, the physical constants as well as parameters, such as apparent resin shrinkage due to cure and the resulting internal stresses, should also be considered in the model. Literature on the characterization of resin matrices addresses such issues as changes in density and internal stress as a function of chemical cure and cure temperature (70-87). By applying these phenomena to the interpretation of fiber/resin failure, the implementation of the mechanistic models is possible.

One of the experimental methods for examining the failure of a composite material is the removal of a single fiber from neat resin. The purpose of this method is to qualitatively (and sometimes quantitatively) evaluate the fiber/matrix interaction. The various sample configurations are classified by two major categories. The first subset is the microtension test where the resin is sheared off the stationary fiber. The second subset is the fiber pull-out test in which the fiber is removed from the stationary resin.

Since the late 1950's and early 60's, embedding and removing a single fiber or filament from neat resin has been used to model the failure of a composite material (1-4). More specifically, this model has been

implemented to compare various fiber surface treatments and embedding matrices. As the research progressed, the interpretation of the data evolved with the development of models through the shear lag hypothesis as applied by Greszczuk (6) and interfacial fracture energy as applied by Outwater and Murphy (7). Key papers are evaluated critically with regard to the single fiber pull-out test and related parameters such as strain energy release rate, residual pressure in the system and the interfacial shear stresses.

Various fiber/resin combinations and many sample configurations are used in single fiber models. "Fibers" of interest include metal rods (3,8,11-15,27,35,37,40), carbon filaments (9,25,30,41,49,54-56,61,62), glass fibers (4,17,20-22,25,26,34,38,41,42,51,53,59,62,68), and polymer fibers such as Kevlar (26,41,42,46,57) and ultra-high density polyethylene (67). These fibers were embedded in matrices of concrete (14,15,35), epoxy (8,9,11-14,17,20,21,25-27,3-,37,338,40-42,46,49,51,54-57,59,61,67,68), polycarbonate (13), polybutylene terepthalate (34), polyethylene (4,21), and polyester (9,51), to name a few. Specimens for the single fiber pull-out test have taken on the form of droplets (34,41,53), cylinders (13,27,37), blocks (10,25,30,42,67), or thick films (35,55,68) situated at the end of the fiber, pastilles at each end of the fiber (9) and fibers completely embedded in blocks of resin (14,51,59).

Each of these sample types provide different information. For example, all specimens offer load values for initial debonding between the fiber and resin, samples which afford long enough embedded lengths accommodate the evaluation of interfacial crack propagation through to completion. All

specimen configurations provide information on the sliding load or stress due to friction and, those which accommodate the removal of the fiber from the resin, potentially afford information on the coefficient of friction.

The interpretation of the load versus displacement traces for single fiber pull-out experiments has changed with the understanding of the failure events. Historically, the interpretation of the microdrop results were inaccurate due to the inability to monitor the debonding process visually and to resolve the debonding events instrumentally (16). Thus, these events contributed to the large extent of scatter in the debonding load results. A recent observation was that the actual onset of the interfacial crack in these small scale specimens does not necessarily coincide with the maximum in the load versus displacement trace (pers. comm. L.S. Penn). To address the interpretation of this load versus displacement trace, classic work by Kelly (8), Takaku and Arridge (11) and Bowling and Groves (14) is presented. On the interpretation of the single fiber pull-out test results from the fracture energy approach, recent work by Morrison, Shah and Jeng (35), Jiang and Penn (67), and Gao, Mai and Cotterell (33) are discussed. Finally, after a discussion of polymeric properties as a function of cure, the interpretation of the test results from a shear-lag venue is presented in terms of interfacial shears stress. Here, references are made to the work of Greszczuk (6), and those researchers implementing Greszczuk's model.

2.1 The Single Fiber Pull-Out Test

The characterization of the failure mechanism for the single fiber pull-out test has been discussed by many researchers. In this section, the early implementation of this test method is presented. The early work consisted primarily of reporting the maximum load of failure which was observed experimentally. Later, research efforts incorporated the propagation of the interfacial fiber/resin crack and some pull-out parameters. Finally, a fracture mechanics approach to modeling the experimental results is presented.

2.1.1 Early Observations of the Single Fiber Pull-Out Test

One of the earliest descriptions of the single fiber pull-out test which detailed the initial debonding, crack propagation, completion, and fiber pull-out was reported by Kelly in 1970 and concerned the work of Sims (8). In that work, a phosphor bronze wire was pulled out of an epoxy resin. The load versus extension trace is shown in Figure 1a. The features of this trace were commented upon as follows, "the region O to X could be markedly nonlinear and sometimes stepped. For a given experimental arrangement, the stress at the point X is very variable. At X the load required to extend the fiber suddenly drops to a new value and the fibre pulls out in a more or less jerky fashion which depends on the rate of loading. The load required to pull out the fibre - Y in the figure - and the value of the load at X both depend markedly on the pressure between the fibre and matrix (internal reference to Bowden 1969, National Physics Laboratory IMS Report, no. 6.)" (8).

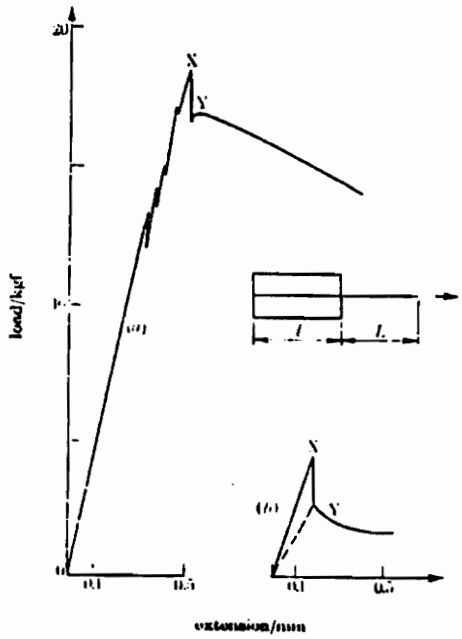

Figure 1. Load versus extension curve for a phosphor bronze wire in an epoxy resin a) etched; b) PTFE coated -Kelly (8).

By using a transparent resin, it was determined that, in the region O to X, the fiber had become debonded and, once the debonding was complete, the frictional stress between fiber and matrix was roughly constant during pull-out. The load value actually used for further interpretation was not clearly stated and the load required for interfacial crack initiation and crack completion were not separated. It was, however, recognized that if the embedded length of the fiber was greater than the length of catastrophic interfacial failure, complete debonding would not occur at once. In the non-catastrophic case, values for the energy per unit area required to

debond the fiber and matrix could be found from the area of the curve and direct observation of the length over which debonding had occurred at each drop in load (8). It was stated that such values were likely to be more reliable than those obtained from catastrophic failure scenarios. However, reported calculations for the debonding energy determined in this way for the phosphor bronze/epoxy system was in the range of 10-500 J/m^2 and for glass/epoxy systems from <200 to $<10^4$ J/m^2. Definitive conclusions could not be drawn from these values.

In contrast, it was reported by Kelly that experiments resulting in catastrophic interfacial failure produced a load versus displacement curve which was linear to point X. At X the bond broke catastrophically and the fiber pulled out, as in Figure 1b. In this scenario, the maximum load corresponded to the load required for debonding over the embedded fiber length of that experiment. This is directly analogous to the microbead/microtension experiments where embedded fiber lengths are very short. Here, the relationship between embedded length and pull-out force has been discussed extensively (see for example work of Piggott, Penn). The bimodal dependence i.e., change in relationship, of embedded length expressed by Piggott and others will be discussed further in a later section.

This same type of load versus displacement curve was also reported by Takaku and Arridge in 1973 (11). In their interpretation of the load versus extension trace shown in Figure 2, they stated that the peak of maximum

load correla[illegible]o "the wire debond[ing] along the full embedded length from the matrix." Takaku and Arridge acknowledged the interpretation reported previously by Kelly, but commented that with their system "the debonding was difficult to detect". They did not account for the element of time needed for the fiber to debond and, once again, the initiation and steady-state or completion loads were not separated. Interpretation and analysis of the experimental results were [illegible]ased upon the maximum load recorded.

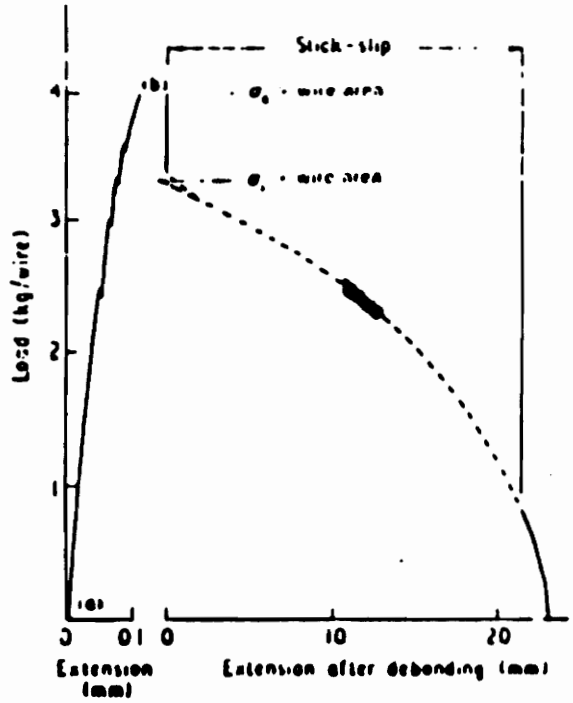

Figure 2. Load versus extension curve for a copper wire in an epoxy resin -Takaku and Arridge (11).

Although the early observations of the single fiber pull-out test included the onset of crack initiation as well as the propagation of this crack along the length of the interface, quantitative distinctions between the events were not made. Here, the maximum load the system was able to withstand was used as the basis of comparison between sample sets. As efforts progressed, however, more details of the failure process were recognized and more appropriate experimental interpretations presented.

2.1.2 Incorporation of Crack Propagation in the Evaluations of the Single Fiber Pull-Out Test

In 1979, Bowling and Groves published a paper describing the pull-out of ductile wires from a brittle matrix (14). In this paper, various events of crack propagation were presented and the role of fiber diameter and embedded length addressed.

The schematic representation of debonding and pull-out via Bowling and Groves, is reproduced in Figure 3. An important feature of their model is that behind the debonding front, the shear stress translates across the debonded region of the interface. This shear stress resulted in an increasing stress on the wire needed to propagate the debonding front. Here, at sufficiently large crack lengths or debond values, the debonding stress exceeded the yield stress of the wire at which time the plastic radial contraction of the wire reduced the interfacial shear stress to zero. From this point until the end of the fiber was reached, the debonding front continued to propagate with a constant stress on the wire. With their

material system, the debonding front typically propagated in small jumps rather than smoothly, and was accompanied by incremental decreases in load, Figure 4. This *steady-state* debonding produced a "debonding plateau" in the load-displacement curve. The magnitude of the plateau debonding stress was interpreted by Bowling and Groves as "the plastic strain needed to remove the interfacial shear traction". For their work, the small scale roughness of the wire surface was deemed critical. However, it was noted that an additional contribution may be required to overcome the radial compressive elastic stress in the matrix arising from the thermal expansion mismatch of the wire and matrix on the cooling from the cure temperature.

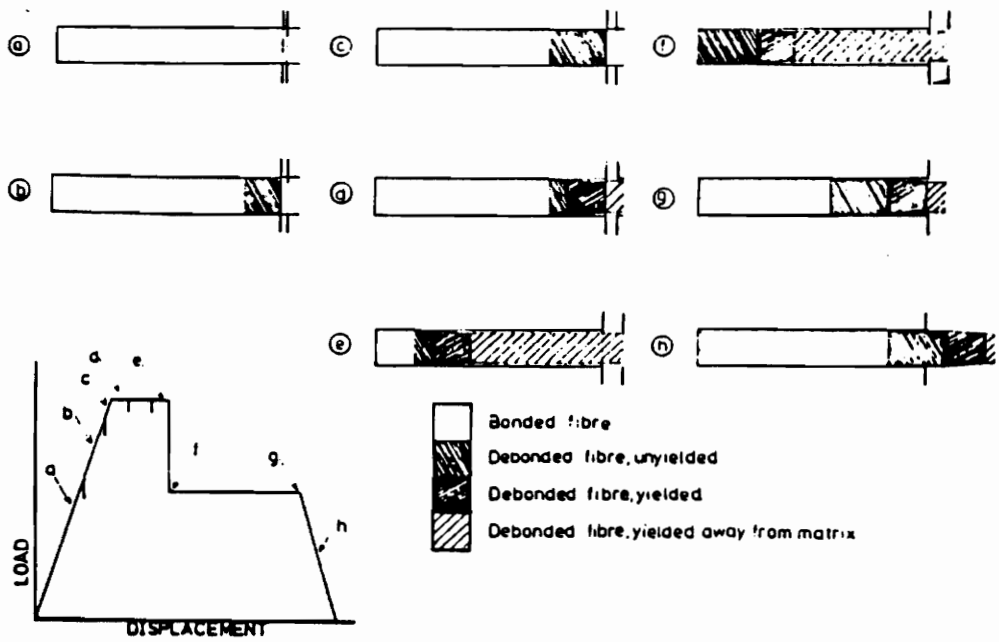

Figure 3. Schematic representation of debonding and pull-out of a ductile wire from a brittle matrix -Bowling and Groves (14).

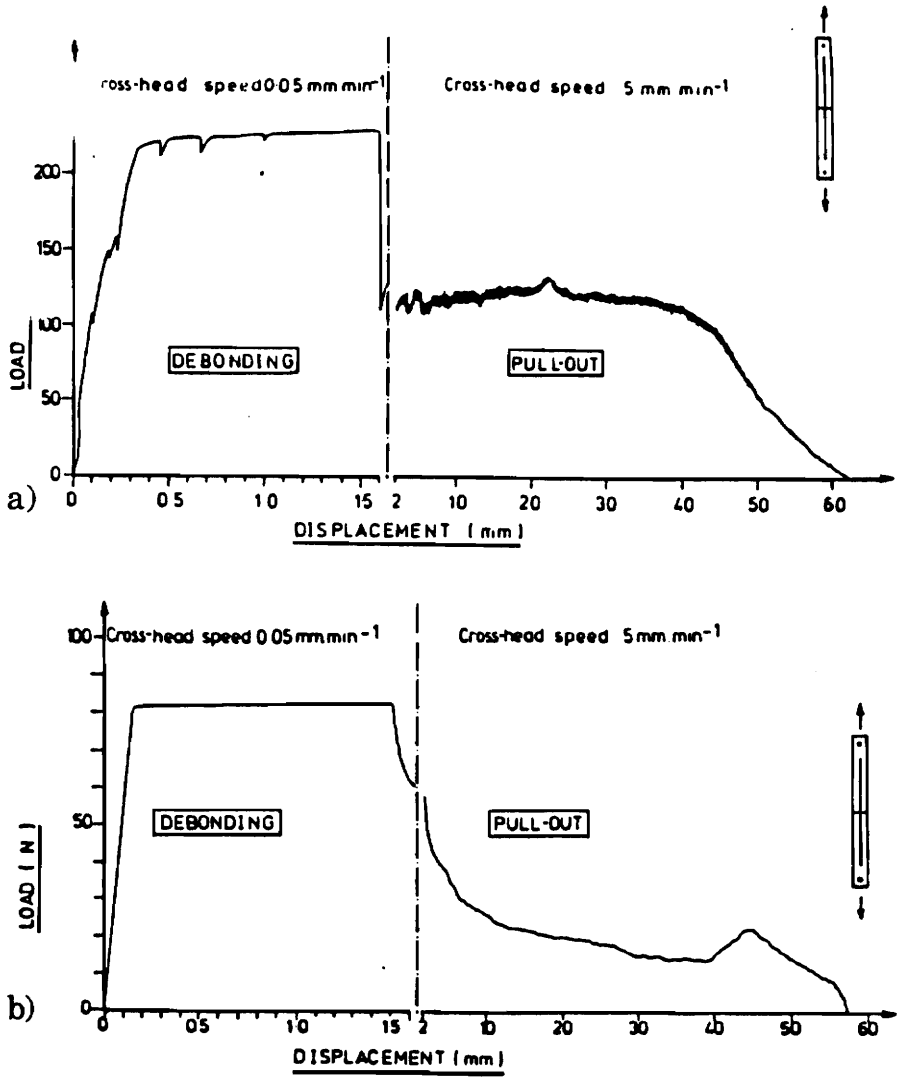

Figure 4. Load versus displacement curve for a) copper/epoxy; b) copper/cement system -Bowling and Groves (14).

For the interpretation of their results, a wire embedded with equal length $l/2$ on either side of the crack which debonded symmetrically on both sides was assumed. The total length remaining in contact with the matrix at the wire end, l_k, was given an alternate interpretation as the length of wire which must be exceeded in order to obtain a debonding plateau. This length was referred to as the *critical length* by Bowling and Groves. Since the shear stress supported by the bonded fiber typically exceeded the shear stress transmitted after debonding, a load drop occurred at the commencement of pull-out. The critical length for metal wire in Araldite MY753 with hardener HY956 epoxy was determined to be 18 mm for a 0.5 mm diameter fiber.

As was observed with the data to be presented, Bowling and Groves found that pull-out generally occurred from one side only of the crack such that the pull-out process was the withdrawal of a "plug" at one end of the wire. The length of this plug was the same as the length at the end of the wire in contact with the matrix at the moment of final debonding, $l_k/2$. The pull-out load remained constant until the beginning of the plug reached the crack surface. The debonding plateau was, therefore, followed by a pull-out plateau. In their paper, the debonding plateau was fairly constant. The comparisons and analysis were done using this debonding stress value.

2.1.2.1 The Change of Fiber Diameter with Tensile Load

The issues to be addressed on the interpretation of the length of the plug during debonding and during pull-out are numerous. In the case of a ductile wire, Bowling and Groves depict the loaded wire as consisting of yielded and unyielded regions. The plug at the end of the wire corresponded to the unyielded zone and the inner length between the two plugs as the yielded zone (14). For this material, the yielded fiber diameter associated with debond completion did not recover when the load drop occurred. Instead, the diameter of the plug i.e., the diameter of the embedded fiber, and the diameter of the yielded length remained essentially the same as when the debonding process reached completion. In cases where the embedding fiber is not ductile, however, the profile of the fiber diameter is determined by the Poisson's contraction of that fiber under a given load and is reversible.

For the fiber with reversible radial contraction, the analogy of a plug at the end of the fiber still applies. However, the profile of the shear stress or interfacial friction cannot be an assumed constant. This is because under a particular load, larger than that required to form a high frictional region or plug, the friction between the debonded fiber and matrix will be greatest behind the debond front and continuously decrease as the fiber length is traversed. Since this is a bi-directional fracture the diameter profile will mirror itself and the frictional interaction will once again increase i.e., a high frictional zone exists behind each debond front and decreases symmetrically to the center of the debonded region.

The total high-friction plug length was defined previously as l_k, and the length at each end of the fiber as $l_k/2$ and was the result of exceeding some critical load so as to yield the fiber and/or overcome the normal pressure exerted on the fiber by the embedding resin. Again, between these two high-friction or primary-frictional zones was a length of fiber whose diameter, due to either yielding or Poisson's contraction resulting from the load, was sufficiently decreased as to not contribute to the frictional dissipation of energy. For the non-ductile system, however, these values are not the same at debonding and at pull-out. As will be seen in Table 1 and as discussed in the next section, the load on the fiber during the debonding process was typically thirty percent greater than the load on the fiber during pull-out. Thus, the resulting Poisson's contraction along the length of the fiber typically resulted in a shorter primary frictional zone (plug) during the debonding process than the primary frictional zone during pull-out. N.B. If the elastic constants of the fiber are such that no radial contraction occurs over the debonding loads, then the entire length of fiber would contribute equally to the interfacial friction.

2.1.2.2 The Relationship Between Debonding Stress and Embedded Length

Bowling and Groves related the variation of the debonding stress, defined as the maximum stress up to completion of debonding, with embedded length. This relationship was bimodal, as seen in Figure 5. Here, the model predicted a constant stress once the embedded length exceeded the critical

length. The experimental deviation from this was attributed to an increased concentration of surface inhomogeneities with increased embedded length. The onset of a constant debond stress was then used to determine the minimum embedded length needed to observe a debonding plateau. This meant that not only was the initial interfacial failure not catastrophic but that it progressed long enough to surpass the primary frictional zone contribution. And, if the embedded length was sufficiently long, steady-state crack propagation would be realized until the fiber end was reached.

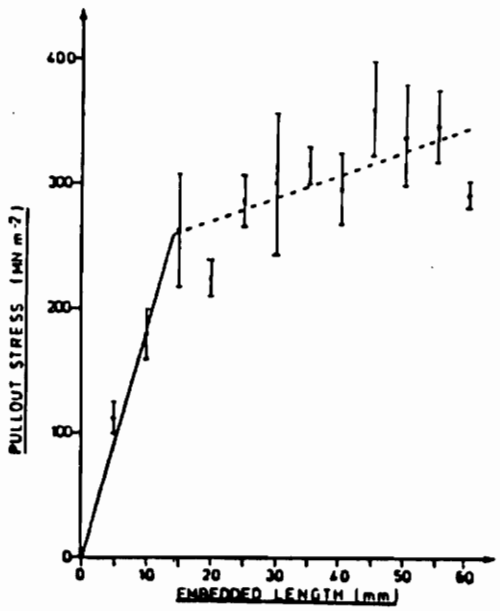

Figure 5. Bimodal relationship between embedded length and stress of steady-state debonding -Bowling and Groves (14).

This bimodal relationship appears to be the same bimodal relationship described by Piggott and others (20-22, 28,46, et cetera) i.e., the maximum load (or stress) as a function of embedded length. However, the load reported by Bowling and Groves was not the load associated with crack initiation unless the debonding of the fiber from the matrix was catastrophic. Instead, it represented debonding plus friction over a given embedded length. The high values of standard deviations associated with the load versus embedded length relationships may partly result from an inappropriate measure or definition of load. While it was thought that the maximum load in the pull-out trace represented the load at initiation, in reality, for fiber lengths greater than catastrophic failure, it represented the load during crack propagation which initially varies as a function of crack length and then levels off as the frictional contribution becomes constant.

2.1.3 The Fracture Mechanics of the Single Fiber Pull-Out Test

Many theoretical models for the pull-out of fibers from a brittle matrix are in the recent literature (7,10,17,24,44,50,52,62,69). These models are based on fracture energy (i.e., 6,10,11,48) or stress analysis (i.e., 7,8,35,46) and have proven insightful. However, the wide use and application of these models to experimental data is limited at best. This is partially due to difficulties in developing micro-scale samples with good experimental reproducibility and the appropriate recording of the failure events for small and sometimes large scale samples. In spite of these problems, efforts to

mathematically model the experimental models of composite failure have been made.

In 1969, Outwater and Murphy presented their work on the fracture energy of unidirectional laminates (7). Their analysis detailed the instability and debonding of a filament within a matrix via "craze induced tension" and the relationship between the debonding of this fiber, the tension in the fiber and the fracture energy of the laminate (7). The basis of their work, and of many to follow, was the general compliance equation expressed as:

$$G = (P^2/2\pi d)\,(dC/da) \qquad (7)[1]$$

where G is the opening mode fracture energy, P is the tensile load on the fiber, d is the fiber diameter and dC/da the compliance of the structure as a function of crack length. Here, the key assumption is the initial existence of an interfacial crack. It is recognized here that the debonding event is mixed mode and after initiation of crack propagation from the resin endface, the failure is predominantly shear (mode II) and not opening (mode I).

The successful model for the determination of the strain energy release rate at both the initiation of crack propagation and for the continuation of the crack front along the fiber length will consider the physical constants of the materials, the response of this material under a load, the response as a function of the material components and ultimately the thermo-mechanical

history of the specimen for a given loading configuration. The following sections detail the efforts of some researchers which have developed methods for the quantitative evaluation of the single fiber pull-out test from fracture mechanics. Their approaches are very similar. Their observations, findings and problems are also very similar. Thus, a fracture energy approach to the problem will only describe a small subset of the single fiber pull-out results with limitations on material properties and fiber lengths as well as material interactions.

2.1.3.1 The Approach of Morrison, Shah and Jeng

In 1988, Morrison, Shah and Jeng published their analysis of the debonding and pull-out of a steel fiber from a cement matrix (35). Here, the primary goal of the investigation was to "identify fracture mechanics based material parameters that could be evaluated from the single-fiber pull-out test". In this work, the total load to debond and pull-out the fiber was separated into two components: that due to frictional resistance and that due to the debonding force. It was assumed that the two load-resisting mechanisms acted independently of each other and that the frictional stress was uniformly distributed over the debonded length. Based on these assumptions, the frictional resistance was described by:

$$P_f = 2\pi r\, a\, \tau_f \qquad [2]$$

where τ_f is the assumed constant frictional resistance of the fiber/matrix interface, a is the length of the interfacial crack and r the radius of the fiber (35).

Resistance offered by the debonding mechanism was determined from the Griffith energy criterion. If the peak debonding resistance occurred at a crack length that satisfied the conditions (35):

$$(E_f/E_m)\,(r/L)^2 \ln (2L/r) << 1 \qquad [3]$$

and,

$$(L-a) / r >> 1 \qquad [4]$$

where L is the embedded length, then the debonding force P_b could be expressed as

$$P_b = (4\,\pi^2\, r^3\, E_f\, G_c\,)^{1/2} \qquad [5]$$

where G_c is the strain-energy release rate associated with crack initiation. Note that $P_{total} = P_f + P_b$ is less than the tensile strength of the fiber, otherwise the fiber fails prior to complete debonding. Rearranging equation [5] allows for the calculation of G_c from the crack initiation load where $P_b = P_{initiation}$.

$$G_{c,init} = P_{init}^2 / [4\,\pi^2\, r^3\, E_f] \qquad (35)\,[6].$$

This was from the standard compliance equation discussed by Outwater and Murphy (7). A schematic depiction of the various loads is reproduced in Figure 6.

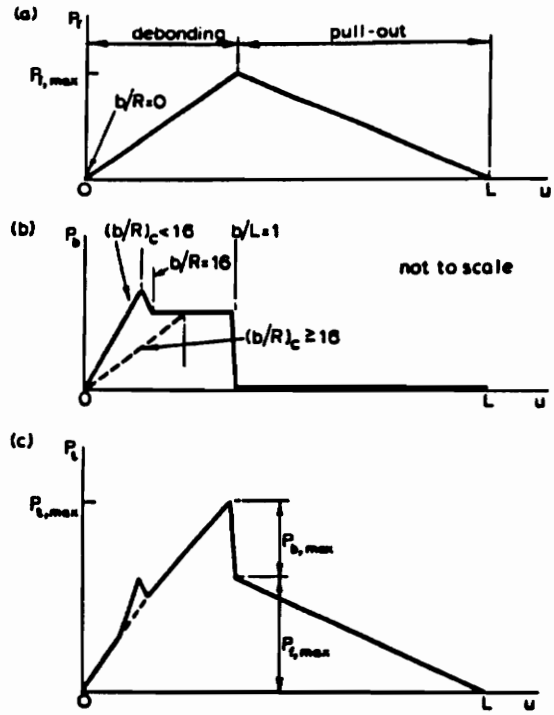

Figure 6. Schematic of load versus displacement when friction dominates: a) contribution of the debonded region; b) contribution of bonded region; c) total resistance to pull-out - Morrison et al. (35).

Morrison et al. determined through the use of finite element analysis, FEM, that the critical maximum crack length for peak interfacial failure was 16r. Conversely, for crack lengths greater than 16r, the frictional dissipation of energy should become a constant. Therefore, if the peak debonding resistance occurred at a crack length smaller than 16r, there would be a drop in load after the maximum resistance had been reached. However, they claimed, a debond plateau would result for post-critical

extensions greater than 16r since the value of G_c was essentially constant for values of a >16r. In taking a close look at the reported data, all embedded lengths were greater than the 16r criterion, thus, according to their hypothesis, steady-state crack propagation should have been realized prior to debond completion. This does not appear to be consistent with how the data was interpreted.

Morrison et al. averaged the maximum pull-out load recorded for each set of embedded lengths. This load was then correlated linearly to the embedded length and a positive slope was assumed. The standard deviations of their data, however, do not show any statistical difference between the sets to encourage such an assumption. Here, the embedded lengths were handled as if they were crack lengths of less than 16r. Because all embedded lengths reported could accommodate crack lengths greater then 16r, steady-state crack propagation - post frictional effects - were, according to their theory, realized. Thus, the maximum load in the pull-out traces correlated to steady-state crack propagation and were constant for the embedded lengths used. Here, where an increase in load was forced, a constant load should have been applied. The increase would have been seen if the embedded lengths were varied less then 16r.

For fiber lengths within the length associated with the primary frictional zone, the contribution of interfacial frictional force to the pull-out resistance would indeed increase proportionally with the debonded length, a, and reach its maximum when debonding was complete (a=L). As described by

their model, the value of P_b would then drop to zero and the resistance to external load could be attributed to the interfacial frictional force. This resistance should then decrease linearly and reach zero as the fiber is completely withdrawn (displacement = L). The total load could then be calculated from the contributions of the debonding force and the interfacial frictional force, $P_{total} = P_b + P_f$.

In addressing Morrison et al.'s interpretation of the load versus extension trace and how it corresponds to the events occurring, the following is suggested. In their interpretation, the load associated with debonding was defined as the difference between the maximum peak load and the load associated with friction at crack completion, i.e., the drop in load post fracture, see Figure 7. Based on the current work, this is not a true value for P_b. Again the load on the fiber plays a role in the amount of interfacial friction experienced by the fiber. Here, by using the lower frictional load of pull-out rather then the frictional load associated with debonding, the frictional contribution was under-estimated when applied to the debonding process. Also, the direct observation of interfacial crack initiation does not necessarily equal the load of initial fiber pull-out determined by this subtraction method. Table 1 contains a listing of the experimentally observed initiation loads, P_i, the load experienced at the end of the primary frictional zone, $P_{friction}$, and the load at the completion of debonding, before and after drop, $P_{complete}$ and P_{drop}, for a series of pull-out experiments to be discussed later. This $P_{friction}$ is the maximum load associated with the end

of the primary frictional zone and is not equal to P_f as defined by Morrison et al.

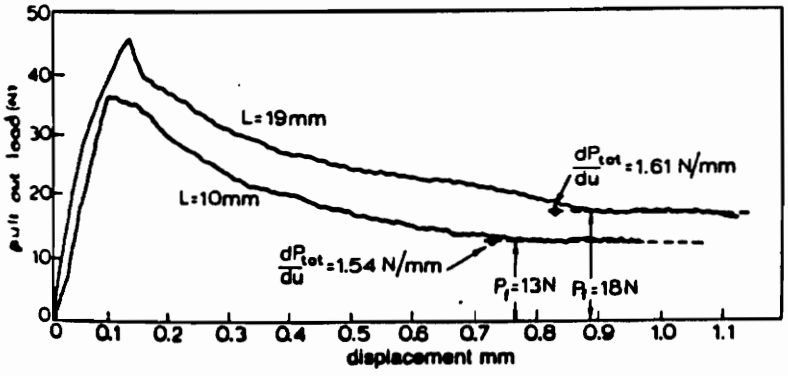

Figure 7. Load versus displacement curve for a steel fiber in cement -Morrison et al. (35).

Table 1. Values for the load on the fiber at various times during the single fiber pull-out test in N; P_{init}, $P_{friction}$, $P_{complete}$, P_{drop} are described in the text.

file	Pinit. N	Ptau. N	Pcomplete. N	Pdrop. N
CD150J	32.9	-	55.78	37.3
CD150K	29.9	-	89.16	62.6
CD177B	78.72	81.96	73.32	59
CD177I	39.74	69.64	73.14	51.6
CD177J	47.44	72.72	69.84	58.3
CD230D	65.98	86.22	89.3	69.5
CD177I	72.38	87.96	66.68	60
CD177J	54.36	66.96	64.86	56
CD177K	60.46	62.42	61.3	53.8
CD250F	51.58	78.22	85.06	60
CD250H	50.3	79.1	91.5	61.5
CD250K	68.48	68.92	105.44	47

Since the determination of P_f accounts for the primary frictional zone and P_{init} accounts for the crack front, the determination of G_c during debonding was estimated with the following equation by Morrison et al.:

$$P_T = 2\pi R^{3/2} (G_c E_f)^{1/2} + 2\pi r\, l\, \tau_f \qquad (35)\ [7]$$

or,

$$G_{c,\tau} = \left[\frac{P_\tau - 2\pi r l \tau}{2\pi r^{3/2}} \right]^2 E_f^{-1} \qquad [8]$$

where l is the length of fiber over which τ acts. Morrison et al. assumed l = L = embedded length, which is inappropriate, as was discussed previously.

Morrison et al.'s work represents an early attempt to appropriately account for the frictional dissipation of energy during debonding. If this were accomplished $G_{c,\tau}$ would equal $G_{c,init}$, i.e., be a constant. This was claimed to have been done, however, because of the questions surrounding their interpretations of the trace and the application of their theory, the conclusion are not substantiated.

2.1.3.2 The Approach of Jiang and Penn

Jiang and Penn (67) have recently reported on their current evaluation of the microdebond test. While the loading configuration differs from the single fiber pull-out test, their approach is worth noting. They attempted to improve their existing analysis of the SFPO test (46) by including the

contributions of matrix compression and of the frictional coupling between the debonded fiber-matrix interface in the wake of the crack tip. In their paper, the strain energy content in the free fiber, the debonded fiber, and the bonded fiber regions of the specimen were derived separately via an energy balance approach. Also, an expression for the work of friction in the debonded region was developed as well as an expression for the critical load for a pull-out specimen.

The primary result of their effort can be expressed as:

$$P_c = A_f \frac{\sqrt{B^2 - 4AC} - B}{2A} + fa \qquad (67)\ [9]$$

where,

$$A = \frac{(1+\alpha) A_f}{2E_f} + \frac{(2+\alpha) A_f \operatorname{csch}^2(ns)}{4E_f} \qquad [10]$$

$$B = -\frac{(1-\alpha)\, fa}{E_f} - \frac{(2+\alpha)\, rf \coth(ns)}{2nE_f} \qquad [11]$$

and

$$C = \frac{f^2(1+\nu_m)\ln\left(\frac{R}{r}\right)}{2n\pi E_f} - \frac{(1-\alpha) f^2 a^2}{2A_f E_f} - 2\pi r G_c \qquad [12].$$

In these equations, A_f is the cross-sectional area of the fiber, r is the radius, f is the frictional relationship between the fiber and matrix (i.e., the pull-out slope, ($dP/d\delta$)), a is the interfacial crack length, and

$$n^2 = \frac{E_m}{E_f\left(1+\nu_m\right)\ln\left(R/r\right)} \qquad [13]$$

$$s = (l-a)/r \qquad [14]$$

$$\alpha = (E_f A_f)/(E_m A_m) \qquad [15]$$

where, R is the matrix radius and l is the embedded length of the fiber. Equation [9] is the fundamental relationship between sample and material parameters and the loading information for crack propagation. Here, the load associated with crack initiation, P_{init}, is denoted $P_{critical}$ or P_c.

Equation [9] was used as a mathematical model to generate a curve of pull-out load versus embedded length, as if for a series of specimens. As was noted in earlier work by researchers using larger specimen geometry's, Jiang and Penn recognized that the maximum pull-out load was identical to P_c only when crack propagation went catastrophically down the entire interface. The details of their computational procedure were dependent upon whether the pull-out load was identical to the critical load (initiation) or was higher than the critical load due to the effect of friction in the debonded region.

As was stated earlier, specimens with large embedded lengths required increased applied load for continued crack growth after initiation and experienced maximum loads that exceed $P_{c,a=0}$ where a is crack length.

The additional load is needed to overcome the effect of friction in the energy balance equation. It was stated in Jiang and Penn's paper that friction, which was given by fa, was proportional to the debonded area and became important only when the embedded length was large enough to allow the development of a significant debonded area prior to complete debonding (67). It was assumed that the unit friction force was not a function of crack length but was uniform along the debond length. This model does not accommodate a fiber whose diameter, over long debonded lengths, decreases to the point of removal from the surrounding matrix cylinder. Therefore, the lengths modeled are either not long enough to surpass the debonding of the frictional zone, or conversely, the model represents a very stiff fiber.

Jiang and Penn were able to confirm directly the process of crack growth in specimens with large embedded lengths. Visual observation of the crack growth process was possible since their resin was somewhat transparent and a change in reflectivity at the interface upon debonding occurred. Crack initiation was observed to occur at P_c, the break point between linear and nonlinear portions of the load versus displacement curve, Figure 8b. The slow and continuous crack growth that occurred after P_c produced the nonlinear portion of the curve. When the crack had completely traversed the embedded length, the fiber lurched upward in the matrix and the load dropped.

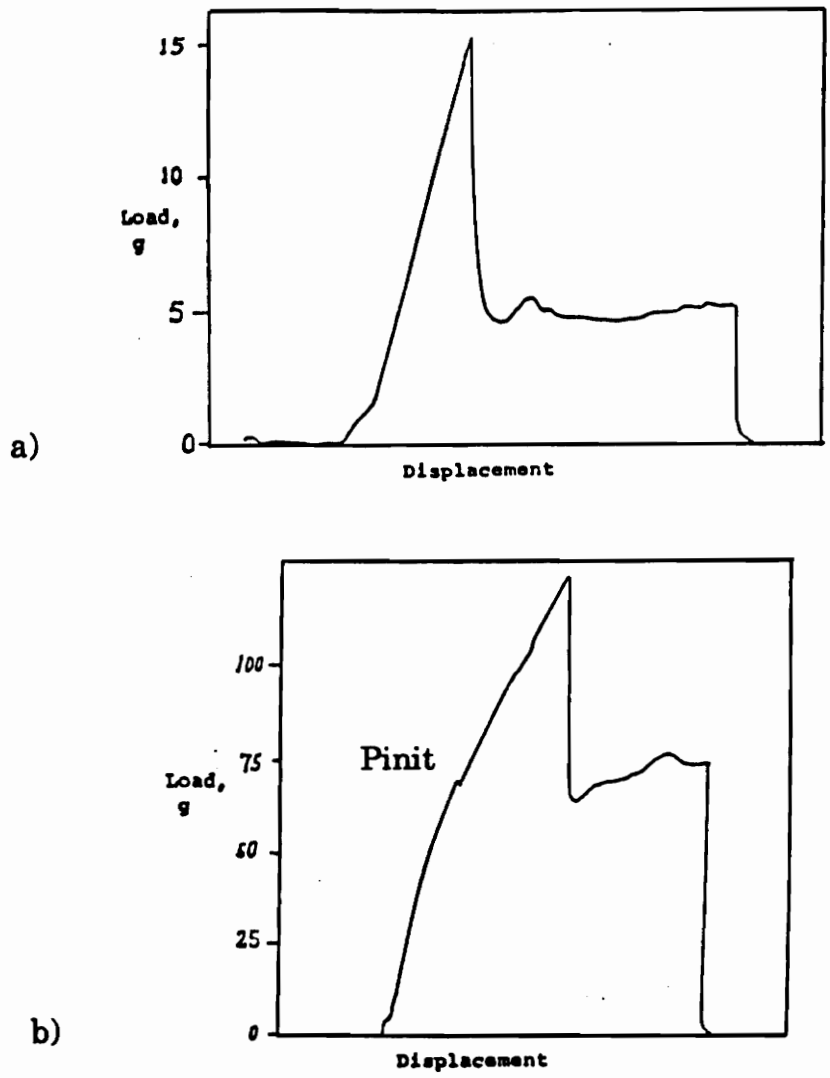

Figure 8. Load versus displacement curve for ultra-high density polyethylene in an epoxy: a) catastrophic interfacial failure; b) crack initiation and propagation -Jiang and Penn (67).

P_c is the only experimentally accessible quantity that gives direct information about the interfacial fracture energy, G_c, between fiber and matrix via equation [9] (67). Although it was stated that the load at initiation could be experimentally observed, this experimental value was never used in the proposed model to determine G_c with the consideration of

interfacial friction. The problem was attributed to pull-out loads obtained at long embedded lengths including friction and were therefore higher then P_c. It is not clear as to why the model, which is supposed to account for this increase in load, was not utilized.

Jiang and Penn's model is based upon an energy balance approach. The energy balance states that the change in external work is equal to the energy released plus the change in internal energy plus the energy dissipated. However, their initial energy balance equation did not account for the change of external work i.e., since frictional forces are present, the total mechanical energy is not constant but changes with the amount of work done (87). Thus, the basis of their model is inappropriate (per. comm. Y-H. Lai).

2.1.3.3 The Approach of Gao, Mai and Cotterell

The most rigorous description of the single fiber pull-out test found in the literature was reported by Gao, Mai and Cotterell (33). In their paper, a fracture mechanics-based debonding criterion which includes friction, was reported. From energy balance considerations, for a crack growth, dA, along a frictional surface, S_F

$$\int_{ST} T\,du\,ds = G\,dA + \int_{SF} \tau_s\,dv\,ds + dU \qquad [16]$$

where T is the tensile force or traction on the surface, du and dv are the displacements in the cracked body of volume V, G is specific work of fracture, $\int_{SF} \tau_s\,dv\,ds$ represents the work of friction and U the stored strain energy of the body (33). For an elastic system

$$dU = 1/2 \int_{ST} T\, duds \; - \; 1/2 \int_{SF} \tau_s\, dvds \qquad [17].$$

Thus,

$$G = \frac{1}{2}\frac{d}{dA}\int_{S_T} T\, duds - \frac{1}{2}\frac{d}{dA}\int_{S_F} \tau_s\, dvds \qquad [18]$$

where $A = 2\pi ra$ and $ds = 2\pi rdy$. Gao et al. applied this equation to the rod in cylinder fiber debonding problem to analyze the debonding process of crack propagation along the fiber-matrix interface.

The fiber matrix pull-out problem is depicted in Figure 9. Here, r is the fiber radius, R the matrix radius, y describes the location along the fiber length where s is the clamped end, l=a is the location of the crack front and 0 is the free edge of the matrix; l (>a) is the debonded depth and τ_s the shear stress acting over the debonded region due to interfacial pressure; T_f and T_m are the tensile forces on the rod and cylinder where $P = T_m + T_f$; also, E_f, E_m and ν_f, ν_m are the Young's moduli and Poisson's ratios for the fiber and matrix respectively.

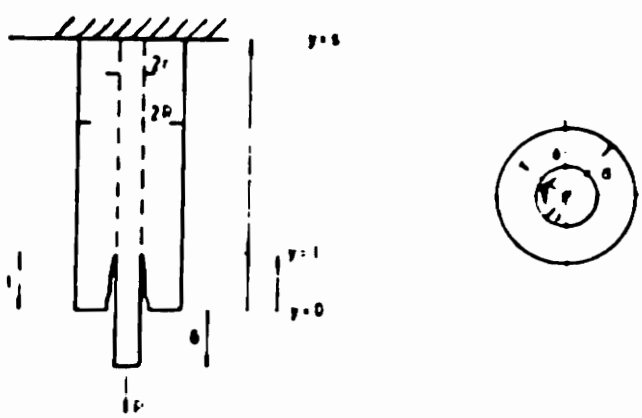

Figure 9. The fiber-matrix pull-out problem -Gao et al. (33).

The debonding toughness, or strain energy release rate, was again given using the well established compliance equation via Outwater and Murphy.

It was shown that the debonding criterion could be described by combining a debonding and frictional term:

$$G = \frac{-P}{4\pi r}\left(\frac{\delta u_f(0)}{\delta l}\right) - \frac{1}{2}\int_0^1 \tau_s \frac{\delta v(y)}{\delta l} dy$$

(33) [19].

The derivative of this equation gave the general debonding criterion as

$$4\pi^2 r^3 E_f(1+\beta)\, G = (1-2kv_f)\left[P-(1+\beta)\, Q\right]^2$$

[20]

and for $G = G_{continue}$, is the strain energy release rate associated with the continuation of an existing crack with the consideration of friction over the existing debonded region,

$$G_{continue} = \frac{(1-2kv_f)\left[P-((1+\beta)\, Q\right]^2}{4\pi^2 r^3 E_f(1+\beta)}$$

[21].

Here,

$$k = \frac{\alpha v_f + \gamma v_m}{\alpha(1-v_f)+1+v_m+2\gamma}$$

[22]

$$\alpha = E_m / E_f$$

[23]

$$\gamma = r^2 / (R^2 - r^2) = c_f / c_m \qquad [24]$$

where c_f/c_m is the volume fraction of fiber in matrix.

$$\beta = \frac{\gamma\left(1-2k\nu_m\right)}{\alpha\left(1-2k\nu_f\right)} \qquad [25]$$

and,

$$Q = T_m(l) = \frac{\alpha\nu_f\left(\tilde{P}-P\right)}{\alpha\nu_f + \gamma\nu_m}\left(e^{\lambda l}-1\right) \qquad [26]$$

where $\tilde{P}$ is a constant which represents the load at the end of the primary frictional zone:

$$\tilde{P} = \frac{\pi r^2 q_o}{\alpha\nu_f}\left[\alpha\left(1-\nu_f\right)+1+\nu_m+2\gamma\right] \qquad [27].$$

Here, q_o is the normal pressure exerted on the fiber due to resin shrinkage during cure plus the differential of the thermal coefficient of expansion between fiber and matrix. Finally,

$$\lambda = \frac{2\mu}{r}\left(\frac{\alpha\nu_f + \gamma\nu_m}{\alpha\left(1-\nu_f\right)+1+\nu_m+2\gamma}\right) \qquad [28]$$

where μ is the coefficient of friction as determined from the tail of the fiber pull-out trace.

Equation [21] shows that the debonding load is a function of crack length, Poisson's contraction, the coefficient of friction at the interface, the volume fraction of fiber and matrix and their Young's moduli. As was the case

with Jiang and Penn, Gao's model was not applied to experimental data which included debonding over the frictional region of the fiber. Instead they addressed the point of crack initiation.

As discussed by Gao et al., if interfacial friction is ignored, the frictionless debonding load, or crack propagation load at very small crack lengths, is expressed as

$$P_o = 2pr^{3/2}\left[\frac{E_f G\,(1+\beta)}{1-2kv_f}\right]^{1/2} = P_{init} \qquad (33)\ [29]$$

and for $G = G_{initiate}$, is the strain energy release rate associated with the initiation of propagation of an existing crack without the consideration of friction over the vanishingly small existing debonded region,

$$G_{initiate} = \left[\frac{P_{init}}{2pr^{3/2}}\right]^2 \left(1 - 2kv_f\right)\left(E_f\left(1+\beta\right)\right)^{-1} \qquad [30]$$

For systems with relatively low fiber volume and fiber modulus, this equation is essentially the same as the compliance equation expressed via Outwater and Murphy. As will be shown later for the work to be presented, there is very little difference between the values of G_c calculated with the compliance equation [1] and Gao's [30].

The evaluation of the single fiber pull-out test has produced a variety of mechanistic models to describe the onset of fiber/matrix interfacial failure and the propagation of this event. While no values for the strain energy release rate during debonding could be found in the literature, the critical strain energy release rate associated with crack initiation, estimated by implementing various forms of Outwater and Murphy's equation, are presented in Table 2.

Table 2. Strain energy release rates for the initiation of crack propagation as reported in the literature.

System	Strain Energy Release Rate, N/m	reference	comments
steel/cemen	2.49 ± 0.05	35	
carbon/epoxy	50	30	
glass/epoxy*	50 ± 14	31	no heat
glass/epoxy*	79 ± 8	31	24 hr at 60
glass/polyester**	57 ± 3	31	no heat
glass/polyester**	190 ± 30	31	6 hr at 80°C
stainless steel	200****	33	

*not specified

**Shell Epon 815 with Shell Ancamine XT

***Ashland Crystic 2-491-PA with methyl ethyl ketone

**** Ginitiate

The variability of the physical parameters in the material systems in Table 2 which are not accounted for with this SERR estimate prevents any comparison of data. Only a model which can account for the various experimental and material parameters as well as the interaction between the joined materials will allow for accurate quantification of the data generated by the single fiber pull-out test.

2.2 The Effect of Cure Temperature on T_g, Density and Internal Stress

In bringing two materials together, the mismatch in their physical properties can be used to optimize the physical properties of the system. Of specific interest here is the embedding of a stiff fiber in a polymer matrix. The matrix properties directly effect the failure of the embedded fiber. To address this issue, literature concerning the densification of thermosetting resin with cure and the subsequent build-up of internal stresses is presented.

A significant amount of research has been published on the physical characteristics of epoxy based resin systems. Regarding the use of these epoxy systems for materials development, the effect of cure temperature on degree of conversion and the glass transition temperature, T_g, has been studied (72,73,75,76,78,79,81-84). Also, parameters such as density and internal stresses have been characterized as a function of cure temperature (71,74,77,81-84). These parameters affect the load carrying and load transfer abilities of a fiber reinforced polymeric resin. The mechanical and

sometimes chemical adhesion which results at the fiber/resin interface provides for the transfer of load or stress between fiber and resin. The mechanical adhesion is the result of the normal pressure on the fiber due to chemical shrinkage of the resin during the crosslinking process as well as the shrinkage of the resin via thermal contraction upon cooling. The extent of this normal pressure has an optimum value for the particular material of interest. Here, there are two functions of the fiber reinforced composite to be considered. First, the extent of load transfer between fiber and resin increases with mechanical (and chemical) adhesion. Second, with the occurrence of composite failure, the ability for these fibers to debond and pull-out provides for the dissipation of energy such that failure is arrested.

Chemical conversion via T_g and internal pressure via densification and shrinkage are evaluated regarding the single fiber pull-out test. To this end, work by Oleinik is addressed regarding critical conversion at different temperatures of cure, T_{cure}. The characterization of epoxy based resins is therefore presented. Here, the density, or volume, of the system as related to the T_g, or extent of conversion, is described for various epoxy systems. This is followed by work of Gillham et al. who have produced a series of papers evaluating the physical properties of high-T_g amine-cured resins (75,81-84). Specifically addressed by Gillham and co-workers was the change in density of the resin as a function of cure temperature and time.

The densification of the polymer and resulting normal pressure on the embedded fiber effect the loading and fracture parameters in the single

fiber pull-out test. Specifically addressing the normal pressure on the single embedded fiber were Broutman (5), Harris (74), and Jang et al. (77) as well as Gao et al. (33). These articles are also evaluated with respect to the current research.

2.2.1 Extent of Reaction and T_g

The transition of a polymer from a liquid or rubbery state into a glassy state occurs over a temperature range associated with the glass transition temperature, T_g. The glass transition temperature is characteristic of a particular material and is a function of its chemical and physical parameters as well as its thermo-mechanical history. With respect to thermosetting materials, as the extent of reaction increases, the average molecular weight of the polymer chains also increases, thus, an increase in T_g occurs.

The relationship between glass transition temperature and the extent of chemical reaction has been addressed by many researchers. The onset of the change in mechanical properties associated with a change of state of the materials has been evaluated by TMA (89), DSC (90), density (72,73,75,76,78,79,81-84) and evaluated chemically by FTIR (90,91). Based on the curing phenomena, it is accepted that as the extent of reaction proceeds the glass transition increases toward a value associated with the theoretical infinite molecular weight matrix.

2.2.2 The Density and Volume of the Epoxy Resin

As a thermosetting material cures, its molecular weight and glass transition temperature increase. As the glass transition temperature approaches the cure temperature, the material may vitrify. If vitrification takes place, the crosslinking process changes from kinetic to diffusion-controlled. If, however, the cure temperature remains greater than the glass transition temperature, the entire cure process is kinetically-controlled. With the embedding of a fiber into a thermosetting resin, two events may occur depending on the relationship between the cure temperature, T_{cure}, and the glass transition temperature, T_g. For the case where $T_{cure} < T_g$, vitrification occurs during the cure process and internal stresses due to chemical shrinkage result. On the other hand, for $T_{cure} > T_g$, vitrification does not occur during the crosslinking process and minimal or no internal stresses result from chemical shrinkage. It is recognized that some internal molecular stresses evolve at the very last stages of cure. For cases of $T_{cure} > T_{R.T.}$, where $T_{R.T.}$ is room temperature, there is a net internal stress due to cooling which must also be considered.

Many epoxy-based resin system have been studied regarding the effect of cure temperature and cure time on both T_g and density. On the evaluation of Bisphenol A-epichlorohydrin (DGEBA) based systems, Fisch, Hofmann and Schmid evaluated the relationship between chemical structure and cure conditions on the density, extent of cure and T_g (73). They found, and

it is now well known, that the glass transition temperature was higher than the cure temperature by some constant amount and that the contraction coefficient was dependent upon the curing temperature. In their work, these two factors resulted in 1) a *decrease* in density of the end-product with increase of cure temperature for one set of chemical systems; 2) an initial decrease in density then constant value for a second chemical system; and 3) a system where the density was independent of the curing temperature (73). The interpretation of these results was based upon the T_g-density relationship. In summary, the decrease in density of the end-product at room temperature with increasing cure temperature resulted from a decrease in the contraction coefficient with T_{cure} (73).

In work reported by Cizmecioglu, Gupta and Fedors, the glass transition temperature and density of the TGDDM/DDS epoxy system were found to increase with the extent of cure and be independent of cure temperature given sufficient reaction time (76). According to Kong, who also addressed the TGDDM/DDS epoxy system, the density of this system would then decrease from the as-cast condition with subjection to different thermal histories (78), see Figure 10. Specifically, post-curing the as-cast material with slow cooling resulted in a significant drop in density. Quenching of this post-cured sample reduced the density further. Samples which were then aged below T_g in nitrogen displayed in increase in density with time.

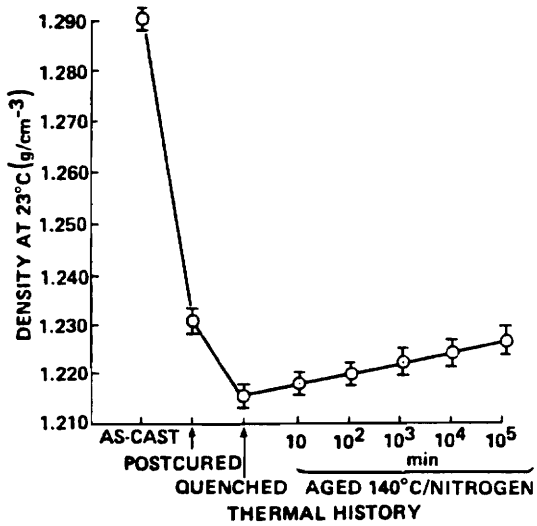

Figure 10. Density versus thermal history of a TGDDM/DDS epoxy system as a function of thermal history -Kong (78).

The significant decrease in the density of the post-cured specimens in Kong's density work were attributed to the escape of unreacted DDS and/or other low molecular weight species. However, via Enns and Gillham (75), another interpretation was offered. This type of density change via Gillham et al., was attributed to a higher-crosslinked system via the higher temperature treatment resulting in a material which was further from the equilibrium glassy state then a material which was not at this elevated temperature. From the literature, it appears that for any given resin system, data is available to support both increasing and decreasing changes in density. As presented in the following sections, the degree of shrinkage and density of a thermoset is a function of thermal history.

Extensive research on the T_g and density relationship to the time and temperature of cure has been reported by Gillham et al. Of specific interest is the recently reported anomaly to the density-T_{cure} relationship. It was observed that the room temperature density, ρ_{RT}, increased with cure time for low T_{cure}. However, ρ_{RT} decreased with increasing time of cure (and T_g) at higher values of T_{cure}. In this regard, Pang and Gillham discussed the room temperature density of a di-functional epoxy monomer cured with a tetra-functional aromatic diamine as a function of time and temperature of cure (81). Here, the T_g was approximately 25 °C greater than the cure temperature of the system; cure took place in the glassy state. T_g was used as an index for the progress of cure.

When the crosslinking process begins, an initial increase in ρ_{RT} is expected via densification due to the crosslinking reaction occurring in the liquid and rubbery states. As the cure time proceeds, the material will either form a glass due to the approach of T_g, or, form a rubber due to gelation. If the material enters a glassy state, $T_g > T_{cure} + x°C$, the density is expected to level off due to minimized molecular relaxation's. Up to a critical extent of reaction, this theory holds. If, however, the crosslink density of the material reaches the conversion value related to gelation prior to the onset of T_g, the material becomes a rubber. After gelation, the system will relax less completely towards equilibrium and the density will not increase as much as prior to gelation. Thus, at room temperature, the apparent density will begin to decrease as a function of cure time and temperature. Stated simply, for $T_{cure} < T_g$, density is a function of cure prior to

vitrification, and a function of chemical and physical aging post vitrification, for $T_{cure} > T_g$, post gelation, density is a constant for a given cooling rate.

In the same study by Pang and Gillham, the volume-temperature relationship was determined for their epoxy system. It is generally accepted that as the extent of cure varies, the volume-temperature relationships between T_{cure} samples are linear and parallel (81). Also, the T_g is predicted to increase with cure with the transition occurring at successively lower specific volumes (81). Gillham et al. found, however, that at higher conversions the specific volume increased. This phenomena is depicted in Figure 11. This anomaly was explained as follows: "In the latter stages of cure, it appears that the effect of increase in T_g due to increased extent of cure can be more dominant than the effect of cure shrinkage. Consequently, the specific volume at room temperature can increase with increasing T_g as the shrinkage at T_{cure} is smaller than the loss of contraction on cooling in the rubbery state due to a higher T_g." Based on these conclusions, a material would be expected to have a higher specific volume on cooling to room temperature when cured at a higher temperature if the thermal coefficient of expansion of the reacting resin is more dominant than the shrinkage due to cure (81).

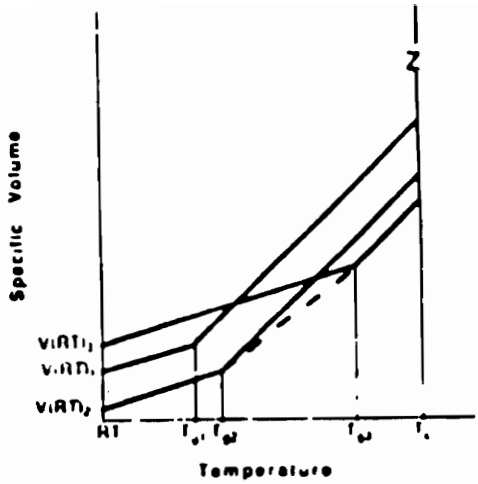

Figure 11. Schematic diagram of specific volume (V) versus temperature (T) for epoxies cured to different extents (1<2<3) -Pang and Gillham (81).

In applying these conclusions to a fiber embedded in neat resin for the single fiber pull-out test, the following discussion is presented. For $T_{cure} < T_g$, as the extent of reaction progresses prior to vitrification, the density increases, free volume decreases and internal stresses remain minimal. Thus, the normal pressure on the embedded fiber is also minimal at this time. Once T_g approaches and passes T_{cure}, the system vitrifies, the reaction becomes diffusion controlled, the free volume decreases at a slower rate and internal stresses begin to build. The normal pressure on the fiber then builds as a function of time spent in the vitreous state at T_{cure}. With cooling from the cure temperature, the glassy material shrinks via thermal contraction, the extent of which is a function of $T_{cure} - T_{R.T.}$ Thus, the normal pressure the resin exerts on the embedded fiber when $T_{cure} < T_g$ is the result of chemical shrinkage post vitrification plus the extent of thermal contraction upon cooling.

During the cure process where $T_{cure} > T_g$, the density of the resin increases, free volume decreases, and internal stresses are minimal. In this case, the system is in the liquid and, with gelation, rubbery states. In these states, relatively little normal pressure is exerted on the fiber due to chemical shrinkage. When cooling commences from this cure temperature, the material is rubbery until the glass transition region is passed and vitrification is complete. In cooling from T_g to room temperature, thermal contraction of the glassy material results in a normal pressure on the embedded fiber. Therefore, the normal pressure exerted on a fiber embedded in a resin cured above T_g is the result of thermal contraction of cooling from T_g to $T_{R.T.}$.

In summation, the normal pressure exerted on a fiber embedded in a polymeric resin will increase as the cure temperature increases and then decrease to a constant value when the cure temperature accommodates chemical cure in the rubbery state.

2.2.3 Internal Stress in a Tetra-Functional Epoxy System

While the density of an epoxy resin is a function of both the chemistry of the system as well as the cure conditions, the extent of internal stresses is primarily a function of cure temperature and time. As previously discussed, this is due to the relationship between the glass transition temperature of the material and the temperature of cure.

In 1991, work was reported by Ochi, Yamashita and Shimbo on the mechanism for the occurrence of internal stress in 1,1,2,2,-tetraphenylglycidyletherethane (TPGEE), a tetra-functional epoxy resin system whose T_g was higher then T_{cure} (86). Internal stress was measured via a strain gauge on a steel ring configuration; changes in density due to chemistry were measured via the change in buoyancy in silicone oil; density change due to the cooling process was calculated from the change of sample length, which was measured by using a thermomechanical analyzer (TMA).

The measured density change due to chemistry was converted to shrinkage by using the following equation:

$$S = (1/\rho_o - 1/\rho_t) / (1/\rho_o) \times 100\ (\%) \qquad (86)\ [31]$$

where ρ_o and ρ_t are the density of uncured samples and the density at curing time, t, respectively. The density due to cooling was determined from:

$$\rho_T = \rho_{cure} / \{1+3\alpha(T-T_{cure})\} \qquad (86)\ [31]$$

where ρ_T and ρ_{cure} are the density of cured sample at temperature T and cure temperature T_{cure}, respectively. The linear thermal expansion coefficient, α, was measured by TMA.

The build up of internal stress in this epoxy resin system occurred in both the curing and cooling processes. The T_g of this system was 308°C, higher than the curing temperature, and the cured resin vitrified during the course of the thermal process.

As depicted in Figure 12, Ochi et al.'s conclusions stated that the shrinkage in the curing process was the sum of the curing shrinkage from the progress of the curing reaction and the cooling shrinkage from cooling from peak temperature [via exothermic reaction] through curing temperature, to room temperature (86). Unfortunately, no samples were prepared above the T_g and so the transition to reduced internal stresses was not evaluated.

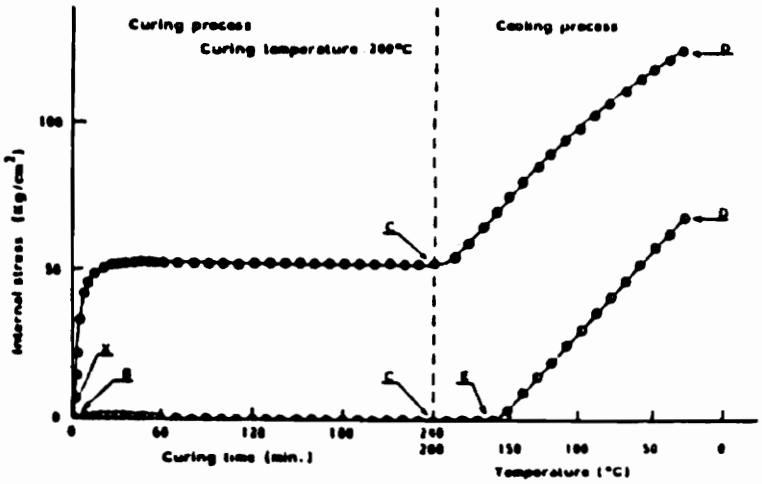

Figure 12. Internal stress during the curing and cooling processes for epoxide resins; top curve is TPGEE/DDM, T_g = 308°C; bottom curve is DGEBA, T_g=165°C -Ochi (86).

The internal stress for all cured systems increased linearly with increasing shrinkage after vitrification. These results support the theory of increased

internal stresses with increased extent of cure for cure temperatures below T_g.

2.3 Residual Stress and the Single Fiber Pull-Out Test

Broutman, who addressed the residual stresses on the single fiber pull-out test (5), stated that in order to determine what effect the glass-polymer joint has on the failure properties of a composite, one must first determine what types of stresses are present at the glass-polymer interface. It was specifically noted by Broutman that during the preparation of the composite, residual stresses are induced due to the polymerization or crosslinking shrinkage of the polymer matrix when cured at elevated temperatures. It was reported that with increasing cure temperature, the bond strength reached a maximum and then decreased as the cure temperature was further increased (5). Here, the increase in bond strength was attributed to thermal shrinkage of the resin, however, the decrease via higher cure temperature was not commented upon. Based on the earlier discussion of residual stresses being a function of cure temperature and time, the decrease of bond strength in Broutman's work may have been a direct result of normal pressure resulting only from thermal contraction.

The determination of the residual stress or normal pressure when considering a reinforced material is a key factor in the characterization of materials. The following section covers methods for quantitatively evaluating the normal pressure on an embedded fiber.

2.3.1 Calculation of Residual Pressure Due to Cooling From Above T_g

A simple model was proposed by Harris to calculate the residual stress in glass-fiber/polyester-resin composites that arose when the material was cooled from the post-curing temperature (74). An elementary elasticity solution for shrink-fit stresses was employed. It was assumed that cure-contraction stresses were relieved during post-curing of the composite at T_{post} and that residual stresses develop as a result of cooling from the post-curing temperature ($\Delta T = T_{post} - T_{R.T.}$). N.B. Based on Section 2.2, for $T_{post} > T_g$, a more appropriate ΔT might be $T_g - T_{R.T.}$.

A rough estimate of the lateral interfacial pressure when a single, infinitely-rigid fiber was embedded in a resin was given approximately by $P \approx E_m \Delta T \Delta\alpha$ (74). Upon expansion, this lateral pressure, which developed when the resin contracted onto the fiber during cooling, was reported as:

$$p = \frac{\delta/c}{\dfrac{1}{E_m\left[(1-\nu_m)\left(c^2/b^2\right) + (1+\nu_m)\right] + \dfrac{(1-\nu_f)}{E_f}}} \qquad (74)\ [33]$$

"where δ is the difference between the radial displacements of the fiber and matrix surfaces at the interface radius, c, i.e. the amount by which the room temperature radius of the fiber exceeds the bore hole that would have been left in the resin had the fiber not been present." For details of the calculation, the reader is referred to the reference. From this equation, p as a function of the ratio c/b for a single fiber embedded in resin, is obtained. From this relationship, the limiting thickness of a resin block

that will grip the fiber with some maximum force was determined to be about twenty times the fiber diameter (74).

2.3.2 Calculation of Residual Stress Due to Curing and Cooling

Jang, Hwang and Lieu (77) separated some of the possible sources of the residual stresses with respect to the single-fiber matrix system. They addressed both the chemical shrinkage of the resin during crosslinking and the mismatch in thermal contraction between the fiber and resin with cool-down.

With respect to the single fiber pull-out test, this radial compression, or normal pressure, results in better contact at the interface and an increased hold on the fiber during a fiber pull-out test (77). Based on the thick cylinder model (TCM), Jang et al. reported the following equation for pressure at the interface of a cylindrical fiber in an infinite medium (77). This equation included the effects of curing or solidification shrinkage:

$$p = \frac{(\alpha_m - \alpha_f)\Delta T + \varepsilon_c}{(1+\nu_m)/E_m + (1-\nu_f)/E_f} \qquad (77)\ [34]$$

where α, ν, T and E denote the usual constants and ε_c is "the linear shrinkage in matrix due to cure". Except for ε_c, this is the same equation introduced by Gerard and Giebert in 1957 (70).

Both the first and second term in the numerator of the equation depend on the temperature of cure and the third term accounts for shrinkage resulting from chemical cure. By obtaining the interface pressure p as a function of T_{cure}, the results of the above arguments were determined to be valid in a qualitative manner. The experimental details are briefly presented below:

By evaluating the bond strength at the interface via the single fiber pull-out test, the magnitude of the residual thermal stress should indirectly be determined (77). Several model material systems each containing a single filament passed perpendicularly through a thin disc of resin were studied. Since the objective of the study was to determine the mechanical interaction between fiber and matrix, the chosen materials had minimal chemical bonding at the interface, if any. Complimenting this first set of experiments was a second series in which the fiber surface was coated with a thin layer of silicon oil prior to embedding. Thus, the interfacial adhesion resulted solely from the mechanical interaction between fiber and matrix.

In Jang et al.'s work, the composite system, a polypropylene fiber in an epoxy, was cured at several different temperatures to permit the formation of different residual stresses. The 'debonding' load was assigned to be the maximum load in the force-displacement curve which was taken as a measurement of the pressure exerted on the fiber by the matrix. The data obtained from the polypropylene-epoxy system appeared to be at least qualitatively consistent with equation [34]. This suggested that the pressure

exerted on the fiber by the matrix was roughly proportional to ΔT, the difference between the cure temperature and the end-use temperature. No calculation using this equation was reported for comparison to the fracture results.

Since the samples in Jang et al.'s study were cured at different temperatures, it was necessary to make sure that the only variable was thermal mismatch and to eliminate extraneous variables. To evaluate the degree of cure in the resin, no matter what the cure temperature, a DMTA was used to measure the viscoelastic properties of the resin after various cure times at selected temperatures. When the relative rigidity and damping characteristics of the test resins were similar, the degrees of cure were considered to be equivalent (77). The results of Jang et al.'s work is reproduced in Figure 13. Based on these experiments, the degree of cure or *extent of cure shrinkage*, ε_c, was assumed to be constant.

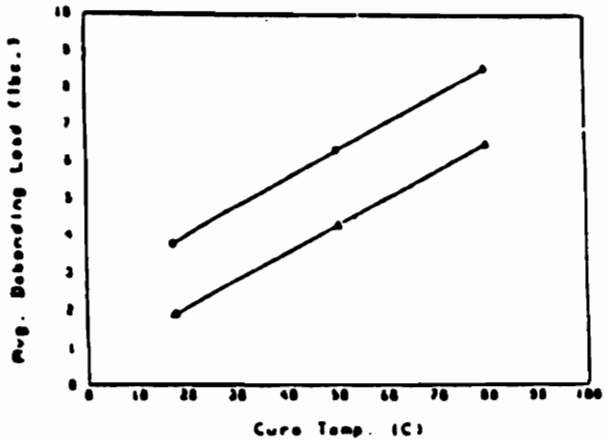

Figure 13. Debonding load versus cure temperature; top curve is a polypropylene/epoxy system; bottom curve PP/E with lubricant applied to the fiber surface -Jang et al. (77).

2.3.3 Calculation of the Residual Stress From Fracture Mechanics

In regards to the normal pressure on the fiber resulting in interfacial friction, the work by Gao, Mai and Cotterell also addressed what they termed the *threshold initial pressure*. This was defined as the normal pressure which the loaded fiber must overcome via Poisson's contraction in order to debond without the frictional interaction between fiber and matrix. This threshold pressure was determined by letting the frictionless load pressure, P_{init}, equal $\widetilde{P}$ in equation [30]. This resulted in the equation:

$$p_{th} = \left[\frac{2\alpha\nu_f}{\alpha(1-\nu_f) + 1 + \nu_m + 2\gamma}\right]\left[\frac{E_f(1+\beta)\,G}{r\,(1 - 2k\nu_f)}\right]^{1/2} \qquad (33)\ [35].$$

This means that when the normal pressure on the fiber which results from chemical cure shrinkage and thermal mismatch is below this threshold pressure, there will be no physical interaction between the fiber and the surrounding matrix during debonding. For a fiber which has some particular set of elastic constants, the length of fiber needed to overcome the threshold pressure of p_{th} can be calculated from:

$$l_T = r / (\mu(\alpha\nu_f + \gamma\nu_m)) \qquad [36].$$

In theory this is the same fiber length discussed by Bowling and Groves via their critical fiber length associated with the primary frictional zone.

The physical parameters of the polymer matrix of a single fiber composite are a function of its chemistry as well as its thermal history. Thus, the

characterization of a given system requires not only the knowledge of the elastic constants of the material but the cure procedure as well. Methods for the determination of the normal pressure exerted on an embedded fiber due to chemical cure of the polymer resin coupled with thermal contraction upon cooling have been presented although not directly applied to the single fiber pull-out test results. The application of a particular method should be dependent upon the thermal history of the specimen. If the material has been or can be considered annealed, the simple method of Harris can be employed with cooling considered from T_g to the use temperature. If, however, the material vitrifies during cure, the build-up of internal stresses due to chemical crosslinking should be considered, as attempted by Jang et al. For the evaluation of the material performance, a fracture approach can be implemented like that presented by Gao et al.

2.4 Interfacial Shear Stress Between Fiber and Resin

In the single fiber pull-out test, the interfacial shear stress can be determined at different experimental times to describe various events. Initially, at the onset of crack propagation, the interfacial bond shear stress is determined from P_{init} in the case of $P_{init} = P_{max}$ for catastrophic interfacial failure (11,26,33,34,41,57,61). For $P_{init} \neq P_{max}$, once crack propagation begins, the debonding interfacial shear stress is determined from the change in load required for crack propagation and for steady-state debonding (14). When debond is completed, a pull-out interfacial shear strength (27,51) can also be determined. Researchers have used the different interfacial shear stress values, as well as the coefficient of friction

(22,25,27,40,47), as a means of quantitatively evaluating and comparing single fiber pull-out data.

In discussing the various aspects of the interfacial shear stress, the mechanism of stress transfer from matrix to fiber is addressed first; various embedded lengths are considered. The calculation of interfacial shear stress with respect to the single fiber pull-out test is then presented.

2.4.1 Stress Transfer From Matrix to Fiber

For a composite under tension along a sufficiently long fiber axis, the tensile stress, σ, and shear stress, τ, at the interface can be depicted as in Figure 14c. This assumes good adhesion between the fiber and matrix such that the relative elongation for each phase is the same and the portion of stress transferred to the fiber is proportional to $E_f E_m$ (see for example 80 and 69). The mechanical equilibrium equation for an end segment, denoted x, can be expressed as:

$$\sigma_x \pi r^2 = \int_0^x \tau(x)\, 2\pi r\, dx + \sigma_m \pi r^2 \qquad \text{... [37]}$$

where $\sigma_x \pi r^2$ is the tensile load transmitted to the end segment by the rest of the fiber, $\int \tau(x) 2\pi r\, dx$ is the portion of the tensile load transmitted by the tangential stresses developed at the interface to the side of the fiber and $\sigma_m \pi r^2$ is the portion of the tensile stress transmitted by normal stresses from the matrix to the fiber endface. This last term becomes negligible at large x. The limit to the values of the applied stress is the tensile strength of the fiber or matrix. For a composite with a more brittle fiber then matrix,

at the ultimate stress for the fiber under tension, the fiber will break to a critical length, l_c. This is the basis for the single fiber fragmentation test.

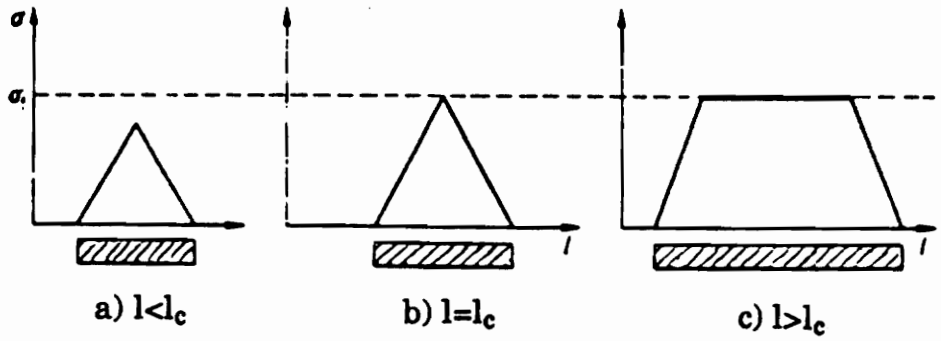

Figure 14. Tensile and shear stresses at the fiber/matrix interface for fiber length, l; a) $l<l_c$; b) $l=l_c$ and c) $l>l_c$.

As the load on a single fiber composite increases, fragmentation continues until all fiber lengths are l_c. There is actually a distribution of fragment lengths and the tensile stresses associated with these fragments are depicted in Figure 14a-c. As the length of fiber decreases from l_c, the amount of load transmitted to that fiber from the matrix also decreases. The implementation of this phenomenon for the characterization of the fiber matrix interface has been used extensively by researchers. It is a methodology which compliments the single fiber pull-out, as well as the microindentation test. However, it will not be until the failure mechanisms and material parameters of these model tests are fully characterized that the quantities associated with the fiber pull-out, critical fiber length and micro-indentation tests will be interchangeable.

The term critical fiber length has been used to describe many phenomenon. It has been applied to the weighted average fiber length resulting from fiber fragmentation tests (18,23,24,51,65), to the primary frictional zone associated with debonding and pull-out (14,59), and to the bimodal relationship between embedded length and load to debond (28,69). The common denominator of this descriptor in these applications are the tensile properties of the fiber relative to the matrix and the normal forces exerted by the embedding resin onto the fiber. The following is a brief discussion of the critical fiber length value.

The primary frictional zone which results during debonding and subsequent pull-out is an event related to the Poisson's contraction of the fiber under a given load. The removal of the fiber from the surrounding matrix is realized because the load required for contraction is less then the load required for steady state debonding which is less then the ultimate strength of the fiber. The relationship between fiber length below l_c and the associated stress and the relationship between fiber embedded length and load required to debond is the same. This is the result of the load carrying ability of fibers less then l_c. The heavily documented embedded length versus load required to debond is reproduced in Figure 15a. The initially rising portion of the curve reflects catastrophic interfacial failure of embedded fiber length less then the critical value. Piggott and others initially interpreted the bimodal relationship based on catastrophic interfacial failure. This lead to the forced plateau in the second region of the trace as an attained maximum failure value associated with the

maximum stress at lengths greater than lc, as depicted in the previous figure. This interpretation has since been revised to account for friction, as depicted in Figure 15b. Based on many of the previous arguments the relationship between load to debond and embedded fiber length may be depicted and interpreted as follows, see Figure 16. As the embedded length, l, increases, the required load to debond also increases, i.e. the maximum stress transferred from matrix to fiber increases. Prior to reaching the critical fiber length associated with failure, the Poisson's contraction of the fiber causes interfacial failure, but because of the longer embedded length, the failure is no longer catastrophic; crack propagation occurs. Due to frictional effects, the relationship between embedded length and load required to debond post catastrophic interfacial failure, is also an increase - not a plateau. If the elastic constants and strength of the fiber accommodate steady-state debonding loads less then the ultimate strength of the fiber, a constant debonding load will be realized at embedded lengths greater then the length effected by the primary frictional zone.

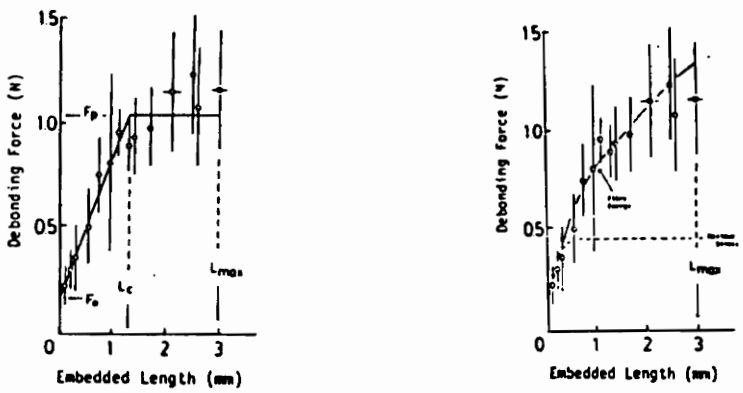

Figure 15. Load to debond versus embedded length a) as initially suggested by Piggott (28); b) revised (69).

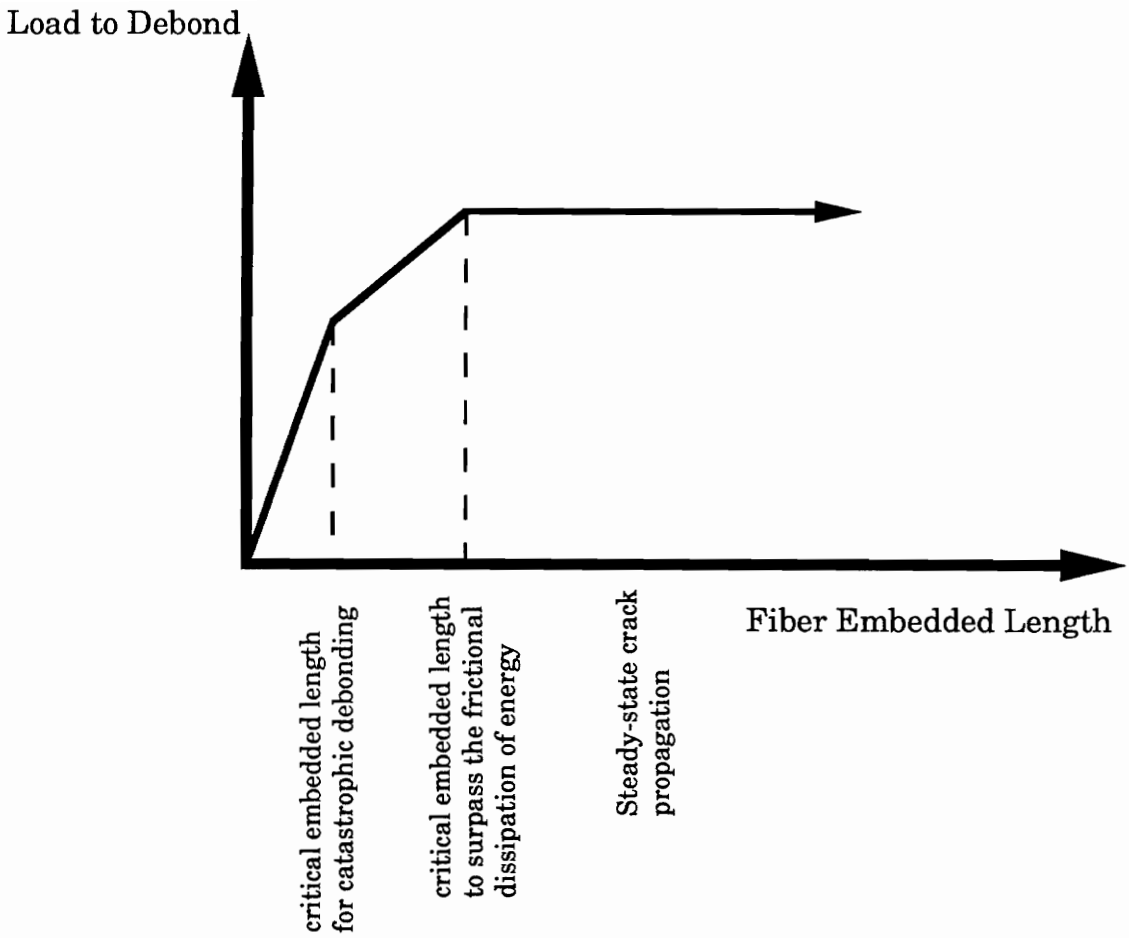

Figure 16. Hypothetical embedded length versus load required to debond.

From the classical shear lag analysis proposed by Cox, a model addressing the interfacial shear stresses of the single fiber pull-out test, was presented by Greszczuk (6). Greszczuk related the force required to initiate debonding, F, to the mean value of the debonding stress, τ, by

$$\tau = F/2\pi rl \qquad [38]$$

with the tensile stress, σ, as

$$\sigma = F/\pi r^2 \qquad (6)\,[39].$$

The plot of σ versus embedded length provides the maximum debonding shear stress from the slope (6). This approach is taken because the true shear strength of the interface would require determination at fiber length $x \rightarrow 0$.

In determining the shear stress values for the current work, the average values are considered. The following represent the approaches taken.

2.4.2 Interfacial Bond Shear Stress

The determination of the interfacial bond shear stress recently detailed and applied by Pitkethly and Doble (55) evolved from Cox's shear lag analysis. Here, the fiber diameter, embedded length and load required for crack initiation were used to determine the maximum value of the interfacial bond shear stress, τ_{bond}, equation [40]. These authors argued that because load transfer from matrix to fiber occurred primarily over the ineffective length of the fiber, the shear strength calculated from a fiber system whose embedded length was greater than this value would be underestimated. This was because a length of fiber was included over which little stress transfer occurred. Pitkethly and Doble also stated that the maximum shear stress should be calculated as the embedded length became exceedingly small. Here,

$$\tau_{bond} = P_{init} / (\pi d l) \qquad [40].$$

Pitkethly and Doble's approach was to calculate the average interfacial shear strength from the above-mentioned parameters and then τ_{ave} was

put into a series of equations used to determine τ_{max}. Here, the typical problem of scatter plagued their results. However, τ_{max} values were calculated and fairly good agreement between experiment and theory was reported.

A study conducted by Biro, McLean and Deslandes, where τ_{bond} was determined as a function of cure temperature (56), is of interest. Measurements were made by the microbond test method for carbon fiber / DGEBA epoxy. The results of their work are reproduced below in Table 3. They found that the interfacial shear stress as determined using P_{max} via equation [40] above, was a function of cure. It was found that an increase in T_g and τ_{bond} paralleled an increase in tensile strength of the matrix. Here the interfacial shear strength increased substantially as compared to the tensile strength of the resin.

Table 3. **Effect of cure on the interfacial shear stress between resins systems -Biro et al. (56).**

Formulation	Cure Schedule	τ_{avg} Average of Tests (MPa)	τ_{avg} From Slope of Regression (MPa)	N*
Host System	B-stage	18.5 ± 3.7	19.5 ± 0.5	38
	Cure I	44.2 ± 11.8	43.3 ± 2.7	23
	Cure II	—	—	—
	Cure III	—	—	—
	Cure IV	50.2 ± 6.7	50.6 ± 1.2	33
System A	B-stage	21.2 ± 4.5	20.7 ± 1.2	16
	Cure I	40.6 ± 7.8	43.3 ± 2.0	12
	Cure II	30.0 ± 9.0	26.4 ± 1.7	19
	Cure III	58.4 ± 12.8	61.4 ± 2.5	27
	Cure IV	66.6 ± 10.8	67.5 ± 1.[illegible]	53

Note: Variation is expressed as standard deviations.
*Number of specimens.

2.4.3 Interfacial Debond Shear Stress

In regards to the single fiber pull-put test, once crack propagation begins there is a debonding interfacial shear stress which results in a frictional dissipation of energy. This is how the initial rise in the debonding portion of the pull-out trace was explained. If the simplifying assumption is made that this is the only cause of the increasing load with displacement, the interfacial shear stress of this region, τ_{debond}, can be determined. However, it is not the load versus displacement relationship but the load versus crack-length relationship which must be implemented. As noted later via the birefringence data, load versus crack-length has a linear relationship - at least over the initial primary frictional zone of debonding. Therefore, from the slope, dP/da, τ_{debond} can be calculated from:

$$\tau_{debond} = (dP/da)\,(1/\pi d) \qquad [41].$$

2.4.4 Interfacial Sliding Shear Stress

With the completion of fiber debonding, frictional sliding takes place. The interfacial shear stress of sliding can be calculated from the tail of the load versus extension trace (27,51). Here,

$$\tau_{pull\text{-}out} = (dP/d\delta)\,(1/\pi d) \qquad [42].$$

Literature values for the interfacial shear stress as determined for the different events of the single fiber pull-out test are compiled in Table 4. The materials and specific stresses determined are noted.

Table 4. Experimentally determined values for the interfacial shear stress as reported in the literature.

	<tau>bond, MPa	<tau>pull-out, MPa	comments	reference
glass/polybutylene terepthalate	31.1			34
Kevlar 29/DEGBA epoxy†	40			41
Kevlar 49/DGEBA epoxy†	41.4			41
Celion/DGEBA epoxy†	65.3			41
stainless steel/epoxy*	20			33
glass/DGEBA epoxy†	33.1			26
Kevlar/DGEBA epoxy†	39.3 ± 7.8			26
Kevlar/DEGBA epoxy ††	21.6 ± 0.51			57
copper/epoxy**	1.4		with release agent	57
copper/epoxy**	0.13			57
carbon/DEGBA epoxy†	27			61
steel/epoxy*		21.8		27
nickle/epoxy*	3.6 E6 ^			14
glass/epoxy**		21 ± 5	no heat	51
glass/epoxy**		34 ± 10	24 hr at 60°C	51
glass/polyester***		7 ± 7	no heat	51
glass/polyester***		10 ± 5	6 hr at 80°C	51
carbon/DGEBA epoxy†	21.2 ± 4.5		Tcure = R.T.	56
carbon/DGEBA epoxy†	40.6 ± 7.8		Tcure = 60°C	56
carbon/DGEBA epoxy†	30.0 ± 9.0		Tcure = 120°C	56
carbon/DGEBA epoxy†	58.4 ± 12.8		Tcure = 165°C	56
carbon/DGEBA epoxy†	66.6 ± 10		Tcure = 180°C	56
stainless steel/epoxy****	1.13 Kg/mm2			11
AU carbon/DEGBA epoxy †	24.1 ◊			18
AS carbon/DEGBA epoxy †	74 ◊			18
As (300) carbon/DEGBA epoxy †	71.7 ◊			18
AS (600) carbon/DEGBA epoxy †	68 ◊			18
AS (750) carbon/DEGBA epoxy †	65.58 ◊			18

†Shell Epon 828
†† Ciba Geigy 6010 and Aldrich triethylene tetramine
*not specified
**Ciba-Geigy Araldite 502 with Hardener 956
***Shell Epon 815 with Ancamine X†
****DGBA+BAS-A, MY750
^ debond plateau
◊ ias measured by critical length tensile test

To date, the quantitative evaluation of the single fiber pull-out test has been primarily reported as the maximum load required to debond the fiber from the resin. Because variables of the experiment are not addressed, this type of reporting does not accommodate meaningful data comparisons between laboratories. In order to build a data base of information regarding the removal of fibers from neat resin, data reduction methods such as those presented here should be implemented. To this end, the previously discussed models and methods of data manipulation are applied in the current work, their appropriateness and limitations are discussed.

Chapter 3

Experimental

In this chapter, the materials used for the various experimental sets are first described. This is followed by the method of sample preparation and loading procedure. For the optimization of the single fiber pull-out test, a new sample configuration was developed (59). Here, the fibers were embedded lengthwise in a neat resin dogbone as shown in Figure 17. The sample was notched across its width, prior to elongation, to allow for the load measurement to be of the fiber/matrix interface. This notched sample was mounted onto a tensile load frame. This load frame was in turn mounted onto a microscope stage outfitted with cross polarizers and a camera system which enabled the viewing of samples, their birefringence patterns and interfacial crack lengths in real time.

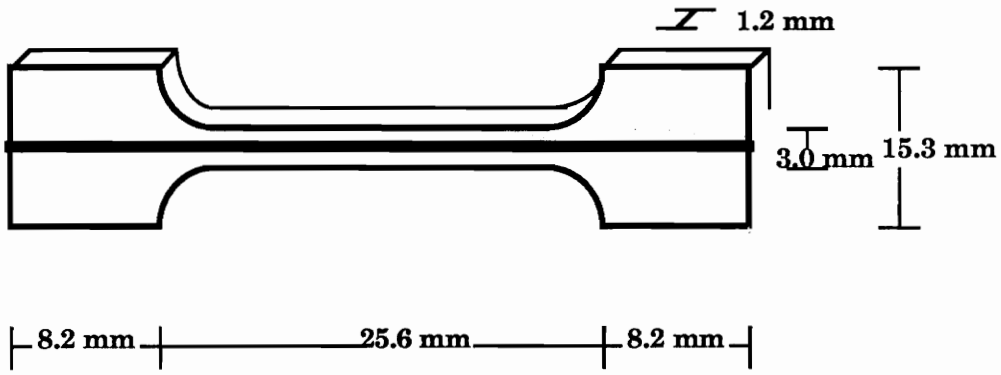

Figure 17. Sample configuration for the embedded optical fiber in a neat resin dogbone.

The experiments for the characterization of the fiber/coating/resin systems were conducted as described in the following test. The final series of experiments, however, consisted of minimizing experimental variables such that only the temperature of cure varied between sample sets. Fibers were from the same manufacturing run, the epoxy resin from the same production lot and handling and preparation of samples were maintained as consistent as possible; all pull-out and DMTA experiments were done within 24 hours after samples were prepared, all TMA was complete within 4 days of sample manufacture and the FTIR spectra were collected in as timely a manner as possible. For these sample sets the imaging microscope was modified to capture the entire sample throughout the run. This facilitated recording the true debond length for those specimens which experienced crack propagation in both directions off the notch. Also, the Minimat load-frame data was collected over shorter displacement lengths then in previous experiments to facilitate a higher data collection

frequency. This was to address the debonding zone such that the frictional contribution to debonding could be detected.

3.1 Optical Fibers

All fibers were commercially-available, glass on glass optical fibers. All fibers, except those which were treated with the coupling agent, were acetone-cleaned prior to embedding. For the determination of fiber coating choice (Section 4.2), the acrylate-coated fibers were from SpecTran Corporation [50/125/500μ (core/clad/coating diameter)] and the polyimide coated fibers were from Polymicro Technologies, Inc. [part # FLP105125150 (105/125/150μ)]. For the constant resin experiments (Section 4.3), the various polyimide-coated fibers were received from Polymicro Technologies, Inc., AT&T, SpecTran Corporation, Fiberguide Industries, Inc., General FiberOptics, and CeramOptec, Inc. [UV (100/110/125)]. For the evaluation of resin chemistry and the related cure cycle on the single fiber pull-out test (Section 4.4), Polymicro polyimide fibers were employed. Finally, a series of experiments were performed to determine the role of cure temperature and resulting normal stress by varying the extent of cure of an uncatalyzed TGDDM/DDS epoxy resin. Here, Polymicro polyimide-coated fibers (part number FLP105125150, lot number AA708) were used. Unless otherwise specified, all test scenarios were repeated in sets of six or more.

3.1.1 Coupling Agent Coating

The coupling agent, Dow Corning Z6040, a glycidoxypropyltrimethoxy silane, was applied to SpecTran fibers which had been coated initially with

acrylate. The acrylate was removed by swelling with acetone and then stripped mechanically. The fibers were then acetone wiped, heated to 60°C for twenty minutes, cooled to room temperature and dipped into the coupling agent. They were then dried at room temperature in a fume hood for 24 hours.

3.2 Resin Systems

Different resins were used for the various experiments. For all samples cured at elevated temperatures, the resin was melted and degassed (125°C, 100 torr, 1 hr) prior to pouring into the preheated molds. To evaluate the initial performance of coated optical fibers when embedded in neat resin and subjected to the fiber pull-out experiment (Section 4.2), two resins were employed: Micromeasurement Group PLM-9, a butylglycidyl ether of bisphenol-A (BGEBA) with epichlorohydrin and Hercules 3501-6, a BF_3MEA catalyzed TGDDM/DDS epoxy. Their cure procedures are: the Micromeasurements Groups PLM-9 epoxy components were mixed, then cured for 48 hours in a 25°C oven, and the catalyzed TGDDM/DDS epoxy was heated at a rate of 4°C/min to 177°C, held at 177°C for 2.5 hours then cooled via bench-top equilibration to room temperature. For the evaluation of fibers with different polyimide coatings in one resin (Section 4.3), Fiberite 976 an uncatalyzed TGDDM/DDS epoxy was the resin of choice. The uncatalyzed TGDDM/DDS epoxy was heated 1°C/min to 150°C, held for 3 hours, cooled at 3.3°C/min to 65°C then cooled 5°C/min to room temperature. In continuing the evaluation of the effects of embedding one manufacturers fiber in different resin systems (Section 4.4), the resins were

BGEBA, uncatalyzed TGDDM/DDS, catalyzed TGDDM/DDS and an in-house toughened bismaleimide: 57% by weight of Matrimide 5292A (4,4'-bismaleimidodiphenyl methane) and 43% by weight of Matrimide 5292B (0,0'diallyl bisphenol A), toughened with 10 % by weight of Amine terminated poly(arylene ether sulfone) (Mn = 15760) (92). The toughened BMI / Diallyl / Bisphenol A was heated 20°C/min to 200°C, held for 1 hour, heated at 20°C/min to 250°C, held for 2 hours and then cooled 1°C/min to room temperature. For the final set of experiments which evaluated the fiber/matrix interaction as a function of cure, uncatalyzed TGDDM/DDS was employed.

For this final cure series, samples of Polymicro polyimide fibers in uncatalyzed TGDDM/DDS were prepared as stated above but brought through the following cure cycles: (i) held at 130°C for one hour, cooled 3.3°/min to 65° then 5°/min to 35°, (ii) heated from 130° to 150°, 1°/min, held three hours and cooled as in (i), (iii) 130°, 3 °/min to 150°, held one hour, 1°/min to 177°, held two hours and cooled as in (i), (iv) 130°, 3 °/min to 150°, held one hour, 1°/min to 210°, held one hour, 1°/min to 230°, held two hours and cooled as in (i), (v) 130°, 3 °/min to 150°, held one hour, 1°/min to 230°, held one hour, 1°/min to 250°, held two hours, cooled as in (i).

3.3 Sample Preparation

Samples were prepared by placing a single acetone-cleaned, optical fiber in the center of a dog-bone-shaped mold, and preheating to 125°C. This mold was then overfilled with resin and covered with a Teflon sheet followed by

preheated weights; the BGEBA resin samples did not require *preheated* mold/weights and were left to cure in a 25°C oven at this point. All samples were cured per the schedules detailed above. Cured samples were notched with a cold razor blade approximately 12 mm from one end of the dogbone. Initial notching was to insure crack propagation *across* the dogbone at minimal or no load, i.e. the fiber alone bridged the two pieces of the specimen. Fiber pull-out tests were performed on a Polymer Laboratories Miniature Materials Tester (Minimat) Tensile Stage. This stage was mounted on an Olympus SZH microscope to permit visual examination of the samples during the test. To perform the test, the samples were clamped onto the tensile stage and the clamps displaced thus supplying sufficient load to extract the optical fiber from the surrounding matrix. The stresses which developed during debonding and pull-out, birefringence bands via cross-polarized light, were examined by optical microscopy. Data was collected in a load-versus-extension format. Since fiber diameters varied between manufacturers, the statistical evaluation of load was normalized to stress. Extension was not converted to strain because the length of fiber over which the load was dissipated changed as a function of clamp displacement.

3.4 Thermal Mechanical Experiments

Thermal mechanical analysis for the characterization of the embedding resin. To this end thermogravimetric analysis, differential scanning calorimetry and thermomechanical analysis was conducted.

3.4.1 Thermogravimetric Analysis

To determine the mass loss of the resin as a function of temperature, thermogravimetric analysis (TGA) was implemented. Here, a Perkin Elmer 7 Series Thermal Analysis System was employed. The temperature was ramped from 25 to 750 °C at a rate of 10°C/min.

3.4.2 Differential Scanning Calorimetry

To quantify heat flow as a function of temperature of residual heat of reaction and determination of the glass transition temperature, a DuPont 2100 differential scanning calorimeter (DSC) was used. Experiments were run from 30 to 300 °C at a rate of 3°C/min.

3.4.3 Thermal Mechanical Analysis

To evaluate the relative change in volume in the resin due to chemical cure and thermal contraction, thermomechanical analysis (TMA) experiments were conducted on a Perkin Elmer System 7. Here, a specimen was placed in the TMA in expansion mode using a 1 mm diameter flat probe. The load on the sample was 1 mN. The initial sample height was measured at 26°C (as were all height measurements). The assembly was then brought through the cure cycle of interest.

3.4.4 Dynamic Mechanical Thermal Analysis

To determine the T_g of the variable cure of uncatalyzed TGDDM/DDS epoxy resin, DMTA experiments were done on a Polymer Laboratories instrument. Here, the neck region of the above mentioned dogbone

specimens were used via dual cantilever. Strain was set at x4, the temperature was ramped from 75 to 300 °C at 3 °C/min. Data was collected at 1 and 10 Hz.

3.5 Fourier Transform Infrared Spectroscopy

Extent of chemical cure states were determined via a diffuse reflectance infrared spectroscopy (DRIFT) method. The spectrometer employed was a Nicolet System 800 operated in the mid infrared (4000 - 650 cm^{-1}) region. DRIFT spectra were obtained using a SpectraTech Inc. Collector™ diffuse reflectance accessory in conjunction with a SiC source, KBr beamsplitter and a mercury cadmium telluride (MCT-A) detector. Samples were prepared with the use of a SpectraTech SiCarb sampling kit which involved abrading specimens upon 320 grit silicon carbide sand paper. Spectra were obtained from the surfaces of the sand paper discs. All spectra were obtained with 256 scans coadded with a 4 wavenumber resolution and Fourier processed with Happ-Genzel apodization. Extent of cure for each specimen was determined via integration of the peak area of the epoxide ring vibration band at 823 cm^{-1} and ratioed to the integrated peak area for an internal reference band. Comparisons were made to the 130°C degassed resin sample.

Chapter 4

The Effect of Fiber Coating and Embedding Resin on the Single Fiber Pull-Out Test

In conducting the single fiber pull-out test on polymer-coated optical fibers embedded in a dogbone of neat resin, many of the features described in the literature have been observed. Complementing these supporting observations were further details accommodating a more enhanced interpretation of the load versus displacement plot.

In this chapter, the single fiber pull-out test as applied and interpreted in this study is discussed first. Following this are the results of various experiments which differ in material choice and therefore physical properties. The chosen series of experiments were conducted to evaluate the single fiber pull-out test method more thoroughly and to relate the polymer chemistry of the embedding matrix to the mechanics of the system. Initial experiments were conducted to determine the physical response of the embedded optical fiber to the pull-out experiment. This was done with fibers supporting various coatings, i.e. acrylate, coupling agent and

polyimide. Next, polyimide-coated fibers from six different manufacturers were embedded in one resin, an epoxy, to determine the various loads and loci of failure to be expected from the given fiber/polyimide/epoxy system. The effect of the resin choice on the single fiber pull-out test was then evaluated. To accomplish this, polyimide coated optical fibers from one manufacturer were embedded in resins of different chemistries and thermal cure cycles.

4.1 The Interpretation of the Single Fiber Pull-Out Test

A generic specimen and failure progression for the following experimental results is depicted schematically in Figure 18. Typical experimental observations are described as follows. Upon notching and clamping the dogbone specimen, it was loaded at a constant rate of displacement. (A small interfacial crack is assumed to initially exist as a result of the notching process via the high stress concentration where the fiber emerged from the resin endface). As the load increased, isochromatic bands, radiating out from the notch and along the fiber, grew and intensified. This continued through the linear elastic region of the material. At a critical load, which was fiber/coating/resin specific, an interfacial crack between the fiber and resin would begin to propagate. This crack, which initially existed as a result of the notching, would propagate along the fiber with clamp displacement. Depending on the fiber/coating/resin system, this crack either flashed quickly to the fiber end or migrated slowly with periodic halts. Visually, a small degree of pulsing or micro-movement would sometimes occur prior to the more dramatic migrations of the crack

front. This may have been the result of the circumferential progression of the crack around the fiber. Also, a constant stress redistribution was seen as changes in the birefringence pattern. Once the interfacial crack had completely debonded the fiber from the resin, the fiber began pull-out and stick-slip activity was generally observed. This activity would continue until the fiber end exited the resin or the fiber fractured. Upon inspection, failure was found to take place at either the glass/coating or coating/resin interface, or in the case of good interfacial adhesion, there was matrix microcracking and fiber failure. If a sample set displayed combinations of these failure loci, it was considered *mixed.*

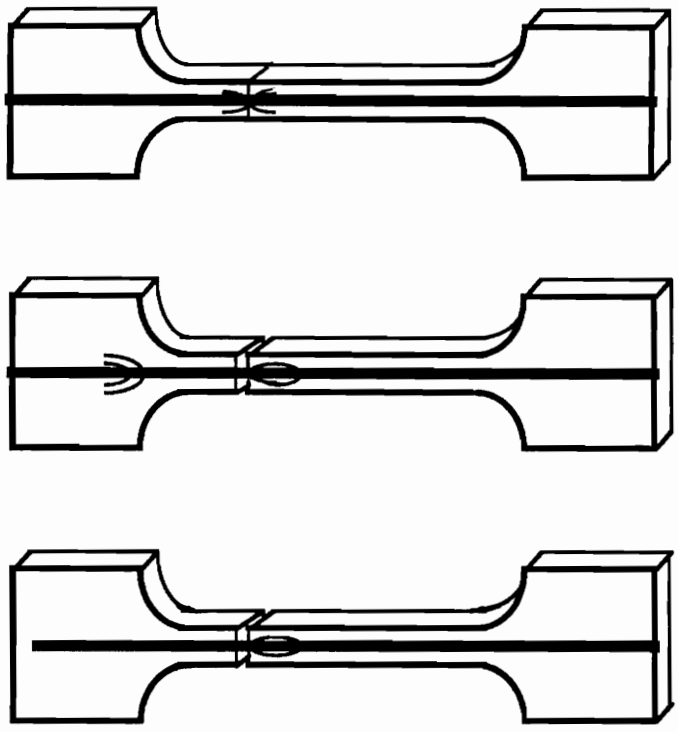

Figure 18. Fiber debonding and pull-out sequence schematically showing the photoelastic birefringence patterns in time.

The stick-slip phenomenon is the result of interfacial frictional sliding. The relationship of this phenomenon to the embedded length of the fiber effected may be of significant importance when considering the toughness of a given composite. This is because the energy absorbed by friction during the fiber pull-out process contributes a substantial portion of the resistance to fracture (40). Here, the sticking phenomenon represents the mechanical hold on the fiber which must be overcome for sliding to proceed. The slip displacement represents the recovery of the fiber to an equilibrium status for a particular load i.e., reversible Poisson effect. It has been found here and by other researchers (40) that the stick slope nearly replicates the slope related to the elastic loading of the system. This means that the mechanical clamping associated with the embedding process provides for the absorption of energy before and after the integrity of the interface is compromised. This is important in the consideration of the systems compliance regarding the toughness of the composite.

Upon embedding the optical fiber, notching and loading the sample, a load versus extension trace was generated. A model load versus extension curve is shown in Figure 19. Here, the linear elastic region began with initial loading and ended at a point depicted as (δ_{init}, P_{init}). Point (δ_{init}, P_{init}) indicates the initiation of propagation of the interfacial crack. The location of this crack initiation on the rising portion of the trace was first reported by Kelly (8) and most recently by Jiang and Penn (67). However, the use of this value for reporting debonding loads or numerical representations has not been forthcoming. From point (δ_{init}, P_{init}) to point

($\delta_{friction}$, $P_{friction}$) and then to ($\delta_{complete}$, $P_{complete}$), the interfacial crack traveled along the fiber length until the fiber was debonded through to one end of the specimen. During the debonding process from P_{init} to $P_{friction}$, there is a significant effect of interfacial friction on the dissipation of energy. However, for fiber lengths which exceed ($\delta_{friction}$, $P_{friction}$) lengths, there was a constant frictional force due to Poisson's contraction of the fiber. This contraction resulted in removal of a portion of the fiber surface from the matrix cylinder thereby removing the frictional interaction for fiber lengths greater then some critical length. Bowling and Groves discussed this phenomenon for a ductile wire embedded in an epoxy matrix (14). They described a frictional plug located at the end of the fiber. Here, the plug was formed over the initial portion of the fiber/matrix debonded area. When a crack front reached the end of the plug (which was primarily dependent upon the elastic properties of the fiber and the cure cycle of the matrix as well as the thermal mismatch between fiber and matrix), the entire plug moved down the fiber, behind the crack front. Behind this plug, then, was a zone of no friction. For a non-ductile fiber, however, it is most probable that the radius of the fiber is a function of location. Therefore, the forces associated with interfacial friction are also a function of location along the fiber length with a maximum value behind the crack front and decreasing to where the fiber emerges from the resin. It is suggested in the current work that there was a critical contact length over which the majority of the friction occurred and this separated the fiber into a primary frictional zone (δ_{init}, P_{init}) $\rightarrow$ ($\delta_{friction}$, $P_{friction}$) and a secondary frictional zone, ($\delta_{friction}$, $P_{friction}$) $\rightarrow$ ($\delta_{complete}$, $P_{complete}$). The

terms primary and secondary are used for convenience to describe the extent of frictional interaction between fiber and matrix. This interaction was a function of fiber location and would best be characterized by nonlinear function describing the decreasing fiber diameter from behind the crack front toward the end of the primary zone, through a transition region and into the secondary zone. This function is not determined here, thus the primary and secondary frictional zone descriptors. It should be noted that point ($\delta_{complete}$, $P_{complete}$) may or may not represent the maximum load the fiber carried during crack propagation but physically, it did correspond to the point of crack completion.

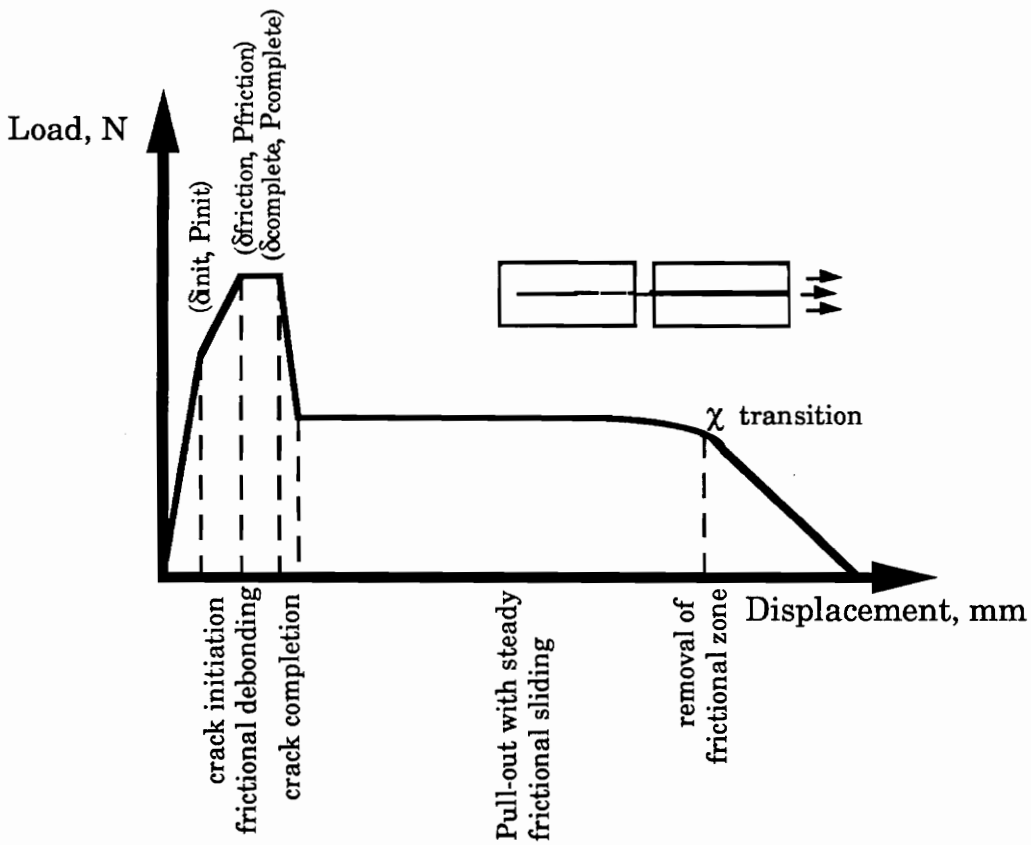

Figure 19. Model load versus extension trace.

Once the interfacial crack completely debonded the fiber from the resin, the fiber was pulled out and, depending on the system, stick-slip behavior observed. Also, depending on the length of fiber which was debonded from the resin and the degree of interfacial friction over that length, there may have been a drop in load following completion, Figure 20a, or alternatively, a steady decrease in load until fiber removal as in Figure 20b. For the situation where there was minimal or no drop in load, this was thought to correspond to the entire length of debonded fiber significantly contributing to the interfacial friction i.e., the end of the plug was not reached. In most systems, however, there was a drop in load post $P_{completion}$ and a relatively small load-extension slope was observed until some critical point. At this critical point, χ, the beginning of a more substantial linear decrease in load with resident fiber length began.

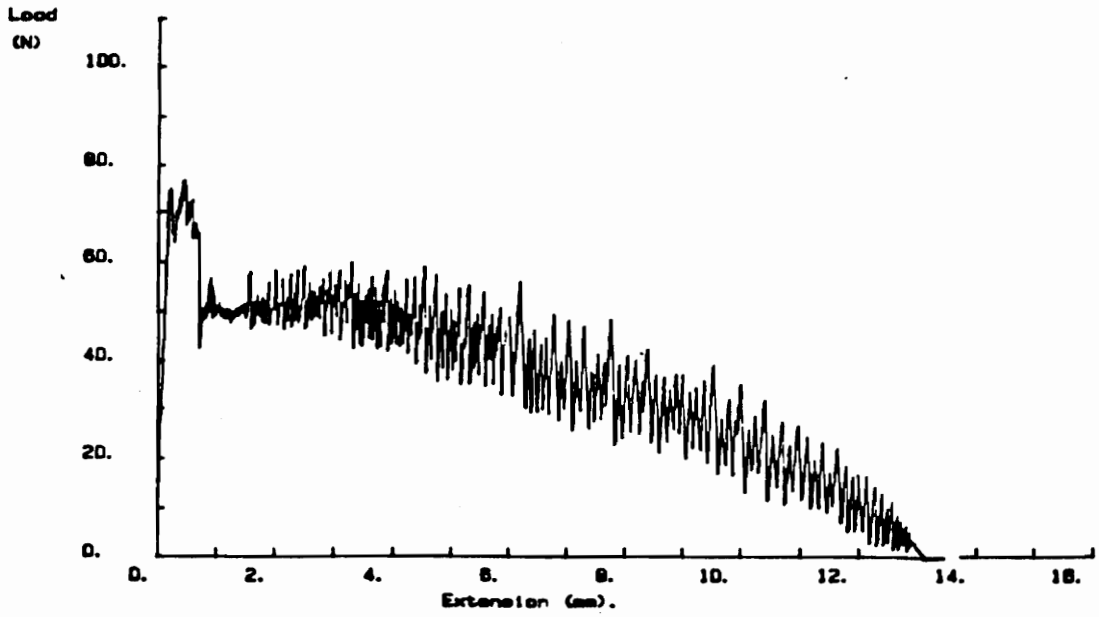

a)

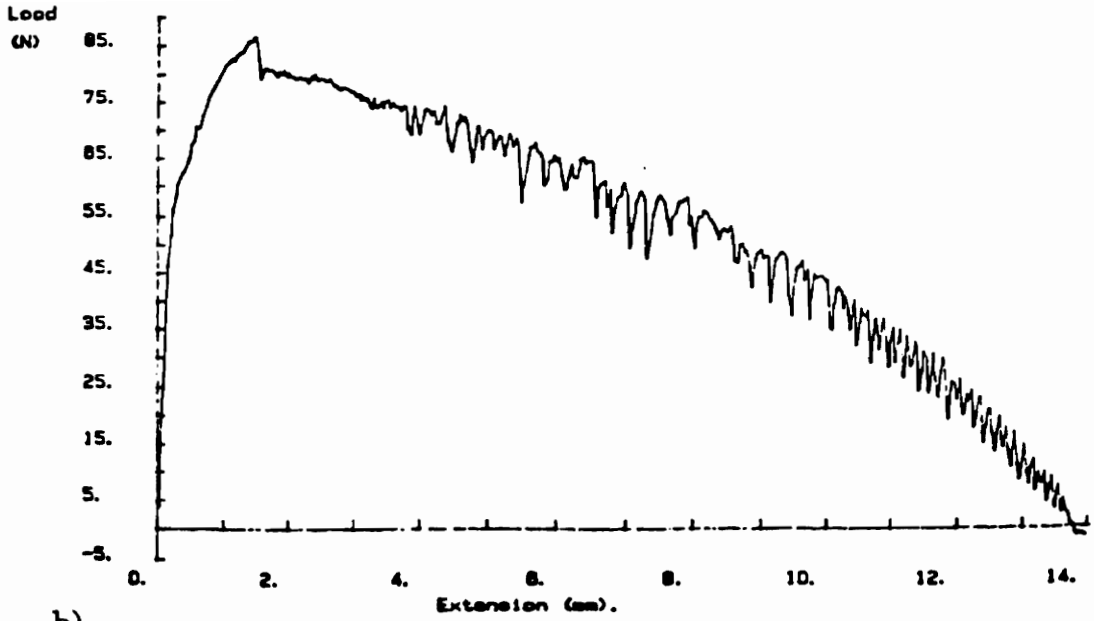

b)

Figure 20. Experimental load versus extension traces showing a) all described debonding and pull-out regions and stick-slip activity; b) no plateau regions.

The interpretation of the load versus extension trace has varied from researcher to researcher. Due to some of the small sample sizes and the difficulty in viewing the failure process, substantial stipulations on the failure events have been made. For experiments where the sample size was large enough to view the debonding process, the various regions of the pull-out trace were defined. In this regard, it was recognized early on by Kelly (8) that the initiation of the fiber/matrix interfacial crack occurred at some point prior to the maximum load the system was to carry. This was noted both visually via a change in reflectivity and experimentally via the load frame response. Although later research efforts from different groups also noted that initiation occurred at some time prior to the maximum

point, utilization of this value for the quantitative interpretation of the test has not been made.

It is reported here that upon debond initiation, the interfacial crack initially propagated with a significant amount of friction. As this applied load increased, the effects of friction began to diminish due to Poisson's contraction of the fiber. At some fiber length, which was fiber, resin and thermal history dependent, the debonding became a steady-state event and the load required for crack propagation a constant. Based on this interpretation, the use of values from the load versus extension trace can be quantitatively evaluated via debonding and pull-out. As will be shown, stresses associated with the initiation of crack propagation, debond continuation and completion as well as frictional sliding and removal, can be quantitatively interpreted from the combined use of fracture mechanics and shear lag theories.

Previous interpretations of the single fiber pull-out test have primarily evolved around the use of the maximum point in the load versus extension trace. If this maximum was the result of catastrophic interfacial failure, the embedded length of the fiber was less than or equal to the length that would otherwise be the crack initiation length. Use of this data point for comparisons between sample sets requires specific consideration of the embedded length. Extensive work has been presented in this area by researchers implementing the microdebond test. However, if the maximum in the load versus extension trace was not the result of

catastrophic interfacial failure, the same data handling cannot be implemented. The frictional effect of the debonded region of the fiber must be considered.

It has been found that the linear elastic region of the fiber/matrix system and the debonding of the primary frictional zone are not readily resolved in the load versus extension trace, i.e., to realize the difference in the slopes requires sufficient data collection and/or significant expansion of the displacement axis. Regarding much of the experimental results reported to date, this similarity may be one of the reasons for the extent of experimental scatter associated with the single fiber pull-out test data. While the visual observation of crack initiation was certainly accommodated in many of the large samples described in the literature, small sample sizes are a problem. Penn and Lee (46) reported visually observing, [with loading] "a circumferential crack appears at the interface where the fiber enters the matrix. Loading is continued with no apparent visible event, and then suddenly an upward displacement of the fiber with respect to the matrix occurs.". The initial crack was not recorded on the load versus extension trace. This was not unique to Penn and Lee, many researchers have reported the same results of a maximum in the trace with a precipitous drop. Unless the time scale of the experiment is increased via longer embedded lengths or the data collection rate is increased, the crack initiation event may be missed as perhaps it has in the past.

In the recent article by Jiang and Penn (67), the observation of crack initiation and propagation was directed toward small scale samples. Here, crack initiation loads were resolved by the load frame and the debonding frictional zone recorded. Apparently the embedded lengths of their high strength fibers were still less than the critical length required for steady-state crack propagation. Unfortunately, their model does not account for these longer embedded lengths.

Information regarding the extent of load transfer from fiber to resin is not only obtained from the debonding of the fiber and matrix, but from the removal of the fiber from the matrix as well. With removal of the debonded fiber from the resin matrix, the resulting change in load with fiber removal gives direct information on the sliding interfacial shear stress of the system as well as the effect of Poisson's contraction. This interfacial shear stress reflects the normal pressure exerted on the fiber, and the length over which this pressure acts. This length can be used as a guide for the determination of the load carrying ability of the fiber in the debonding process. As suggested in Chapter 5, the interfacial shear stress and corresponding fiber length is sensitive to the fiber, resin and thermal history of the system.

4.2 The Effect of Fiber Coating on the Single Fiber Pull-Out Test

This first set of experiments was designed to evaluate the performance of the different optical fiber coatings when the fiber was subjected to the single fiber pull-out test. Of interest were SpecTran's acrylate-coated, Dow

Corning's coupling-agent-treated and Polymicro polyimide-coated optical fibers. The resins of interest were BGEBA (25°C for 48 hours) and the catalyzed TGDDM/DDS (177°C for three hours). The results of the experiments where fibers were coated with coupling agent, acrylate and polyimide were very different from each other in a given resin and between resins via birefringence patterns, loads of initiation, acoustic activity during debonding, and loads associated with pull-out.

4.2.1 Bisphenol-A Based Epoxy Resin

The BGEBA resin was chosen since there would be minimal thermally induced stress seen by the embedded fiber. Three repetitions per fiber set were performed. The initiation stresses were 18.06 (single value), 696.0 ± 336, and 901.5 ± 101 MPa for the SpecTran acrylate, Polymicro polyimide and Dow Corning's coupling-agent-coated fibers, respectively. These results are compared in Figure 21.

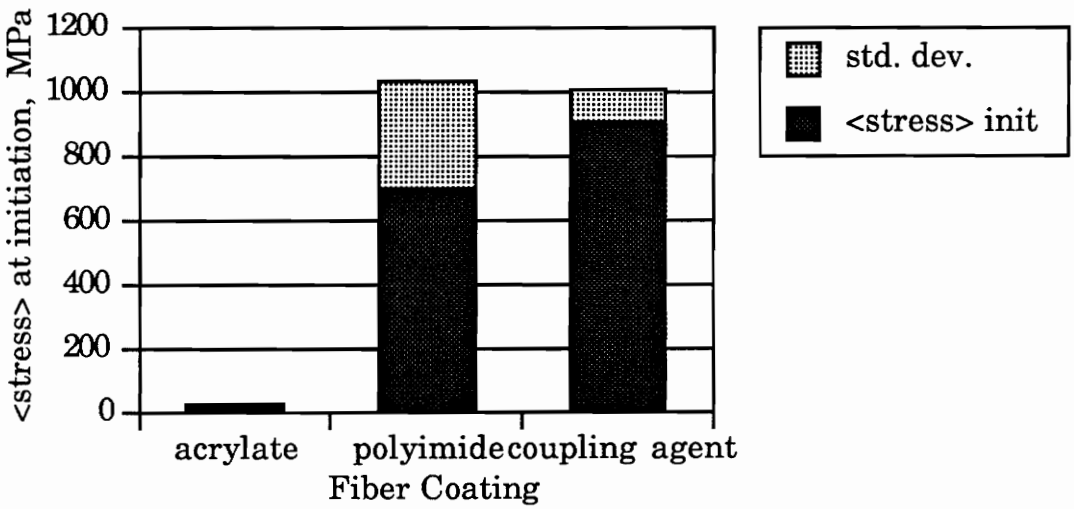

Figure 21. Fibers supporting various coatings embedded in the BGEBA resin system.

Visually, the acrylate coated fiber samples displayed minimal stress transfer via the birefringence pattern. With the onset of clamp displacement, debonding would begin almost immediately. There was migration of the interfacial crack along the fiber from both sides of the notch; this migration was immediate and with no hesitations. The system appeared to "unzip". At crack completion, the fiber began to pull-out. In this resin the removed, coated fibers surface was not damaged i.e., failure appeared to take place at the coating/resin interface. Interestingly, when the fiber was removed from the resin the coating extended beyond the glass fiber end. This probably resulted from slippage of the entire coating (rather than coating deformation) and the fiber end which was still embedded likely displayed a corresponding small region of uncoated glass fiber. This was not verified.

The coupling agent treated fibers also displayed low transfer stresses via the load frame data and the birefringence patterns. Here, there was a nonlinear load response to the extension of the sample i.e., the interfacial crack displayed halts and hesitations while propagating to the end of the fiber. These fibers did pull-out in an uneventful manner i.e. minimal stick-slip and a linear decrease in load with extension.

The polyimide-coated fibers exhibited a comparatively large amount of stress transfer activity in the form of birefringence patterns which migrated in a non-linear fashion along the fiber. As will be shown, the

birefringence patterns seen here were minimal when compared to the samples cured at elevated temperatures. With the polyimide samples there was a pull-out plateau at the low loads of 225-550 MPa. The locus of failure was at the polyimide/resin interface.

4.2.2 Catalyzed TGDDM/DDS Epoxy Resin

In this set of experiments, the coupling agent coated fibers were not used because of the difficulty in pre-notching the specimens without causing fiber failure. Fibers removed from the catalyzed TGDDM/DDS epoxy resin responded in a more dramatic fashion than fibers embedded in the BGEBA system. Upon loading, the acrylate coated samples exhibited crack initiation stresses of 27.2 ± 0.74 MPa. As with samples in the BGEBA system, these samples displayed minimal stress transfer via the birefringence pattern and interfacial crack propagation along the fiber from both sides of the notch. Again, the system unzipped. At crack completion the fiber began to pull-out and, visually, one could see that the integrity of the coating was compromised. Although some bare fiber was seen, it was observed that the locus of failure was primarily cohesive in the acrylate coating as it was severely torn. Figure 22 is a load versus extension trace for the acrylate coated fiber in catalyzed TGDDM/DDS epoxy (N.B.. the superimposed cosine was an instrument perturbation which was later removed). None of these samples displayed any stick-slip activity.

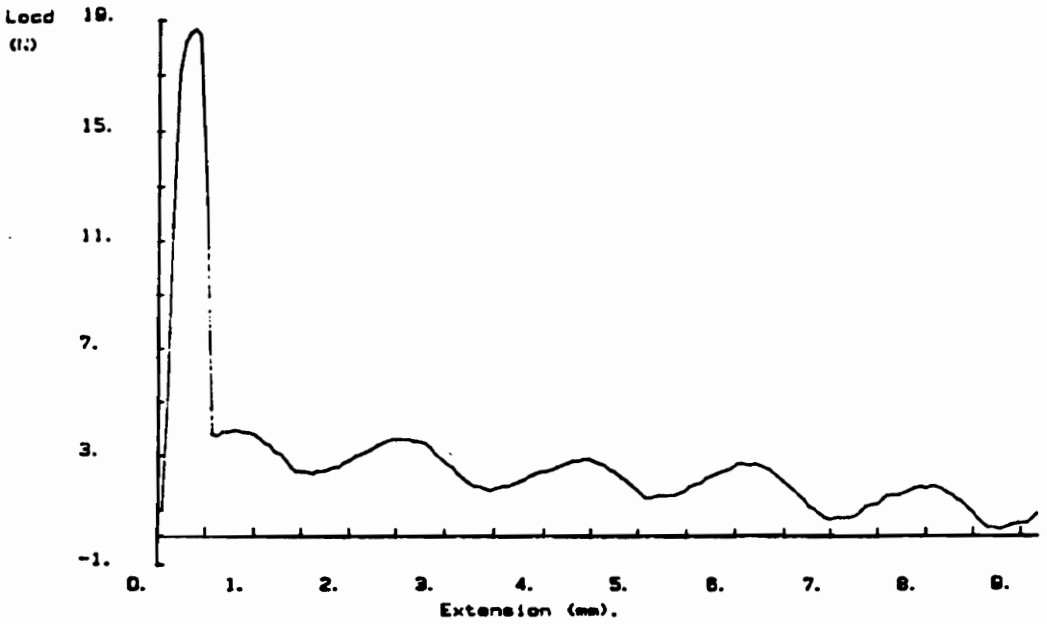

Figure 22. SpecTran acrylate coated fiber embedded in catalyzed TGDDM/DDS.

In contrast to the acrylate in catalyzed TGDDM/DDS and to all fibers in BGEBA, the experiments conducted on the Polymicro polyimide-coated optical fibers in catalyzed TGDDM/DDS revealed a significantly different behavior. Here, there was substantial stress transfer from the fiber to the matrix via birefringence patterns of greater magnitude and higher order. Interfacial crack initiation stresses were 1892.2 ± 367 MPa. For these samples, once the interfacial crack began to migrate, there was a great deal of acoustic activity and, correspondingly, the moving isochromatic bands showed substantial hesitations. These observations appear to represent the effect of increased normal pressures on the fiber resulting from the embedding resin. This concept will be expanded upon in a later section. For all of these samples, the locus of failure visually appeared to be at the

glass/polyimide coating interface. Of these, half resulted in fiber failure with the exposed fiber showing no polyimide intact. Stick-slip activity was prevalent for these samples with increased magnitude at the end of the run which may have been due to the locus of failure.

4.3 The Effect of Fiber Manufacturer on the Single Fiber Pull-Out Test

To determine the most appropriate polyimide-coated optical fiber for embedding in the uncatalyzed TGDDM/DDS epoxy resin for the later evaluation of the cure cycle, fibers supplied by six different manufacturers were examined. Some significant differences between sample sets were found. For specimens obtained from Polymicro Technologies, the dominant mode of failure was polyimide/epoxy debonding with a few cases of glass/polyimide debonding. Data depicted in Figure 20a was typical for this sample set in that all previously described regions were present. For fibers obtained from AT&T, General FiberOptics and SpecTran, there was an inconsistent mixed failure i.e., glass/polyimide, polyimide/matrix and fiber failure. Of the samples which did not result in fiber failure, a typical load-versus-extension plot did not show a pull-out plateau region. Instead, a maximum load was reached and the fiber pulled out in a consistent manner, i.e. decreasing load with extension, as in Figure 20b. For the AT&T and SpecTran samples, stick-slip activity was minimal. General FiberOptics fibers, however, displayed a failure loci of matrix microcracking. This corresponded to excellent interfacial adhesion at both the glass/polyimide and polyimide/epoxy interfaces. For these samples, ultimate failure took place between the polyimide and matrix and stick-slip

did occur. Visually, the stick-slip activity did not necessarily coincide with the sites of microcracked matrix. Fiber specimens obtained from Fiberguide generally failed at the polyimide/epoxy interface and typically showed a great deal of stick-slip activity as seen in Figure 23. CeramOptec fibers primarily displayed failure at the glass/polyimide coating interface. While the loads seen during the runs were unimpressive, there was substantial stick-slip activity which occurred in the last third of the plot after minimal stick-slip occurred in the pull-out plateau region. This is shown in Figure 24. This was possibly due to micro-scale build-up of coating material resulting in a decreased area from which the fiber was being withdrawn N.B. this was typical of specimens failing at the glass/coating interface.

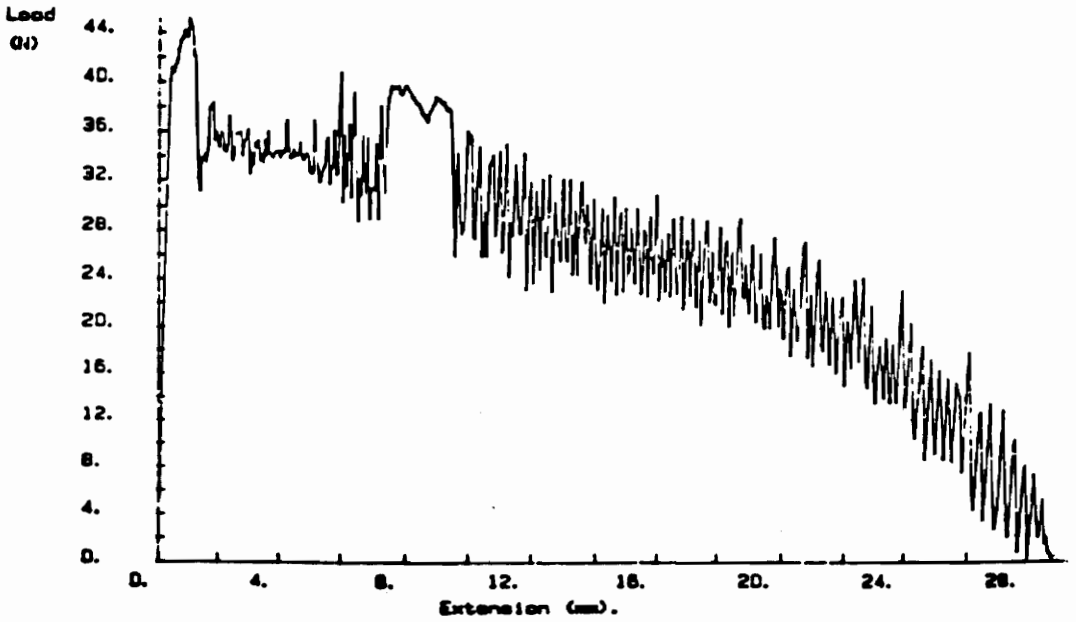

Figure 23. Typical load versus extension trace for coating/resin interface failure. Example from Fiberguide sample set.

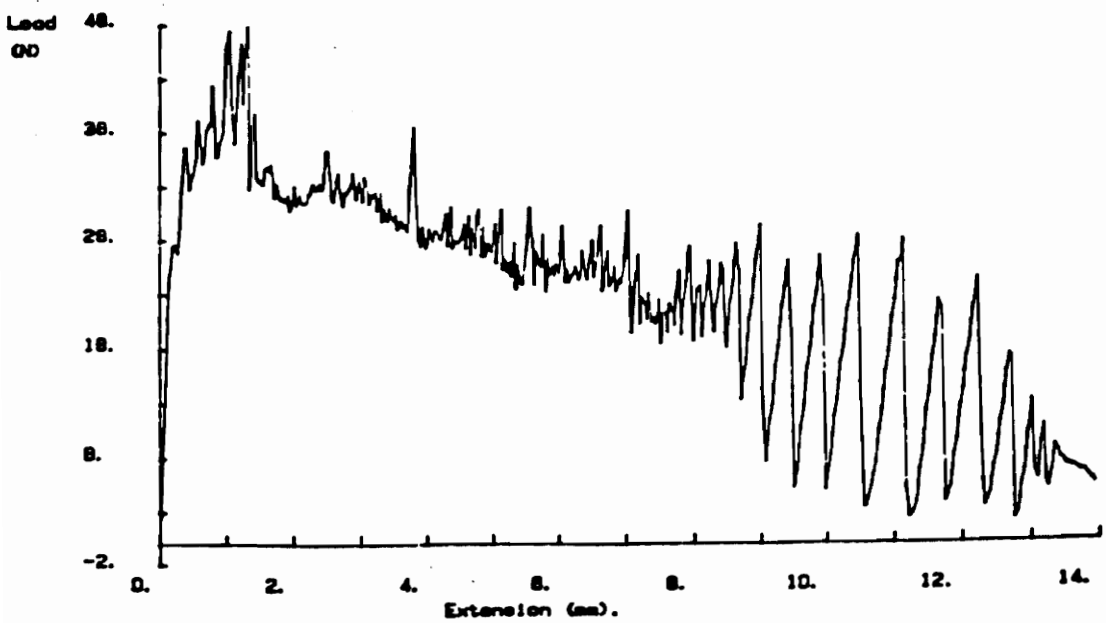

Figure 24. Typical load versus extension trace for glass/coating interface failure. Example from CeramOptec sample set.

The data reported in Figure 25 shows that the failure properties of the optical fiber/epoxy matrix system are dependent upon fiber manufacturer for a given resin. Although standard deviations are high, clear differences in the values of the initial loads, slopes and modes of failure between optical fiber manufacturers were found. N.B. The variability between manufacturers results from different polyimide chemistries, production methods, etc. This figure is complemented by Table 5.

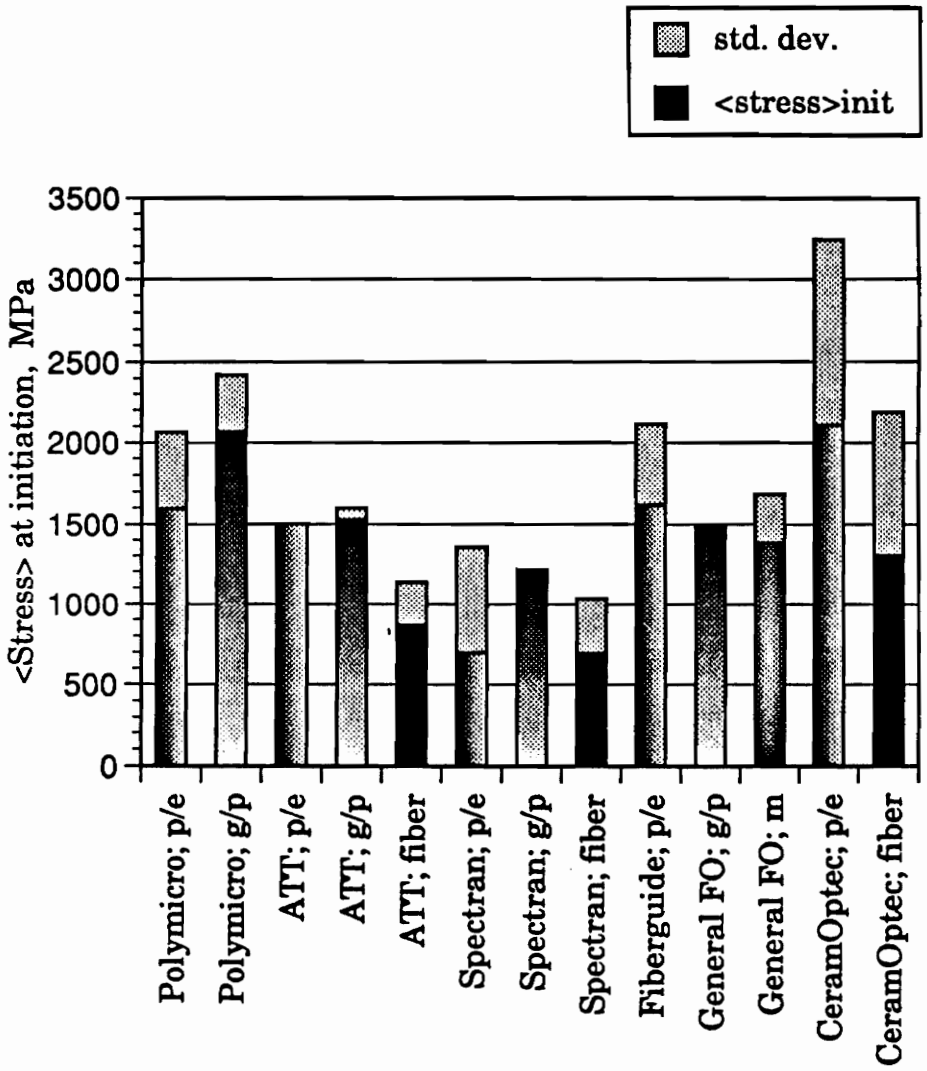

Figure 25. Results of different polyimide-coated fibers embedded in the uncatalyzed TGDDM/DDS epoxy resin.

Table 5. Results of different polyimide-coated fibers embedded in the uncatalyzed TGDDM/DDS epoxy resin.

manfacturer / locus	<stress>init
Polymicro; p/e	15967 ± 469
Polymicro; g/p	2067 ± 355
ATT; p/e	1506
ATT; g/p	1533 ± 70
ATT; fiber	870 ± 269
Spectran; p/e	699 ± 659
Spectran; g/p	1216
Spectran; fiber	696 ± 338
Fiberguide; p/e	1621 ± 494
General FO; g/p	1503
General FO; m	1386 ± 301
CeramOptec; p/e	2109 ± 1137
CeramOptec; fiber	1306 ± 885

4.4 The Effect of Resin Choice on the Single Fiber Pull-Out Test

To evaluate the effect of resin chemistry and cure cycle on the single fiber pull-out test, polyimide coated fibers were embedded in four different resins. Here, the polyimide-coated fiber choice was based on the results of the previous section via the loads associated with debonding and the apparent locus of failure. As was reported, the removal of the debonded polyimide-coated fiber from any particular resin resulted in either unperturbed polyimide coating, or in the case of coating failure, clean glass

fiber. These surfaces are easily seen with the unaided eye but were initially verified by both infrared spectroscopy and x-ray photoelectron spectroscopy. Since manufacturer coating chemistries and procedures were not adjustable for the current work, an appropriate performing polyimide-coated fiber (Polymicro supplied) was embedded in the four resins of interest.

Polymicro's polyimide-coated optical fibers were embedded in BGEBA (25°C for 48 hours), uncatalyzed TGDDM/DDS (150°C for three hours), catalyzed TGDDM/DDS (177°C for three hours) and NH_2 -Polysulfone / BMI / Diallyl / Bisphenol A resin (200°C for 1 hour and 250°C for 2 hours). The data for all experiments conducted to evaluate the tensile performance of Polymicro fibers in various resins is presented in Figure 26 and Table 6. The data includes resin, stress at crack initiation, $\sigma_{initiation}$, interfacial shear stress for final pull-out, $\langle\tau\rangle_{pull\text{-}out}$, and locus of failure. These experiments are detailed in the following text.

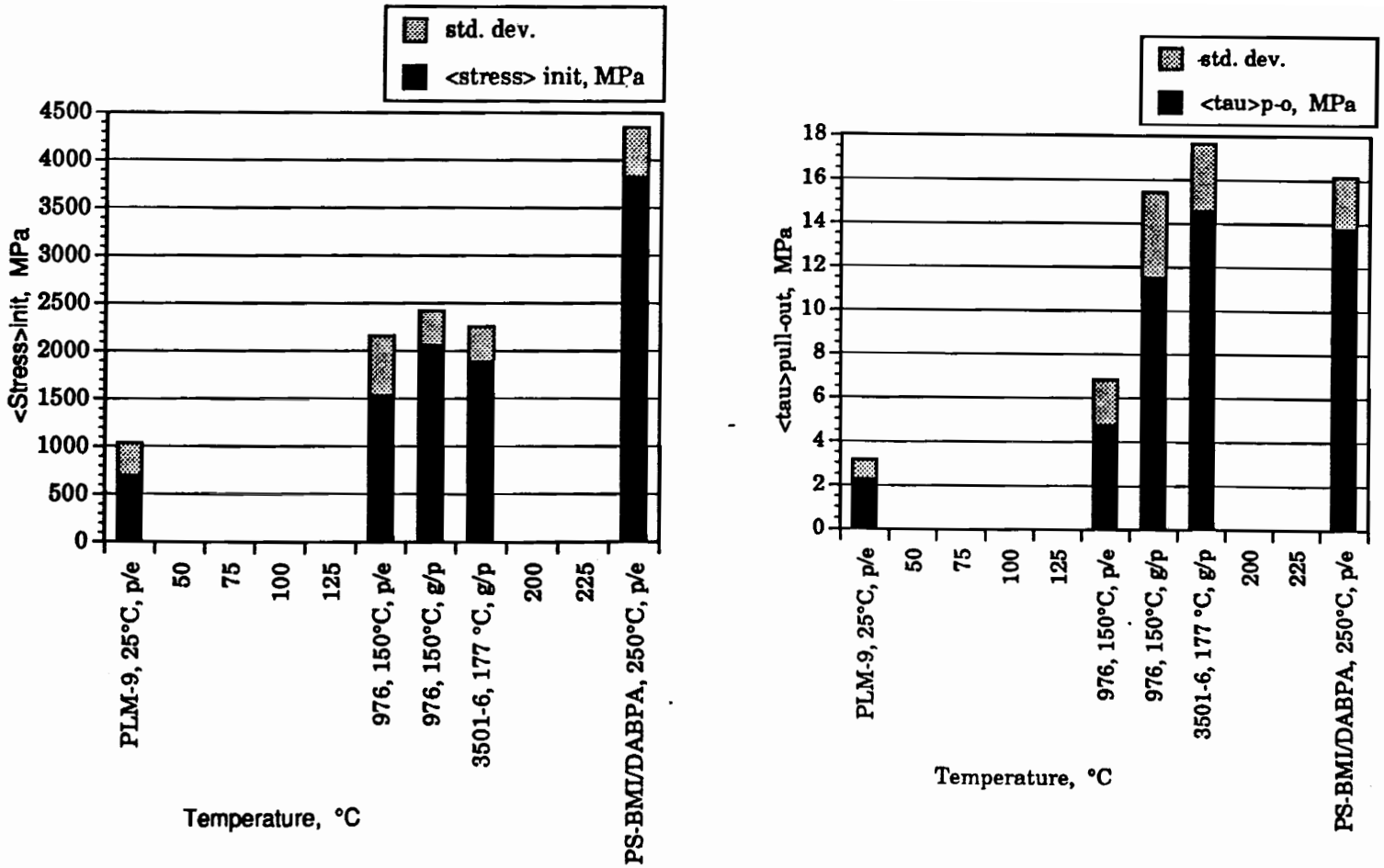

Figure 26. Bar chart of Polymicro polyimide coated fibers embedded in various resins: a) average stress at initiation; b) average interfacial shear stress for pull-out.

Table 6. Experimental results of Polymicro polyimide coated fibers embedded in various resins.

resin, Tcure	locus	<stress> init,	<tau>p-o, MPa
PLM-9, 25°C	p/e	696 ± 336	2.27± 0.86
976, 150°C	p/e	1534 ± 628	4.73 ± 2.1
976, 150°C	g/p	2067 ± 355	11.5 ± 3.9
3501-6, 177 °C	g/p	1892 ± 367	14.55 ± 3.1
PS-BMI/DABPA	p/e	3830.9 ± 523	13.75 ± 2.4

The set of experiments examined BGEBA (room temperature cure, 24 hours). The average initiation load was 696 ± 336 MPa and the observations were detailed earlier in Section 4.2.1.

The sets of experiments which implemented uncatalyzed and catalyzed TGDDM/DDS epoxy systems required elevated temperatures for cure. As the specimen cure cycle temperature increased, the load required for initial debond increased, indicative of resin shrinkage or clamping. Here, there was substantial stress transfer from the fiber to the matrix via birefringence patterns of greater magnitude and higher order. For the uncatalyzed TGDDM/DDS and catalyzed TGDDM/DDS epoxy resin systems the average crack initiation loads were 1596.6 ± 469 and 1892 ± 367 MPa, respectively. For these samples, once the interfacial crack began to migrate, there was a great deal of acoustic activity and, correspondingly, the moving isochromatic bands showed substantial hesitations. At crack

completion, the fiber began pull-out. For the uncatalyzed samples, the locus of failure was at the coating/resin interface. Figure 20a is a typical load versus extension trace for this set of samples. For the catalyzed sample set, the primary locus of failure was at the glass/coating interface. This was probably the result of fibers from different manufacturing lots rather than of the embedding resin. A typical load versus extension trace was described via Figure 24. Indicative of the glass/coating failure is the substantial stick-slip behavior at the tail end of the trace.

For fibers embedded in NH_2 -Polysulfone / BMI / Diallyl / Bisphenol A, the final set of experiments, the average load required for crack initiation was 3830.9 ± 523 MPa. For these samples, the stick-slip load differential was often as high as 1130 MPa. While the coating/resin interface was the primary locus of failure, the fiber would often fail at some time during the run.

This series of experiments has shown that the combined chemistry and thermal cure cycle of the embedding resin substantially effect the results of the single fiber pull-out test. Not only were the stresses associated with crack initiation a function of resin properties but crack propagation and fiber sliding properties were affected as well.

4.5 Summation

For the development of smart structures through the implementation of optical fiber sensors, the extent of stress transfer between fiber and matrix should be known. It has been shown here that the choice of fiber coating as well as embedding resin play a significant role in determining the loads required for the initiation of interfacial crack propagation as well as the locus of the failure. For the development of a strain sensor for relatively small scale perturbations, maximum stress transfer would be desired i.e., a coating system such as a coupling agent which accommodates chemical adhesion at the fiber/resin interface. However, if the sensor is to survive interfacial microcracks, ply delaminations or plastic deformation of the structure, some degree of slippage would be desirable.

To control the extent of fiber slippage in a resin with particular thermal cure requirements, a coating with minimal or no chemical bonding plus minimal compressive properties would be desirable. Since the rubbery acrylate coating deforms with pressure i.e., pressures due to the mechanical clamping of a thermally cured resin or via perturbations to the structure et cetera, in a non-controlled fashion, the coating of choice which is readily available is based on polyimide chemistry.

In regards to the embedding resin, the qualitative performance of the embedded fiber as measured by the load required for the initiation of crack propagation was related to the thermal history of the specimen. It is

recognized that the chemistry between resins varied, however, in viewing the thermal history of the samples, the apparent relationship between the mismatch in thermal coefficients of contraction between fiber and resin appears to play a significant role.

From this qualitative evaluation of load transfer between fiber, coating and resin via the single fiber pull-out test, it was found that the load response of the fiber was directly related to the fiber coating and manufacturer as well as the thermal and chemical properties of the embedding resin. The detailed interpretation of these results are limited due to insufficient physical data pertaining to the embedding resins. This problem is directly addressed in the following chapter.

Chapter 5

Cure Study: Variable Cure of Uncatalyzed TGDDM/DDS Epoxy and Its Effect on the Single Fiber Pull-Out Test

It has qualitatively been shown that the failure of the interface between the fiber and resin is a function of material, sample loading, Young's moduli and Poisson's ratio of the two materials and the mismatch of the thermal coefficient of expansion between the two materials. Regarding the relationships between load required for initial crack propagation and resin chemistry and thermal history, clear differences in the results of the single fiber pull-out tests were demonstrated. The effect of coating properties on the transfer of load from fiber to resin were significant, as was the normal pressure exerted in the fiber due to resin chemistry and thermal contraction. To exemplify these results, the comparative study via variable cure was conducted. Here, it was expected that as polymer properties changed with cure temperature, the failure of the single fiber composite would also change and in a predictable way.

To specifically address the residual stresses on the embedded fiber, the single fiber composite was thermally cured at various temperatures for the same amount of time. Polymicro polyimide-coated optical fibers from one production run were embedded in the uncatalyzed TGDDM/DDS epoxy resin. These specimens, brought to various temperatures were physically characterized by TMA and DMTA, and chemically characterized by FTIR spectroscopy. The failure results of this final series of experiments were evaluated for the determination of the strain energy release rate and interfacial shear stress as a function of thermal history.

In this series of experiments, as the cure temperature of the resin was elevated from sample set to set with time at T_{cure} a constant, many of the physical characteristics of the resin changed, see Table 7. Here, not only did the glass transition temperature increase but the extent of cure and the modulus also increased, as expected. The effect of the change in the polymer resin parameters via the fracture mechanics of the single fiber pull-out test was to increase the strain energy release rate at crack initiation and have a greater influence on the interfacial shear stress and coefficient of friction via the increased normal pressure on the fiber. This effect was thought to be the result of the T_{cure} - T_g relationship. As such, the trend of these parameters was to increase as T_{cure} increased but to then decrease when T_{cure} approached T_g.

Table 7. T_{cure}, T_g (DMTA), modulus (minimat), percent cure (FTIR relative to 130°C degassed samples) for the uncatalyzed TGDDM/DDS epoxy system.

	Tg, °C	Modulus, MPa	% epoxide ring
150	180	4120	34.6
177	220	5720	65
230	260	6540	67.4
250	260	7540	72.4

This chapter presents and discusses how the choice of cure cycle was made and its effect on the single fiber pull-out test with respect to the strain energy release rate. These results are then interpreted through the determination of residual pressure via chemistry and temperature, Section 5.3, and the interfacial shear stress and coefficient of friction, Section 5.4. Finally, a summary discussion is presented in which the fracture mechanics of these single fiber pull-out tests are quantitatively correlated to the physical properties of the polymer matrix.

5.1 The Choice of Cure Temperature

For evaluating the role of cure temperature on the single fiber pull-out test, an appropriate array of temperatures was determined. To this end, the determination of complete cure of the epoxy was made by thermal characterization. This consisted of running Thermal Gravimetric Analysis, TGA, Differential Scanning Calorimetry, DSC, and Thermal Mechanical Analysis, TMA, experiments on the uncatalyzed TGDDM/DDS resin samples.

TGA was run to determine mass loss of the sample with temperature. This experiment provided the percent weight loss of the sample as a function of time and temperature. Weight loss of 2% occurred at 275.3°C and 5% at 331.8 ° in N_2, see Figure 27a. The DSC provided the heat flow of the sample as a function of time and temperature as related to sample chemistry. The DSC results for the resin system are shown in Figure 27b. Here, the measurement was of heat flow as a function of temperature. The experimental heat/cool cycle was repeated five times. The first cycle displayed a significant exotherm: onset at 160°C. This was indicative of incomplete cure of the resin system. The second through fifth heat cycles showed no exotherm and the traces were reproducible. Next, a TMA was run to measure the change in volume with temperature. Expansion of the sample was measured as a function of temperature. As with the DSC experiments, the TMA revealed a significant expansion which began at approximately 160°C and with consecutive heats this expansion was no longer seen, see Figure 27c.

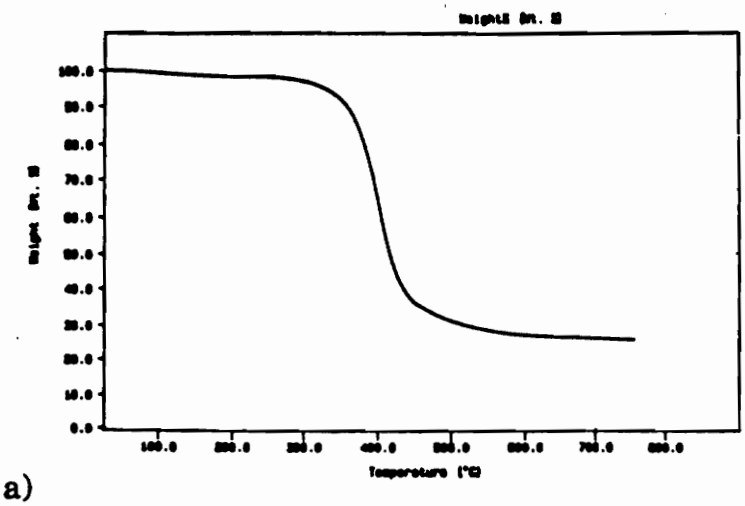

a)

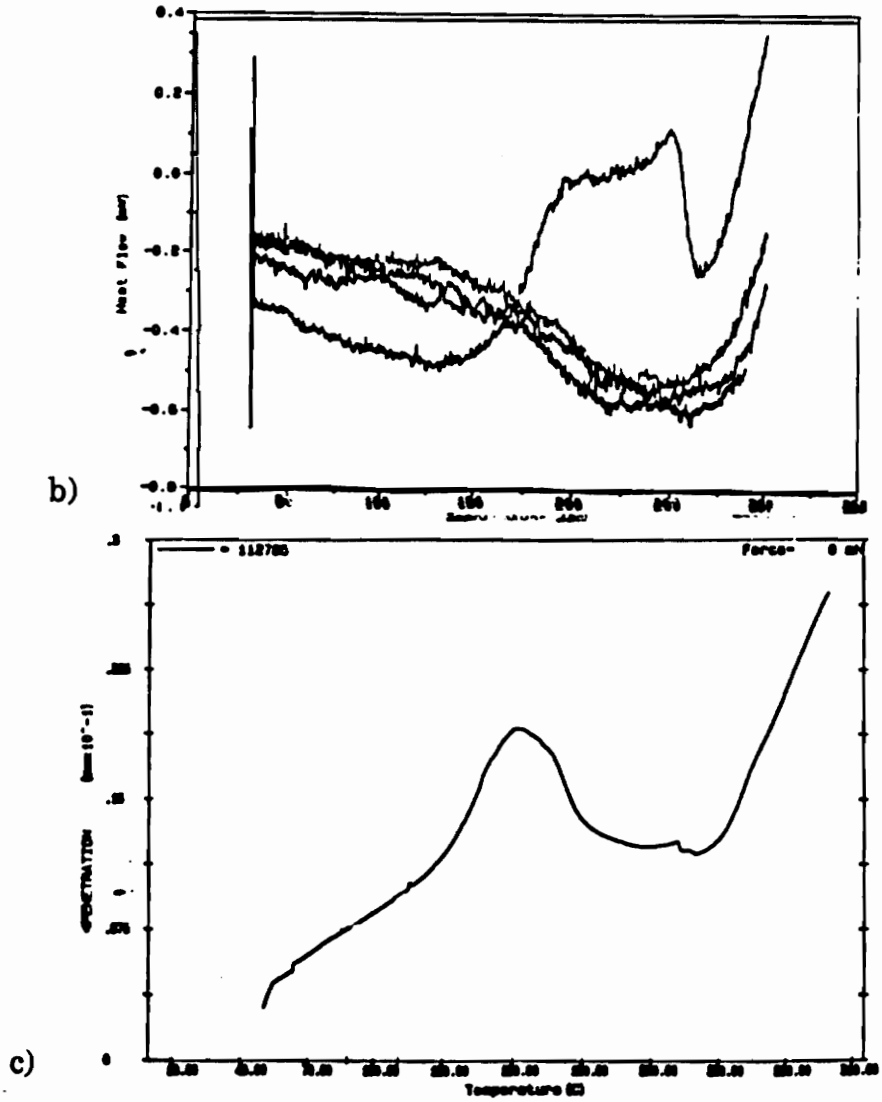

Figure 27. a) TGA; b) DSC; and c) TMA of the uncatalyzed TGDDM/DDS epoxy resin.

The post cure scenario with maximum temperatures of 230°C completely cured the epoxy as per a TMA set of experiments. N.B. A post cure with T_{max} = 200°C was insufficient as per the presence of an exotherm via TMA.

Based on these experiments, cure temperatures of 150, 177, 230 and 250°C were employed. These cure temperatures were chosen for the following reasons: 150°C is the cure temperature employed by a major user of this resin (and partial sponsor of this work); 177°C is the manufacturers

recommended cure temperature, 230°C was the temperature found to complete the cure chemistry via mechanical properties (TMA), and 250°C was chosen to determine near T_g effects.

5.2 Results and Interpretation of the Single Fiber Pull-Out Test as Cure Temperature is Increased

The single fiber pull-out experimental results and calculation of the strain energy release rates are presented below. Here, the load required for interfacial crack initiation was implemented for the determination of the critical strain energy release rate. The strain energy release rate during the propagation of this crack was also calculated with the consideration of frictional effects during crack propagation through the high frictional region. The experimental results and model calculations support the hypothesis that the residual stresses are a function of the T_{cure} : T_g relationship.

5.2.1 Experimental Results

For a given cure temperature sample set, the minimum number of experiments was eight. The pull-out response of the various samples varied significantly. For example, a *model response* was that which exhibited a $P_{init} < P_{friction} = P_{s\text{-}s;debond}$, both a debonding and pull-out plateau region and, of course, a pull-out tail. Four or more experiments from each sample set did exhibit this model response. The remaining experiments resulted in load relationships which did not follow the model i.e., P_{init} equal to the maximum load such that $P_{friction}$ was $\leq P_{init}$ or, no

debonding plateau post $P_{friction}$. Since fiber surface inhomogeneities and fiber alignment play a significant role in this type of study, these varied pull-out responses were not unexpected. For the reported results and calculations, only the data points which were relevant to the particular discussion were used for any given calculation; an appropriate explanation concerning this is provided at that point. Only samples which debonded at the polyimide/resin interface were considered. If the number of points in a reported average was less than four, this is noted in the text. All pull-out traces discussed in this section are located in Appendix A, these traces were not corrected for load offsets whereas the data reported in the text was. Some of the traces displayed a change in stick-slip activity during pull-out; no comment can be made at this time as to why this occurred. However, this change of amplitude was noted in a paper by Cook, Thouless, Clarke and Kroll (40), as relating to a change in pull-out rate. No intentional change in rate was made here and this phenomenon was observed more than once.

The results of this cure study are shown in Table 8. Listed are the values of stresses associated with crack initiation, σ_{init}, completion of the primary frictional zone, $\sigma_{friction}$, the steady-state debonding plateau, $\sigma_{s\text{-}s;debond}$ and pull-out plateau, σ_{drop} and σ_{chi} in MPa. Since the pull-out plateau typically displayed a slight slope, this plateau value is reported as a pair. The first value was the stress dropped to at the onset of pull-out and the second value was the stress associated with the onset of the chi transition region. The average of this pair is also listed.

Table 8. Stresses in MPa for interfacial crack initiation, σ_{init}, the end of the primary frictional zone, $\sigma_{friction}$, and steady state debond and fiber pull-out: σ_{drop} and σ_{chi}.

	initiation	friction	s-s debond	plateau, drop	plateau, chi	<plateau>	Comments
150 C	3288.9	4957.0	4130.8	2889.2	2362.2	2625.7	model pull-out
150 J	1992.7	-	3513.0	2259.2	969.1	1614.2	no p-o plateau
150 K	1811.0	-	4663.8	3791.6	2362.2	3076.9	perfect model
150 M	4248.3	3242.9	3452.5	2128.4	1401.6	1765.0	Pinit = Pmax, no p-o plateau
177 B	4768.0	4964.3	4685.6	3573.6	2483.3	3028.5	model
177 E	4478.5	4447.0	-	3173.8	1817.1	2495.5	perfect model
177 I	2407.0	4218.0	4127.2	3125.4	2210.8	2668.1	model, d plateau w/ change of debond direction, stick-slip anomoly
177 J	2873.4	4404.6	4258.0	3531.2	2786.2	3158.7	perfect model
230 A	-	-	5015.1	3985.5	3694.7	3840.1	initial clamp slippage
230 D	3996.4	5222.3	5360.4	4209.6	3028.5	3619.0	model, d plateau w/ change of direction
230 I	4384.0	5327.7	4464.0	3634.2	2931.6	3282.9	model
230 J	3292.5	4055.7	3755.3	3391.9	-	1695.9	no p-o plateau, stick-slip anomoly
230 K	3662.0	3780.7	3803.8	3258.6	2241.1	2749.8	perfect model
230 L	4854.0	4277.4	4300.4	3452.5	2453.1	2952.8	Pinit = Pmax
250 E	4203.5	-	3755.3	2386.4	-	1193.2	np p-o plateau
250 F	3124.2	4737.7	4906.1	3634.2	2059.4	2846.8	perfect model
250 H	3046.6	4791.0	5027.3	3725.0	3513.0	3619.0	perfect model
250 K	4147.8	4174.4	4361.0	2846.8	2089.6	2468.2	Pinit = Pmax, d plateau w/ change of direction

The single fiber composite specimens of this cure study displayed different birefringence patterns when placed under a load. Since the material parameters of the various sets were the same, the photoelastic response of the systems represented the transfer of load from fiber to matrix. Here, the number of birefringence bands remained constant, however, the width of these bands increased with the elevated cure temperatures i.e., there was greater load transfer in the 230°C sample set than the 150°C set. This observation was also made in the series of experiments where resin chemistry was varied. As noted below, no conclusion could be drawn about the relative birefringence patterns when the chemistry of the embedding resin changed.

When Polymicro polyimide-coated optical fibers were embedded in resins of different chemistry and cure temperature the resulting birefringence patterns dramatically changed and increased in both order and magnitude as the cure temperature between sample sets increased. No direct conclusions could be made regarding load transfer, however, even though the values correlating to the fracture of the specimens also increased with sample-set cure temperature. This was because the chemistry between sample sets varied and the contributions to the resulting birefringence could have been from more than photoelastic events. By implementing the one resin and varying the extent of cure, the birefringence variables were maintained constant. Here, the changes in photoelastic patterns represented changes in load transfer with extent of cure. The key

parameter of this effect was the residual pressure on the fiber which resulted from the chemical cure plus the thermal contraction of the resin relative to the fiber as the system was cooled from the cure temperature.

5.2.2 Strain Energy Release Rate as a Function of Cure

The strain energy release rate was calculated for the above data with and without the consideration of friction. Neglecting friction, the basic compliance model, equation [1] and Gao's model, equation [30], were employed. Considering the effects of friction, the model of Gao et al., [21], was used. The calculations were done using a spreadsheet and the program can be found in Appendix B. Each of these equations are listed here for easy reference.

Strain energy release rate at crack initiation is

$$G_{init} = P_{init}^2 / [4 \pi^2 r^3 E_f] \qquad [6]$$

and

$$G_{initiate} = \left[\frac{P_{init}}{2pr^{3/2}}\right]^2 \left(1 - 2k\nu_f\right)\left(E_f\left(1 + \beta\right)\right)^{-1} \qquad [30].$$

Strain energy release rate during crack propagation is

$$G_{continue} = \frac{\left(1-2k\nu_f\right)\left[P-\left((1+\beta)Q\right]^2\right.}{4\pi^2 r^3 E_f\left(1+\beta\right)} \qquad [21].$$

5.2.2.1 Critical Strain Energy Release Rate

Using the compliance equation and Gao's equation for SERR without friction, Table 9 was generated; Figure 28 compliments this information.

Table 9. Average critical strain energy release rate in N/m for the model pull-out experiments.

File	Ginit	Ginitiate	<Ginit>	<Ginitiate>
150 C	2760	2550		
150 J	1013	937		
150 K	837	774	1536 ± 1063	1420 ± 982
177 B	5801	5480		
177 I	1476	1400		
177 J	2103	1990	3126 ± 2337	2956 ± 2205
230 D	4075	3870		
230 I	4905	4660		
230 J	2766	2630		
230 K	3422	3250	3792 ± 914	3602 ± 868
250 F	2491	2380		
250 H	2369	2260		
250 K	4390	4200	3083 ± 1133	2946 ± 1087

Figure 28. <SERR>initiation, bar chart using Ginitiate.

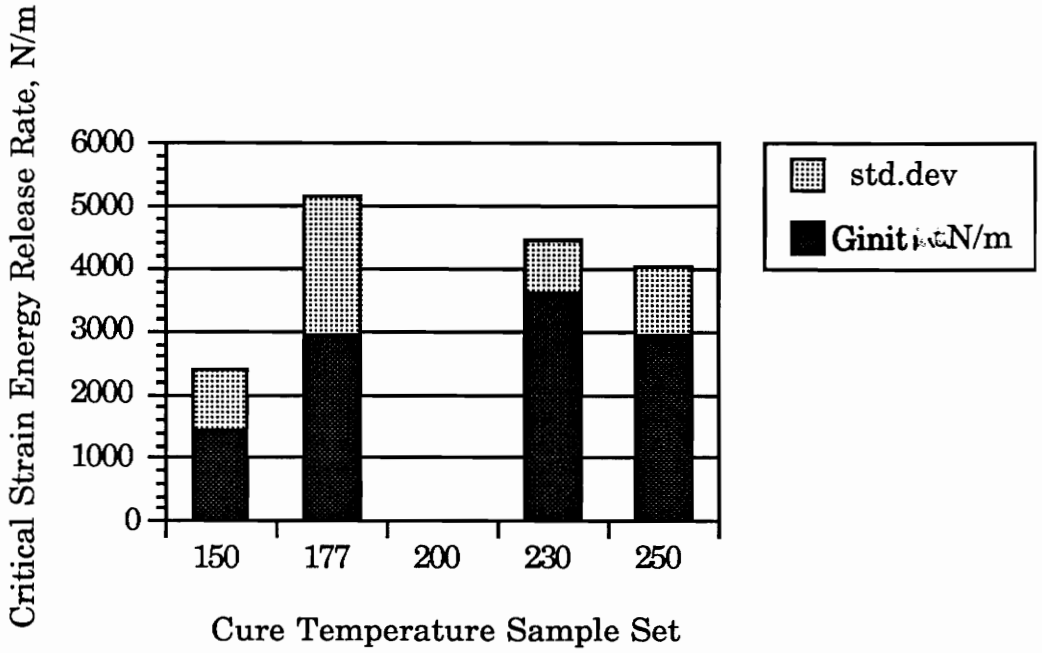

Due to high values of standard deviation for the sample sets of a particular cure cycle, no statistical difference between the individual sample sets of the cure study experiments can be claimed. This prevents drawing definitive conclusions for the relatively small temperature increments. However, the trends of the data do follow the expected outcome of increasing values for the stress at crack initiation, the critical strain energy release rate values with cure temperatures well below T_g. The strain energy release rate associated with the sample set cured at 250°C is lower then the values associated with 230°. Again, since T_{cure} was within Tg - 30°C this was expected. In taking a closer look at the 150°C and 230°C cure cycle sample sets, statistically significant differences in fracture properties of the specimens are seen.

5.2.2.2 Debonding Strain Energy Release Rate

To evaluate both the experimental data of debonding and the mathematical models for this event, the strain energy release rate was calculated with the consideration of the frictional dissipation of energy. The equation of Gao Mai and Cotterell was implemented. In order to minimize the variability of the experimental results, specific model experiments of the different cure cycles are reported, not the average of the sample set. Table 10 displays these calculations. Reported are the experimentally determined normal pressure implementing Gao's equation, the interfacial shear stress of pull-out and the load associated with crack initiation. The strain energy release rate was determined for a debond length associated with the middle of the high frictional zone, $G_{continue}$.

In the presentation of Gao et al.'s model, $\widetilde{P}$ was explained to represent the maximum load in the system due to the contribution of frictional forces. Experimentally, this has been referred to as $P_{friction}$. The calculation of $\widetilde{P}$ via equation [27] underestimated the experimental value of $P_{friction}$ and its implementation in equation [26] resulted in negative strain energy release rates. Therefore, the experimentally determined $P_{friction}$ was used for $\widetilde{P}$. Excluding samples 150J and 150K, the experimental models which displayed the theoretically predicted response, $G_{continue}$ came very close to $G_{initiate}$.

Table 10. **Strain energy release rate calculated with the consideration of friction via Gao et al.'s model.**

	normal pressure, MPa	iss at pull-out, MPa	load for initiation, N	load at continuation, N	Ginitiate, N/m	Gcontinue, N/m
150 C	11.6	12	54.3	68.1	2550	2610
150 J	11.6	6.15	32.9	44.3	937	2230
150 K	11.6	11.4		56.1	774	2770
177 B	18.2	23.4	78.7	80.3	5480	5430
177 I	18.2	18.5	39.7	54.7	1400	1120
177 J	18.2	20.2	47.4	60.1	1990	1630
230 D	38.22	20.2	66	76.1	3870	5130
230 I	38.22	11.3	72.4	80.2	4660	5270
230 J	38.22	20	54.4	60.7	2630	2840
230 K	38.22	11.3	60.5	61.4	3250	3370
250 F	38.12	19	51.6	64.9	2380	2980
250 H	38.12	15.2	50.3	64.7	2260	3030
250 K	38.12	17.5	68.48	68.6	4200	4230

To contrast these fracture results to the polymer properties associated with a particular cure temperature the properties of all sets were evaluated. However, due to the experimental scatter inherent to the single fiber pull-out test, only the statistically different sample sets will be compared to the polymer parameters. To this end, the relationship between the 150 and 230°C data sets is discussed in regards to the physical properties of the polymeric matrix. This then develops into a discussion on the translation of load from fiber to matrix and the observed birefringence patterns. From there, the quantitative evaluation of the experiments and correlation's between the polymeric properties and fracture mechanics of the single fiber pull-out test is made.

5.3 Polymer-Based Considerations Regarding the Single Fiber Pull-Out Test

It has been presented that the normal pressure exerted on a fiber embedded in a polymeric resin will increase as the cure temperature increases and then decrease to a constant value when the cure temperature accommodates chemical cure in the rubbery state. The trend of the experimental results of the single fiber pull-out test supports this theory. To better evaluate this phenomenon the residual stress as a function of cure cycle was calculated implementing TMA experimental results. This is followed by the calculation of the various interfacial shear stress terms from the single fiber pull-out test results of interest. Finally, these values, the normal pressure and interfacial shear stress, are used to determine the

coefficient of friction for the polyimide coated glass fiber embedded in a TGDDM/DDS epoxy resin.

5.3.1 Residual Stress Exerted on the Embedded Fiber

In order to quantify the degree of densification due to both chemical crosslinking of the epoxy network and reduction in resin temperature (89), a series of thermomechanical analysis (TMA) experiments were conducted. Resin samples which were degassed in the usual way and then lightly crosslinked at 150°C for one hour (to prevent flow in the TMA) were evaluated.

Table 11 shows the percent change in associated with the chemistry and cooling regions of the experiment. Figure 29 shows the expansion versus temperature plots of these runs. Assuming an isotropic, homogeneous material,

$$(\Delta V)_{Chem} = [(height_{Tinitial} - height_{Tfinal}) / height_{Tinitial}] \times 3 \times 100\ (\%) \quad [43]$$

and,

$$(\Delta V)_{Temp} = [(height_{Tmax} - height_{T=20°C}) / height_{Tmax}] \times 3 \times 100\ (\%) \quad [44]$$

Table 11. T_{cure}, $(\Delta V)_{Chem}$, $(\Delta V)_{Temp}$, $(\Delta V)_{total}$ in percent decrease for the uncatalyzed TGDDM/DDS epoxy system.

Tcure	(DV)chem	(DV)temp	(DV)total
150	0.95 ± 0.12	1.923 ± 0.008	2.88 ± 0.12
177	0.63 ± 0.16	1.95 ± 0.16	2.583 ± 0.06
230	1.47 ± 0.5	3.61 ± 0.28	5.38 ± 0.5
250	2.59 ± 0.59	5.98 ± 2.3	8.57 ± 2.9

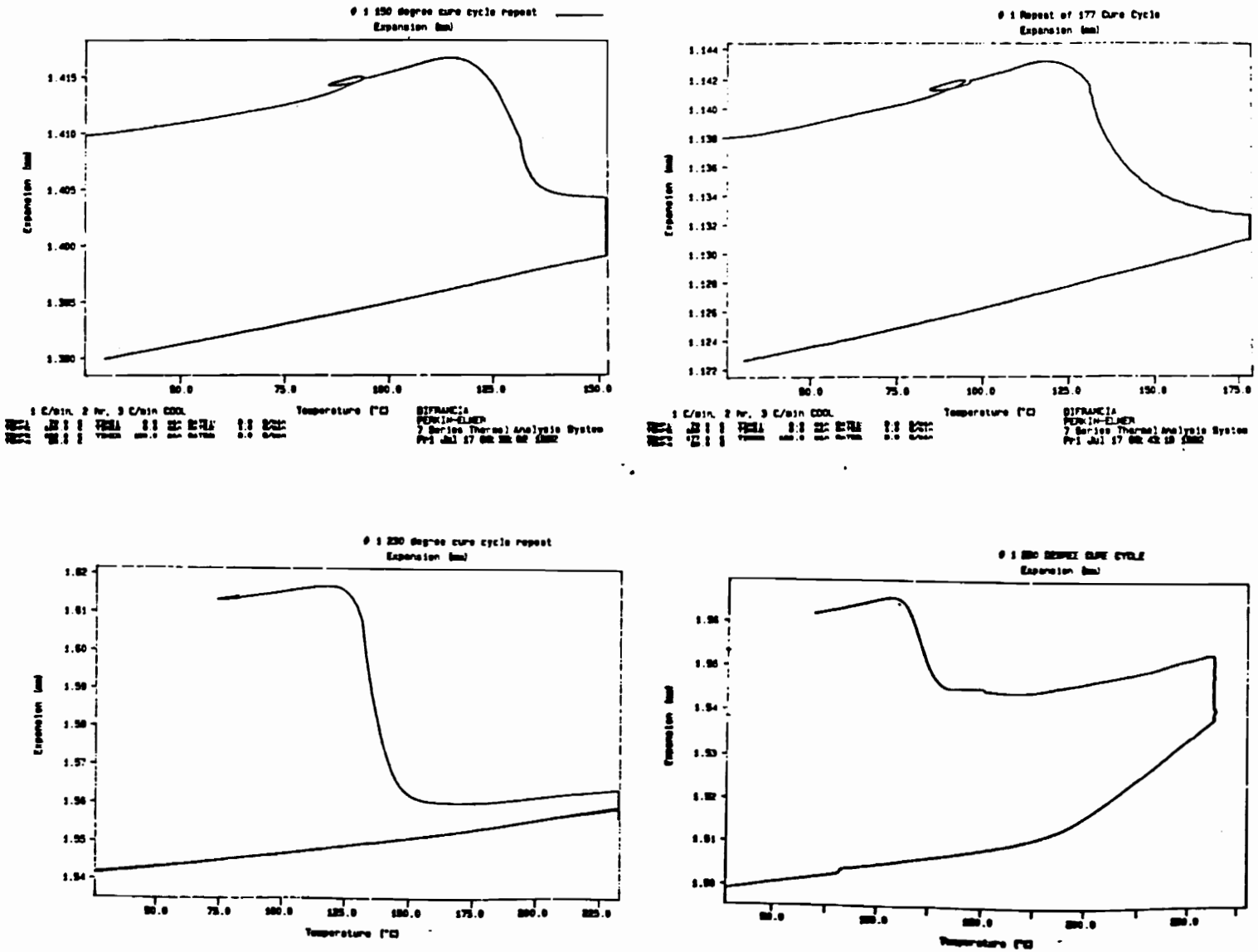

Figure 29. Expansion versus temperature for T_{cure} a) 150; b) 177; c) 230 and d) 250°C.

The relative change in volume via the TMA experiments accommodated a quick determination for the degree of shrinkage due to both chemical crosslinking and thermal contraction. This can only be accomplished for cure in the glassy state based on the assumption of no flow during cure. Since the cure temperature of 250° is very close to the T_g of the resin, the TMA results are not meaningful for this sample set.

In regards to the 177°C TMA results, the anomalous behavior with respect to the theory of continuous shrinkage during vitreous cure, is unexplained. It is worth noting that the fracture results gave a standard deviation of sixty percent. This resulted in data which spread across both the 150 and 230°C sample sets.

5.3.2 Determination of Residual Stresses

The normal pressure exerted on the embedded fiber by the surrounding matrix was determined by implementing Gao's approach via the single fiber pull-out test. Here, $[G_o]$ was applied via the single fiber pull-out test results. These critical strain energy release rates as well as the values for α, k and β are listed in Table 12 with the determined normal pressure.

Table 12. Residual pressure normal to the fiber surface via Gao et al.'s equation.

Tcure	alpha	kappa	beta	Ptotal, MPa
150	5.8 E-2	6.94 E-3	7.88 E-2	14.95
230	9.21 E-2	10.2 E-3	4.96 E-2	34.68

In contrast, a calculation based on the cure of the polymer was also made by implementing the approach of Harris. To determine the normal pressure exerted on the fiber due to thermal contraction of the matrix upon cooling, Harris's equation was implemented where the thermal coefficient of expansion of the fiber and matrix are 5 E-7 and 5 E-5 /°C (from TMA) and Poisson's ratio of the fiber and matrix were taken as 0.14 and 0.33, respectively. While these are not precise, they afford good estimates for the calculation. By in-situ measurement of the reaction temperature via a Luxtron 750 Fluoroptic™ Thermometry System and via the thermal read-out from the TMA cure study, the reaction temperature was within 2 degrees of the programmed cure temperature and so the cure cycle temperature, T_{cure}, was used in the calculation. The moduli of the epoxy matrix were reported in Table 7, the modulus of the fiber was 71 GPa.

Harris's equation does not account for the normal pressure resulting from the cure chemistry. By implementing the previously discussed TMA results, pressure due to cure shrinkage and, therefore, the total normal pressure on the fiber can be estimated. To do this the ratio of the TMA volume change of thermal to total was equated to the ratio of the calculated thermal contraction to the unknown total pressure. The amount of pressure due to chemistry was then the difference between P_{total} and P_{temp}. Table 13 shows the normal pressures due to temperature and the total resulting pressure as seen by the embedded fiber.

Table 13. Residual pressure normal to the fiber surface via TMA and Harris's equation.

Tcure	rm, E-5m	Ptemp, MPa	Ptotal, MPa
150	7.2037	18.95	28.38
230	7.1755	47.39	70.63

In comparing the results of the two approaches, the difference in the normal pressure on the fiber cured at 230°C compared to 150°C is 2.3 and 2.5 times greater from a fracture and polymer based approach, respectively. This disagreement suggests that the sensitivity of the single fiber pull-out test to the physical state and history of the polymer matrix is significant. As the polymer network formed at the two cure temperatures of interest, the modulus of the material as well as the degree of shrinkage due to chemical curing increase. Here, three hours at 150°C did not fully cure the TGDDM/DDS system and the physical properties of this partially cured resin reflected it. As the shrinkage increased with cure, the pressure exerted on the embedded fiber increased and the load required to overcome this pressure increased.

5.4 Interfacial Shear Stress and the Coefficient of Friction

The interfacial shear stress and coefficient of friction are related through the pressure in the system. The coefficient of friction is a constant for a given pair of materials and the interfacial shear stress varies as a function of pressure. For the single fiber pull-out test the pressure corresponds to the normal pressure discussed previously. When the fiber was loaded,

however, the pressure on the fiber was a function of crack length and radial contraction for a given location. To account for this effect, the interfacial shear stress was calculated from experimental data resulting from initial debonding, debond propagation over the primary frictional zone, and for the final removal of the fiber from the matrix. The coefficient of friction was also determined. By means of comparison, it was calculated for the debonding of the primary frictional zone and for the final removal of the fiber.

5.4.1 Interfacial Shear Stress

Values for the interfacial shear stress were determined for debond initiation, τ_{bond}, debond propagation in the primary frictional zone, τ_{debond}, and for the final removal of the primary frictional region, $\tau_{pull\text{-}out}$. These values were calculated in the following way:

In applying the shear lag theory to the variable cure data, bond strength, τ_{bond}, was determined using

$$\tau_{bond} = P_{init} / (\pi d l) \qquad [40]$$

where d is the fiber diameter and l is the length of fiber over which the initial debond occurs. In the current research, this length was determined visually via the birefringence pattern. In a typical experiment, the stress pattern was typically a series of three isochromatic bands forming the shape of an eye. At the very first increment of debonding, the *eye* displaced a distance equal to the location of the inner-most isochromatic band relative

to the edge or notch of the sample. This was the distance used for l in the above equation and was on the order of three to five fiber diameters.

The radial contraction of the fiber under a load caused the debonding in the frictional zone to result in a linear load versus displacement relationship for some time, then a transitional knee was sometimes displayed and steady-state crack propagation observed. This type of knee was seen during fiber pull-out in the χ region of the trace also. For the progressive debonding and for the final removal of the fiber, the interfacial shear stress was calculated from

$$\tau_x = (dP/dq)_x \, (1/\pi d) \qquad [45]$$

where q is crack length a, or displacement δ, and x is debond or pull-out.

As a point of interest, the length over which this shear stress acted during the debonding process versus the pull-out process was oftentimes the same. This assisted in the determination of the primary frictional zone during debonding as correlating to the pull-out tail length. This estimate was not too far off as seen in the Figure 30 which shows a pull-out trace from the 230°C cure sample set. The point of crack initiation and completion of the primary frictional zone are indicated in the blow-up. This ($\delta_{friction}$, $P_{friction}$) point was determined by noting the load which corresponded to a crack length of 3.5 mm. This crack length corresponded to the length of the tail of the pull-out region of the trace. The assumption of $l_{s\text{-}s,p\text{-}o} = l_{s\text{-}s,d}$ was therefore viable.

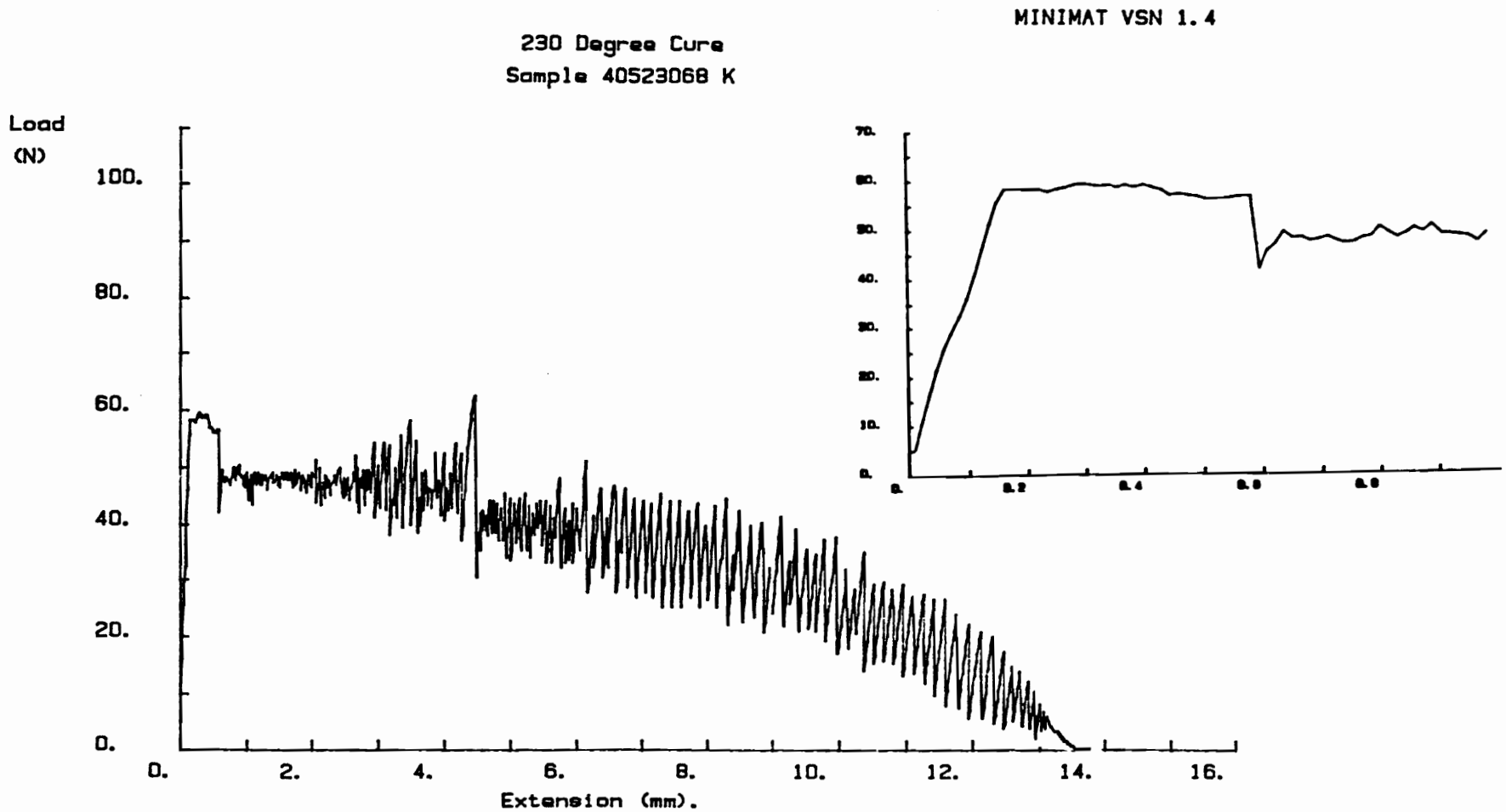

Figure 30. Load versus extension trace from the 230°C sample set. The debonding region of the trace is exploded to show the frictional effects on the debonding load.

5.4.2 The Coefficient of Friction

The coefficient of friction has been determined from both the slope of the debonding frictional region and the tail of the pull-out trace using:

$$\tau = \mu p \qquad (63)\ [46]$$

where τ is the interfacial shear stress calculated from the appropriate place on the trace, and p is the normal pressure on the fiber resulting from chemical shrinkage and thermal mismatch during cure. The averages of the various interfacial shear stress terms are listed in Table 14 along with the coefficients of friction which were determined by implementing values for the normal pressure as determined with Harris's equation.

Table 14. Various interfacial shear stresses in MPa and coefficients of friction for the same experimnetal values implemented in the determination of the critical strain energy release rate.

Tcure	<tau> bond	<tau> debond	<tau> pull-out	<mu> debond, Harris	<mu> pull-out, Harris
150	197 ± 67	493 ± 238	9.85 ± 3.2	26	0.52
230	319 ± 39	516 ± 205	20.7 ± 0.97	10.89	0.597

The values of the interfacial shear stresses are not as sensitive to the change in the polymeric properties due to cure. For τ_{bond}, this may be due to the use of the visually-determined debond lengths combined with the assumption of a stress-free edge. This assumption is inappropriate with the consideration of these small lengths. The determination of the interfacial shear stress during the debond region, as well as the fracture energy associated with this region is very complex. Here, the change in

load required to continue the propagation of the crack front along the high frictional portion of the fiber was independent of cure temperature. Thus, the statistically same values for τ_{debond} were found. In the analysis of this region from an energy approach, frictional effects as determined from pull-out and not debond, were implemented. For a better understanding of the events occurring during the crack propagation between fiber and polymer matrix, the viscoelastic response of the material will need to be addressed as will the complex three dimensional path of the crack front, etc.

5.5 Summation

For the evaluation of the single fiber pull-out test and its sensitivity and dependencies on the embedding polymer matrix, a controlled cure study was conducted. By the selection of particular cure cycles the physical parameters of the embedding resin were modified and characterized in a controlled way. Through the optimization of the current experimental procedure, the failure process of the single fiber composite was also characterized. By evaluating these two sets of information, the following discussion emerged.

First, the extent of standard deviation associated with the single fiber pull-out test was the result of many variables. In this work in particular, the fiber axis alignment and especially the condition of the initial notch were critical. Manually impinging the dogbone specimen with a cold razor blade introduced a great deal of variability to the quality of the notch; angle and sharpness at the fiber/resin contact area were not easily controlled. This

problem could be addressed in future efforts by developing a simple spring loaded system such that a razors edge impinges on the specimen at a reproducible angle and intensity.

While definitive conclusions between changes in cure temperature of 20°C cannot be made, the hypotheses are supported by the trend of the data. Specifically, the theories presented in the literature described the relationship of the residual stress in the polymer resin with the cure temperature and ultimate T_g. Based on these theories it was expected that as the cure temperature increased the internal stresses increased. In regards to an embedded fiber, as the internal stresses increase, the normal pressure exerted by the matrix onto the fiber also increase. This increase in mechanical clamping would then be reflected in the strain energy release rate and/or the interfacial shear stress at crack initiation. Further, when T_{cure} resulted in chemical crosslinking occurring in a pseudo-rubbery state, the resulting normal pressures would diminish and also be reflected in the fracture of the specimen. Figure 28 clearly displayed this trend.

In order to present a quantitative evaluation of these results, two statistically different sets of results were addressed. The 150° and 230°C cure cycle data sets accommodated an interesting evaluation of the single fiber pull-out test and the correlation of the polymeric properties to the fracture mechanics of the test. Based on the T_g, percent conversion, and relative changes in volume with cure, these two data sets represent an

incomplete and completely cured (by TMA) polymer matrix, both of which were likely cured in the glassy state.

For the comparison between these two data sets, Table 15 is presented. Listed are the physical parameters of the polymer resin, i.e., T_g, normal pressure calculated from Harris's equation, and the values from the single fiber pull-out test, i.e., strain energy release rate, interfacial shear stresses and the coefficient of friction.

Table 15. Descriptors of the 150 and 230°C cure sets

Tcure, °C	Tg, °C	Normal Pressure, MPa -Harris		<mu>p-o, -Harris
150	180	28.38 ± 1.2		0.52
230	260	70.63 ± 6.56		0.597

Tcure, °C	Ginitiate, N/m --Gao	normal pressure, MPa -Gao	<mu>p-o, -Gao
150	1420 ± 982	14.95 ± 0.6	0.659
230	3602 ± 868	34.68 ± 3.2	0.597

<iss>p-o
9.85 ± 3.2
20.7 ± 0.97

By increasing the cure temperature from 150 to 230°C for the two hour cure period, the residual pressure increased by a factor of 2.4. Changes in the strain energy release rate and sliding interfacial shear stress of pull-out were 2.54 and 2.1 fold, respectively. The coefficient of friction, implementing normal pressures determined by both fracture- and polymer-based approaches, remained constant within experimental error as it should for a given material whose only variable is residual pressure.

Chapter 6

Conclusions

To accomplish the objective of this work i.e., test the sensitivity of the single fiber pull-out test to the physical parameters of the polymer matrix, a series of experiments with a progressively decreasing number of variables were conducted. Initially, the single fiber pull-out test was characterized and the dependence of the results on experimental parameters such as notch conditions, fiber alignment, clamping methods and rate of clamp displacement were addressed. This was followed by the evaluation of the fiber coating/embedding matrix combination. The determination of the strain energy release rate and interfacial shear stress of a polyimide-coated optical fiber embedded in an uncatalyzed TGDDM/DDS epoxy system as a function of the relative shrinkage of the resin with cure was then studied.

On the interpretation of the load versus extension traces from the single fiber pull-out tests, the following analysis of the data was made. With displacement of the clamping mechanism of the tensile stage, a load was introduced to the single fiber composite. In response to this load, the

material behaved with linear elasticity. This linear elastic behavior continued until the interfacial crack, which was present after the initial notch, began to propagate. With this initiation of debond propagation, the contribution of frictional forces to the dissipation of energy was significant for most of the material combinations. This resulted in what was termed the primary frictional zone. As clamp displacement continued, the effects of the frictional forces began to diminish due to Poisson's contraction of the fiber. At some fiber length, which was fiber, resin and thermal history dependent, the debonding became a steady-state event and the load required for crack propagation became a constant.

With completion of debonding the load carried by the system dropped to a value associated with the energy dissipated by frictional sliding. As the length of the fiber resident in the matrix became less than the critical length associated with the primary friction zone, the load carried by the materials began to decrease with reduced resident length.

Based on this interpretation of the single fiber pull-out test, the use of values from the load versus extension trace can be quantitatively evaluated. The quantitative interpretation of the single fiber pull-out test can be accomplished from both the data associated with fiber debond and fiber pull-out. In regards to the debonding process, the various events can be numerically characterized in the following way. The stress associated with the initiation of crack propagation can be interpreted via the critical strain energy release rate assuming a stress free edge and no friction, equation

[6], and/or the interfacial shear stress of the interface, equation [39]. The strain energy release rate can be determined during the propagation of the crack front along some known debond length with the consideration of the friction forces via equation [21]. At sufficiently long debond lengths, steady-state crack propagation occurs such that frictional forces are relatively constant over some critical fiber length. Here, the strain energy release rate is a maximum and this value in combination with the critical fiber length are key parameters for quantitatively describing the failure of the material. In regards to the fiber pull-out data, the stress associated with frictional sliding combined with the stick-slip activity describe the residual mechanical interaction between the debonded fiber and the surrounding matrix. With final removal of the fiber, the critical length of fiber associated with the primary frictional zone can be estimated and the interfacial shear stress of sliding and, thus, the coefficient of friction determined. To date, the quantitative evaluation of the single fiber pull-out test has been primarily reported as the maximum load required to debond the fiber from the resin. Because variables of the experiment are not addressed, this type of reporting does not accommodate meaningful data comparisons between laboratories. In order to build a data base of information regarding the removal of fibers from neat resin, data reduction methods such as those employed here should be implemented.

For various fiber/coating/resin combinations, the characterization of the single fiber pull-out experiment was accomplished through the analysis of the loading, debonding and friction of a given fiber/resin combination. It

was found that the physical properties of the fiber coating and the combined chemistry and thermal cure cycle of the embedding resin substantially effected the results of the single fiber pull-out test. Not only were the stresses associated with crack initiation a function of resin properties but crack propagation and fiber sliding properties were affected as well. The detailed interpretation of these results were limited due to insufficient physical data pertaining to the embedding resins.

The final series of experiments were designed to evaluate the induced thermal stresses due to the cure cycle and the effect of these stresses on the single fiber pull-out test results. Here, the TGDDM/DDS epoxy matrix, which was cured at different temperatures for the same amount of time, was characterized through the determination of the relative extent of cure, the degree of shrinkage with cure and the glass transition temperature.

Based on the earlier discussion of the relationship between T_g and T_{cure} and the associated changes in density and specific volume were expected to be seen in the results of the single fiber pull-out test. Here, the normal pressure the resin exerted on the embedded fiber when $T_{cure} < T_g$ was the result of chemical shrinkage post-vitrification plus the extent of thermal contraction upon cooling. For the cure process where T_{cure} approached T_g, the normal pressure exerted on a fiber embedded in a resin was primarily the result of thermal contraction of cooling from T_g to $T_{R.T.}$. The effect of the T_{cure} : T_g relationship was to increase the critical strain energy release rate as T_{cure} increased until the glass transition range was entered. This was

the result of the normal pressure on the fiber resulting from both crosslinking densification and thermal contraction. At $T_{cure} = T_g - 10°C$, the material was approaching the rubbery state, the build up of internal stresses due to crosslinking were reduced and the overall normal pressure was primarily a function of thermal contraction upon cooling. Thus, a net reduction in the strain energy release rate resulted when the specimen was cured at a temperature near T_g.

It was found that over small temperature increments between sample sets, a statistical difference between fracture values could be not demonstrated. However, the trend of the data supported the hypothesis that incremental changes in the polymer-based material parameters effect the mechanical failure of the single fiber composite. By evaluating sample sets with a larger difference in cure temperature, 150 and 230°C, an excellent correlation between the polymeric properties and the fracture mechanics of the single fiber pull-out test was made.

For the quantitative interpretation of these single fiber pull-out test results, a mechanistic approach was used to determine the strain energy release rate for both initiation without friction and for propagation with friction. Also, the interfacial shear stresses associated with initiation, debond propagation and sliding were determined. From the results of the previously-mentioned experiments, the normal pressure on the fiber was determined independently from 1) the polymer characterization experiments and 2) the fracture mechanics experiments. For the

determination of the normal pressure from polymer parameters the relative change in volume via TMA and Harris's equation were employed. For the determination from the fracture experiments via the single fiber pull-out tests Gao's equation was employed. These two approaches each determined the increase in normal pressure with elevated cure temperature to increase by a factor of 2.4. This increase was observed in the debonding data via a factor of 2.5 increase in $<G_{initiate}>$, and the pull-out data via a factor of 2.1 increase in $<\tau>_{init}$.

In conclusion, the single fiber pull-out test was found to be a viable means of modeling the interfacial failure of an embedded fiber loaded in tension. This test method can be used not only for the evaluation of fiber surface treatments as it has in the past, but also to relate the physical properties of the embedding resin to the failure mechanism of the single fiber composite.

Chapter 7

Future Work

The initial motivation of this work involved the attaching or embedding of optical fiber sensors on or in a structure of interest. To this end, questions regarding the adhesion between fiber and matrix and the extent to which the fiber would respond to perturbations in the structure arose. To partially answer these questions the single fiber pull-put test was employed to evaluate stress transfer between matrix and fiber and the locus of failure as well as the effects of various fiber coating and embedding resin materials.

Historically, the single fiber pull-out test was developed as a model for the failure of fiber reinforced materials. With the current understanding and interpretation of this model and the ability to quantify the experimental results, this test could also be employed for other evaluative efforts. Here, improvements on stress transfer could be made by determining the optimal fiber/coating/resin combination for the development of a given sensor or by developing a matrix/coating and coating/fiber interphase with graded properties i.e., modulus.

The experimental apparatus employed in this work could readily be used for the evaluation of the fiber/coating/matrix interface region post exposure to non-ideal environments and/or mechanical aging. This could help in the evaluation of both sensor sensitivity and long term performance.

Finally, through the complete characterization of the fiber/matrix debonding event as described here, the extent of material damage could be assessed. Specifically, based on the response of a strain sensor undergoing interfacial failure and fiber bridging, a non-linear sensor response to structural loading might indicate the initiation of crack propagation at the interface. This would be indicative of ply delamination for example. As the crack would progress, the debonded fiber would first experience a significant amount of interfacial friction. However, as has been shown, once a critical length of fiber has debonded, the frictional dissipation of energy is diminished and steady-state crack propagation occurs.

The initiation of the interfacial crack as well as the debonding with increasing friction and constant friction could be detected with the appropriate optical fiber sensor. In regards to the output signal of the sensor, the response should reflect the degree of stress transfer between sensor and matrix. Thus one would know if steady-state debonding has been attained and thus if the degree of failure is to the point of steady-state propagation and near strain induced sensor failure.

References

1. Chambers and McGarry, 14th Annual Technology and Management Conference, Reinforced Plastics Division, SPI, (February 1957), Section 12-B.

2. Haslett and McGarry, 17th Annual Technology and Management Conference, Reinforced Plastics Division, SPI, (February 1962), Section 14-D.

3. Kelly, A. and Tyson, W.R., "Tensile Properties of Fibre-Reinforced Metals: Copper/Tungsten and Copper/Molybdenum," Journal of Mechanics and Physics of Solids, 13, (1965), 329-350.

4. Broutman, L.J., "Glass-Resin Joint Strengths and Their Effect on Failure Mechanisms in Reinforced Plastics," Polymer Engineering and Science, (July, 1966), 263-272.

5. Broutman, L.J., "Measurement of the Fiber-Polymer Matrix Interfacial Strength," Interfaces in Composites, ASTM STP 452, (1969), 27-41.

6. Greszczuk, L.B., "Theoretical Studies of the Mechanics of the Fiber-Matrix Interface in Composites," Interfaces in Composites, ASTM STP 452, (1969), 42-58.

7. Outwater, J.O. and Murphy, M.C., "On the Fracture Energy of Unidirectional Laminates," 24th Annual Technical Conference, Reinforced Plastics/Composites Division, The Society of the Plastics Industry, Inc., (1969) Section 11-C, 1-8.

8. Kelly, A., "Interfacial Effects and the Work of Fracture of a Fibrous Composite," Proceedings of the Royal Society A, 319, (1970), 95-116.

9. Favre, J.P. and Perrin, J., "Carbon Fibre Adhesion to Organic Matrices," Journal of Materials Science, 7, (1972), 1113-1118.

10. Lawrence, P., "Some Theoretical Considerations of Fibre Pull-Out From an Elastic Matrix," Journal of Materials Science, 7, (1972), 1-6.

11. Takaku, A. and Arridge, R.G.C., "The Effect of Interfacial Radial and Shear Stress on Fibre Pull-Out in Composite Materials," Journal of Physics D: Applied Physics, 6, (1973), 2038-2047.

12. Morton, J. and Groves, G.W., "The Effect of Metal Wires on the Fracture of a Brittle-Matrix Composite," Journal of Materials Science, 11, (1976), 617-622.

13. Hadjis, N.and Piggott, M.R., "The Effect of Matrix Stresses on Fibre Pull-Out Forces," Journal of Materials Science, 12, (1977), 358-364.

14. Bowling, J. and Groves, G.W., "The Debonding and Pull-Out of Ductile Wires From a Brittle Matrix," Journal of Materials Science, 14, (1979), 431-442.

15. Bowling, J. and Groves, G.W., "The Propagation of Cracks in Composites Consisting of Ductile Wires in a Brittle Matrix," Journal of Materials Science, 14, (1979), 443-449.

16. Drzal, L.T., Rich, M.J. and Lloyd, P.F., "Adhesion of Graphite Fibers to Epoxy Matrices: I. The Role of Fiber Surface Treatment," Journal of Adhesion, 16, (1982), 1-30.

17. Emadipour, H., Chiang, P. and Koenig, J.L., "Interfacial Strength Studies of Fibre-Reinforced Composites," Res Mechanica, 5, (1982), 165-176.

18. Drzal, L.T., Rich, M.J., Koenig, M.F. and Lloyd, P.F., "Adhesion of Graphite Fibers to Epoxy Matrices: II. The Effect of Fiber Finish," Journal of Adhesion, 16, (1983), 133-152.

19. Bascom, W.D., Boll, D.J., Fuller, B. and Phillips, P.J., "Fractography of the Interlaminar Fracture of Carbon Fibre Epoxy Composites," Journal of Materials Science, 20, (1985), 3184-3190.

20. Chua, P.S. and Piggott, M.R., "The Glass Fibre-Polymer Interface: I - Theoretical Considerations for Single Fiber Pull-Out Tests," Composites Science and Technology, 22, (1985), 33-42.

21. Chua, P.S. and Piggott, M.R., "The Glass Fibre-Polymer Interface: II - Work of Fracture and Shear Stress," Composites Science and Technology, 22, (1985), 107-119.

22. Chua, P.S. and Piggott, M.R., "The Glass Fibre-Polymer Interface: III - Pressure and the Coefficient of Friction," Composites Science and Technology, 22, (1985), 185-196.

23. Bascom, W.D. and Jensen, R.M., "Stress Transfer in Single Fiber/Resin Tensile Tests," Journal of Adhesion, 19, (1986), 219-239.

24. DiBenedetto, A.T., Nicolais, L., Ambrosio, L. and Groeger, J., "Stress Transfer and Fracture in Single Fiber/Epoxy Composites," in Composite Interfaces H. Ishida and J.L. Koenig, eds., Elsvier Science Publishing Co. Inc., (1986), 47-54.

25. Piggott, M.R., Sanadi, A., Chua, P.S. and Andison, D., "Mechanical Interactions in the Interphasial Region of Fibre Reinforced Thermosets," in Composite Interfaces, eds. H. Ishida and J.L. Koenig, (Elsvier Science Publishing Co. Inc, (1986), 109-121.

26. Miller, B., Muri, P. and Rebenfeld, L., "A Microbond Method for Determination of the Shear Strength of a Fiber/Resin Interface," Composites Science and Technology, 28, (1987), 17-32.

27. Parry, T.V. Wilson, J.M. and Leck, D.C., "Pull-out of Steel Fasteners From a Laminated Composite Subjected to External Pressure," Composites Science and Technology, 28, (1987), 279-290.

28. Piggott, M.R., "Debonding and Friction at Fibre-Polymer Interfaces, I. Criteria for Failure and Sliding," Composites Science and Technology, 30, (1987), 295-306.

29. Piggott, M.R., "The Effect of the Interface/Interphase on Fiber Composite Properties," Polymer Composites, 8, No. 5, (October, 1987), 291-297.

30. Piggott, M.R. and Andison, D., "The Carbon Fibre-Epoxy Interface," Journal of Reinforced Plastics and Composites, 6, (July, 1987), 290-302.

31. Piggott, M.R. and Chua, P.S., "Recent Studies of the Glass Fiber-Polymer Interphase," Industrial and Engineering Chemistry Research, 26, No. 4, (1987), 672-677.

32. Desio, G.P., Miller, B. and Rebenfeld, L., "The Microbond Method for the Evaluation of Interfacial Shear Strengths of Composites," AIChE Annual Meeting, Washington, D.C., November 28, 1988.

33. Gao, Y-C., Mai, Y-W and Cotterell, B., "Fracture of Fiber-Reinforced Materials," Journal of Applied Mathematics and Physics (ZAMP), 39, (July 1988), 550-572.

34. McAlea, K.P. and Besio, G.J., "Adhesion Between PBT and E-Glass Measured with a Microdebond Technique," Polymer Composites, 9, No. 4, (August, 1988), 285-290.

35. Morrison, J.K., Shah, S.P. and Jeng, Y-S, "Analysis of Fiber Debonding and Pull-Out in Composites," Journal of Engineering Mechanics, 114, No. 2, (February 1988), 277-295.

36. Narkis, M., Chen, J.H. and Pipes, R.B., "Review of Methods for Characterization of Interfacial Fiber-Matrix Interaction," Polymer Composites, 9, No. 4, (August, 1988), 245-251.

37. Piggott, M.R., "Debonding and Friction at Fibre-Polymer Interfaces, II. Macroscopic Model Experiments," Composites Science and Technology, 31, (1988), 15-24 .

38. Waite, S.R. and Sage, G.N., "The Failure of Optical Fibers Embedded in Composite Materials," Composites, 19, No.4, (July, 1988), 288-294.

39. Argawal, R.K. and Drzal, L.T., "Effects of Microwave Processing on Fiber-Matrix Adhesion in Composites," Journal of Adhesion, 29, (1989), 63-79.

40. Cook, R.F., Thouless, M.D., Clarke, D.R. and Kroll, M.C., "Stick-Slip During Fiber Pull-out," Scripta Metallurgica, 23, (1989), 1725-1730.

41. Guar, U. and Miller, B., "Microdebond Method for Determination of the Shear Strength of a Fiber Resin Interface: Evaluation of Experimental Parameters," Composites Science and Technology, 34, (1989), 35-51.

42. Latour, R.A., Black, J. and Miller, R., "Fatigue Behavior Characterization of the Fiber-Matrix Interface," Journal of Materials Science, 24, (1989).

43. Overton, B.J. and Taylor, C.R., "Time Temperature Dependence of Dual Coated Lightguide Pull-Out Measurements," Polymer Engineering and Science, 29, No. 17, (mid-summer, 1989), 1169-1171.

44. Palley, I. and Stevens, D., "A Fracture Mechanics Approach to the Single Fiber Pull-out Problem as Applied to the Evaluation of the Adhesion Strength Between the Fiber and the Matrix," Journal of Adhesion Science and Technology, 3, No.2, (1989), 141-153.

45. Penn, L.S. and Jutis, B., "The Effect of Pendent Groups at the Fiber Surface on Interfacial Adhesion," Journal of Adhesion, 30, (1989), 67-81.

46. Penn, L.S. and Lee, S.M., "Interpretation of Experimental Results in the Single Pull-Out Filament Test," Journal of Composites Technology and Research, JCTRER, 11, No. 1, (Spring 1989), 23-30.

47. Piggott, M.R. and Roberedo, M.M., "The Properties of the Interface Between Fibers and Polymers," 34th International SAMPE Symposium, (May 8-11, 1989), 1913-.

48. Sigl, L.S. and Evans, A.G., "Effects of Residual Stress and Frictional Sliding on Cracking and Pull-Out in Brittle Matrix Composites," Mechanics of Materials, 8, (1989), 1-12.

49. Gaur, U. and Miller, B. "Effects of Environmental Exposure on Fiber/Epoxy Interfacial Shear Strength," Polymer Composites, 11, No. 4, (August, 1990), 217-222.

50. Hutchinson, J.W. and Jensen,H.M, "Model of Fiber Debonding and Pull-Out in Brittle Composites with Friction," Mechanics of Materials, 9, (1990), 139-163.

51. Lee, S.M. and Holguin, S., "A New Single Fiber/Resin Interface Test for High Crosslinked Resin Systems," Journal of Adhesion, 31, (1990), 91-101.

52. Leung, C.K.Y. and Li, V.C., "Applications of a Two-Way Debonding Theory to Short Fibre Composites," Composites, 21, No.4, (July, 1990), 305-317.

53. Mäder, E. and Freitag, K-H., "Interface Properties and Their Influence on Short Fibre Composites," Composites, 21, No. 5, (September 1990), 397-402.

54. Penn, L.S. and Chou, C.T., "Identification of Factors Affecting Single Filament Pull-Out Test Results," Journal of Composites Technology and Research, JCTRER, 12, No.3, (Fall, 1990), 164-171.

55. Pitkethly, M.J. and Doble, J.B., "Characterizing the Fiber/Matrix Interface of Carbon Fibre-Reinforced Composites Using a Single Fiber Pull-Out Test," Composites, 21, No. 5, (September, 1990), 389-395.

56. Biro, D.A., McLean, P. and Deslandes, Y., "Application of the Microbond Technique: Characterization of Carbon-Epoxy Interfaces," Polymer Engineering and Science, 37, No.17, (mid-September, 1991), 1250-1256.

57. Chou, C.T. and Penn, L.S., "Chemical Bonding and Physical Interaction by Attached Chains at the Fiber-Matrix Interface," Journal of Adhesion, 36, (1991), 1125-137.

58. Désarmot, G. and Favre, J-P, "Advances in Pull-Out Testing and Data Analysis," Composites Science and Technology, 42, (1991), 151-187.

59. DiFrancia, C.D., Claus, R.O. Hellgeth, J.W., and Ward, T.C., "Characterization of Polyimide-Coated Optical Fibers for Embedding in Epoxy Resin for the Development of Smart Composite Structures", Proceedings of the Adhesion Society Fourteenth Annual Meeting, (Clearwater, FL), 1991.

60. Hughs, J.D-H., "The Carbon Fibre/Epoxy Interface - A Review," Composites Science and Technology, 41, (1991), 13-45.

61. Marshall, P. and Price, J., "Fibre/Matrix Interface Property Determination," Composites, 22, No. 1, (January, 1991), 53-57.

62. Miller, B., Gaur, U. and Hirt, D., "Measurement and Mechanical Aspects of the Microbond Pull-Out Technique for Obtaining Fiber/Resin Interfacial Strength," Composites Science and Technology, 42, (1991), 207-219.

63. Piggott, M.R., "Failure Processes in the Fibre-Polymer Interphase," Composites Science and Technology, 42, (1991), 57-76.

64. Qui, Y. and Schwartz, P., "A New Method for Study of the Fiber-Matrix Interface in Composites: Single Fiber Pull-Out from a Microcomposite," Journal of Adhesion Science and Technology, 5, No. 9, (1991), 741-756.

65. Rao, V. and Drzal, L.T., "The Dependence of Internal Shear Strength on Matrix and Interphase Properties," 12, No. 1, (1991), 48-56.

66. Wang, S.J., Baptiste, D., Bompard, P. and François, D., " Microscopic Failure Mechanism of a Unidirectional Glass Fiber Composite," Fatigue Fracture of Engineering Materials, 14, No. 4, (1991), 391-403.

67. Jiang, K.R. and Penn, L.S., "Improved Analysis and Experimental Evaluation of the Single Filament Pull-Out Test," Composite Science and Technology, *in press*.

68. Moon, C.K., Lee, J.O. Cho, H.H. and Kim, K.S., "Effect of Diameter and Surface Treatment of Fiber on ISS in Glass Fiber/Epoxy and HDPE," Journal of Applied Polymer Science, 45, (1992), 443-450.

69. Piggott, M.R., "Interfaces Properties and Their Influence of Fiber-Reinforced Polymers" in Composite Applications The Role of Matrix, Fiber, and Interface, eds. T. Vigo and B. Kinzig, (VCH Publishers, Inc. 1992), 221-265.

70. Gerard, G. and Gilbert, A.C., "Photothermoelasticity: An Exploratory Study," Journal of Applied Mechanics, ASME, 24, (1957), 355.

71. Bush, A.J., "Measurement of Stresses in Cast Resins," Modern Plastics, 35, (February, 1958), 143-148.

72. Shimazaki, A. "Volume-Temperature Relation of Epoxy Resin-Acid Anhydride Mixtures with Different Degrees of Crosslinking", Journal of Polymer Science, Part C, No. 23, (1968), 555-568.

73. Fisch, W., Hofmann, W. and Schmid, R., "Chemistry of Epoxide Resins. XVII. Influence of Structure and Curing Conditions on the Density, Degree of Cure, and Glass Transition Temperature During Curing of Epoxide Resins", Journal of Applied Polymer Science, 13, (1969), 296-308.

74. Harris, B., "Shrinkage Stresses in Glass/Resin Composites," Journal of Materials Science, 13, (1978), 173-177.

75. Enns, J.B. and Gillham, J.K., "Effect of the Extent of Cure on the Modulus, Glass Transition, Water Absorption, and Density of an Amine-Cured Epoxy", Journal of Applied Polymer Science, 28, (1983), 2831-2846.

76. Cizmecioglu, M., Gupta, A., and Fedors, R.F., "Influence of Cure Conditions on Glass Transition Temperature and Density of an Epoxy Resin", Journal of Applied Polymer Science, 32, (1986), 6177-6190.

77. Jang, B.Z., Hwang, L.R. and Lieu, Y.K., "The Assessment of Interfacial Adhesion," Interfaces in Metal Matrix Composites Proceedings, New Orleans, (March 2-6, 1986), 95-109.

78. Kong, E.S-W., "Physical Aging in Epoxy Matrices and Composites", in Advances in Polymer Science, 80, Epoxy Resins and Composites IV, K. Dusek, ed., (Springer-Verlag Berlin Heidelberg 1986), 125-172.

79. Oleinik, E.F., "Epoxy-Aromatic Amine Networks in the Glassy State. Structure and Properties" in Advances in Polymer Science, 80, Epoxy Resins and Composites IV, K. Dusek, ed., (Springer-Verlag Berlin Heidelberg 1986), 49-100.

80. Whitney, J.M. and Drzal, L.T., "Axisymmetric Stress Distribution Around an Isolated Fiber Fragment," in Toughened Composites, ASTM STP 37, Norman J. Johnston, ed., (ASTM, Philadelphia, 1987), 179-196.

81. Pang, K.P. and Gillham, J.K., "Anomolous Behavior of Cured Epoxy Resins: Density at Room Temperature versus Time and Temperature of Cure," Journal of Applied Polymer Science, 37, (1989), 1969-1991.

82. Taylor, M.A. and Gillham, J.K., "Anomolous Stresses vs Extent of Cure in an Epoxy Composite System," Polymer Materials: Science and Engineering, 61, (Fall, 1989), 806-814.

83. Simon, S.L., Wisanrakkit, G. and Gillham, J.K., "Reaction Kinetics and Calculation of Iso-T_g and Vitrification Curves in the TTT Diagram of a High T_g Epoxy/Amine System," Polymer Materials Science and Engineering, 61, (Fall, 1989), 799-805.

84. Stutz, H. and Mertes, J., "Torsional Braid and Gelation in Thermoset Resins," Journal of Applied Polymer Science, 38, (1989), 781-787.

85. Nimmer, R.P., "Fiber-Matrix Interface Effects in the Presence of Thermally Induced Residual Stresses," Journal of Composite Technology and Research, JCTRER, 12, No. 2, (Summer, 1990), 65-75.

86. Ochi, M., Yamashita, K. and Shimbo, M., " The Mechanism for Occurrence of Internal Stress During Curing Epoxide Reactions," Journal of Applied Polymer Science, 43, (1991), 2013-2019.

87. Tai, D.W. and Penn, L.S., "Relation of Interfacial Adhesion to Residual Stress in Carbon Fiber/Epoxy Composites," Journal of Composite Materials, 25, (November, 1991) 1445-1458.

88. Resnick, R., and Halliday, D., Physics Part I, (Wiley and Sons, 1966).

89. Skrovanek, D.J. and Schoff, "Thermal Mechanical Characterization of Organic Coatings", Progress in Organic Coatings, 16 (1988), 135-163.

90. deBakker, C.J., St. John, N.A. and George, G.A., "Simultaneous DSC-FTIR-NIR Studies of the Cure Kinetics of Epoxy Resins," Polymer Preprints, 33, No. 1, (April, 1992), 374-375.

91. George, G.A., Cole-Clarke, P., St. John, N. and Friend, G., "Real-Time Monitoring of the Cure Reaction of a TGDDM/DDS Epoxy Resin using a Fiber Optic FTIR," Journal of Applied Polymer Science, 42, (1991), 643-657.

92. Jurek, M.J. and McGrath, J.E., "Synthesis and Characterization of Amine Terminated Poly(arylene Ether Sulfone) Oligomers," Polymer, 30, (1989), 1551-1556.

Appendix A

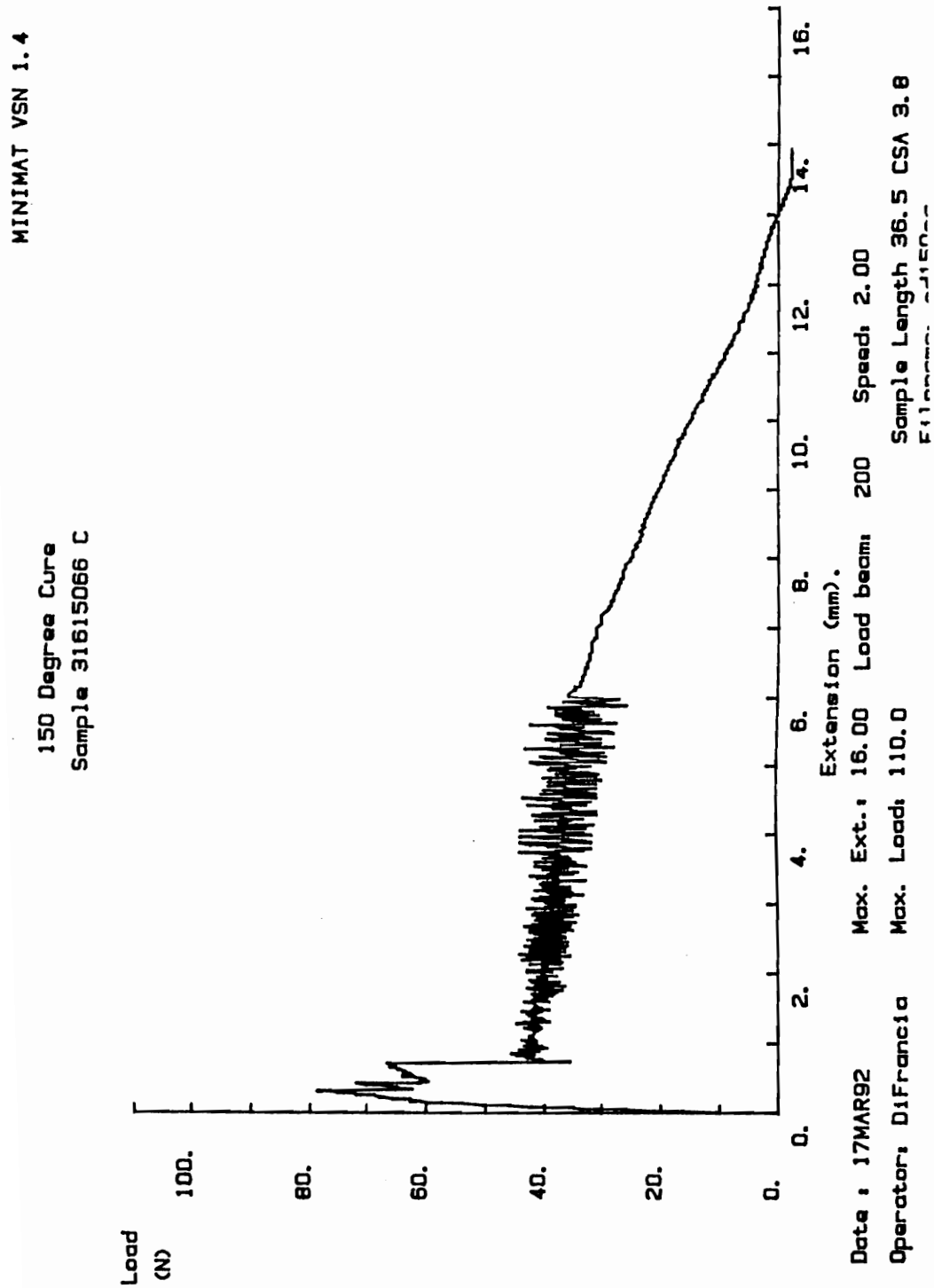
MINIMAT VSN 1.4
150 Degree Cure
Sample 31615066 C
Load
(N)
100.
80.
60.
40.
20.
0.
0.
2.
4.
6.
8.
10.
12.
14.
16.
Extension (mm).
Date : 17MAR92
Max. Ext.: 16.00
Load beam: 200
Speed: 2.00
Operator: DiFrancia
Max. Load: 110.0
Sample Length 36.5 CSA 3.8

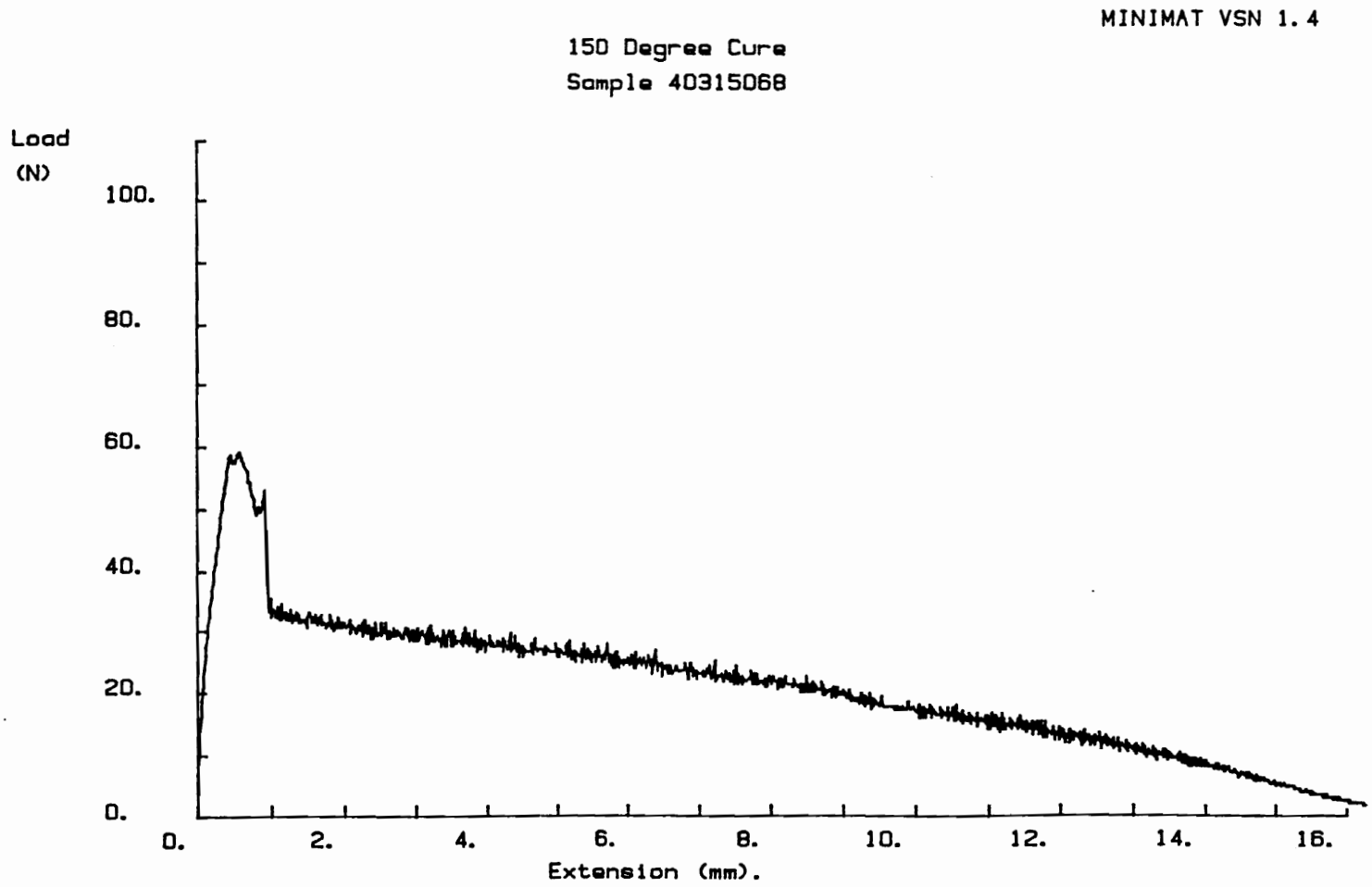
MINIMAT VSN 1.4
150 Degree Cure
Sample 40315068
Load
(N)
100.
80.
60.
40.
20.
0.
0.
2.
4.
6.
8.
10.
12.
14.
16.
Extension (mm).
Date : 04APR92
Max. Ext.: 16.00
Load beam: 200
Speed: 2.00
Operator: DiFrancia
Max. Load: 110.0
Sample Length 30.0 CSA 3.0

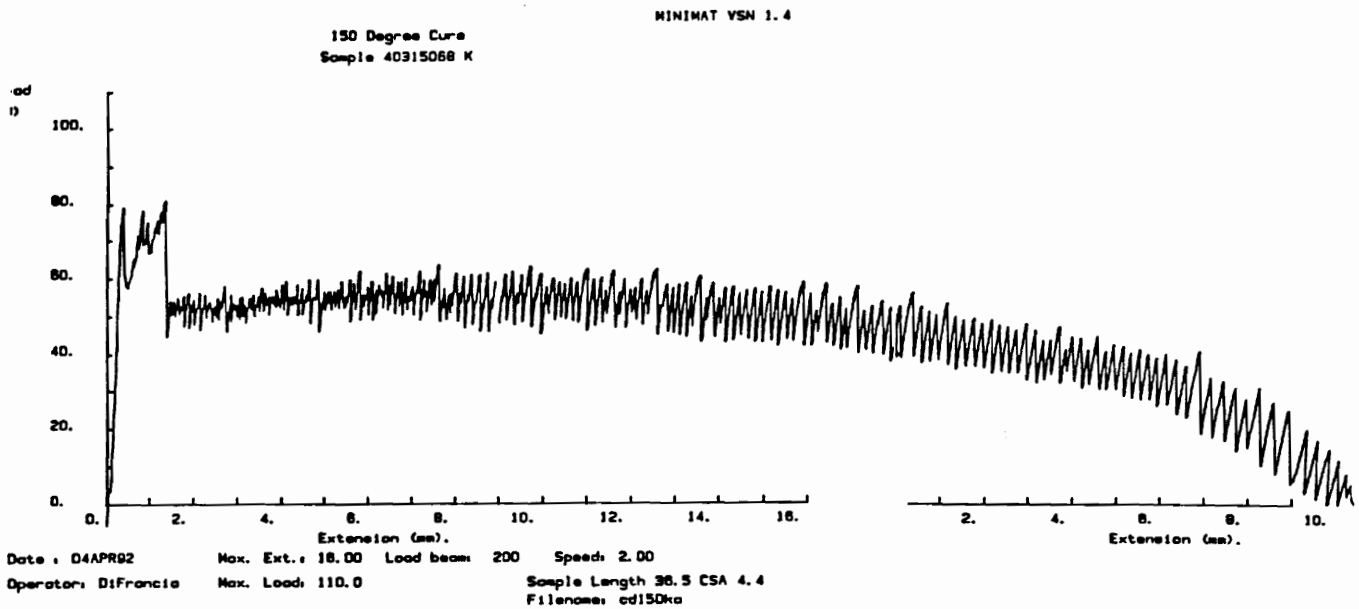
MINIMAT VSN 1.4
150 Degree Cure
Sample 40315068 K
100.
80.
60.
40.
20.
0.
0.
2.
4.
6.
8.
10.
12.
14.
16.
Extension (mm).
2.
4.
6.
8.
10.
Extension (mm).
Date : 04APR92
Max. Ext.: 18.00
Load beam: 200
Speed: 2.00
Operator: DiFrancia
Max. Load: 110.0
Sample Length 36.5 CSA 4.4
Filename: cd150ka

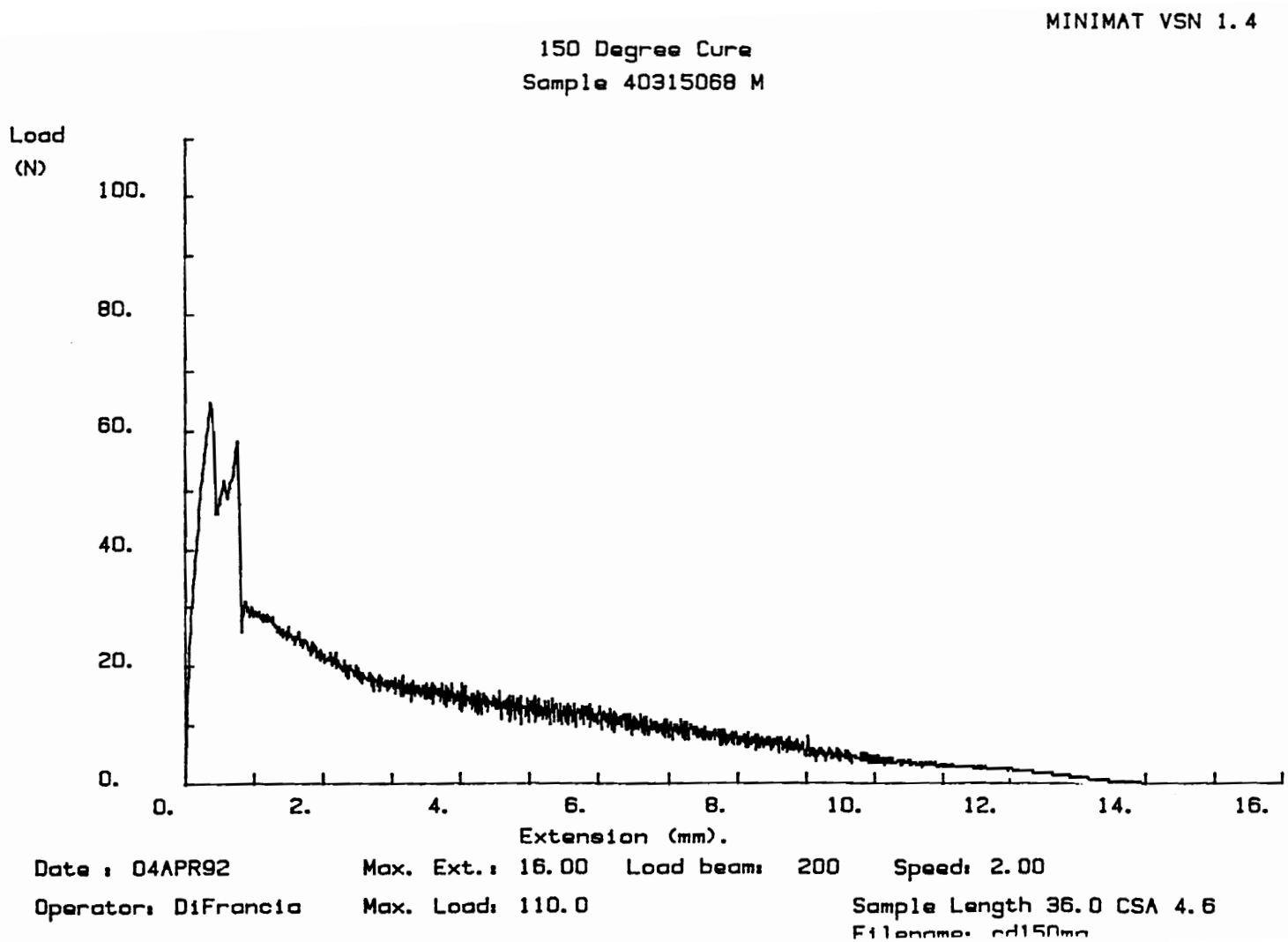
MINIMAT VSN 1.4
150 Degree Cure
Sample 40315068 M
Load
(N)
100.
80.
60.
40.
20.
0.
0.
2.
4.
6.
8.
10.
12.
14.
16.
Extension (mm).
Date : 04APR92
Max. Ext.: 16.00
Load beam: 200
Speed: 2.00
Operator: DiFrancia
Max. Load: 110.0
Sample Length 36.0 CSA 4.6

MINIMAT VSN 1.4

177 Degree Cure
Sample 31717766 B

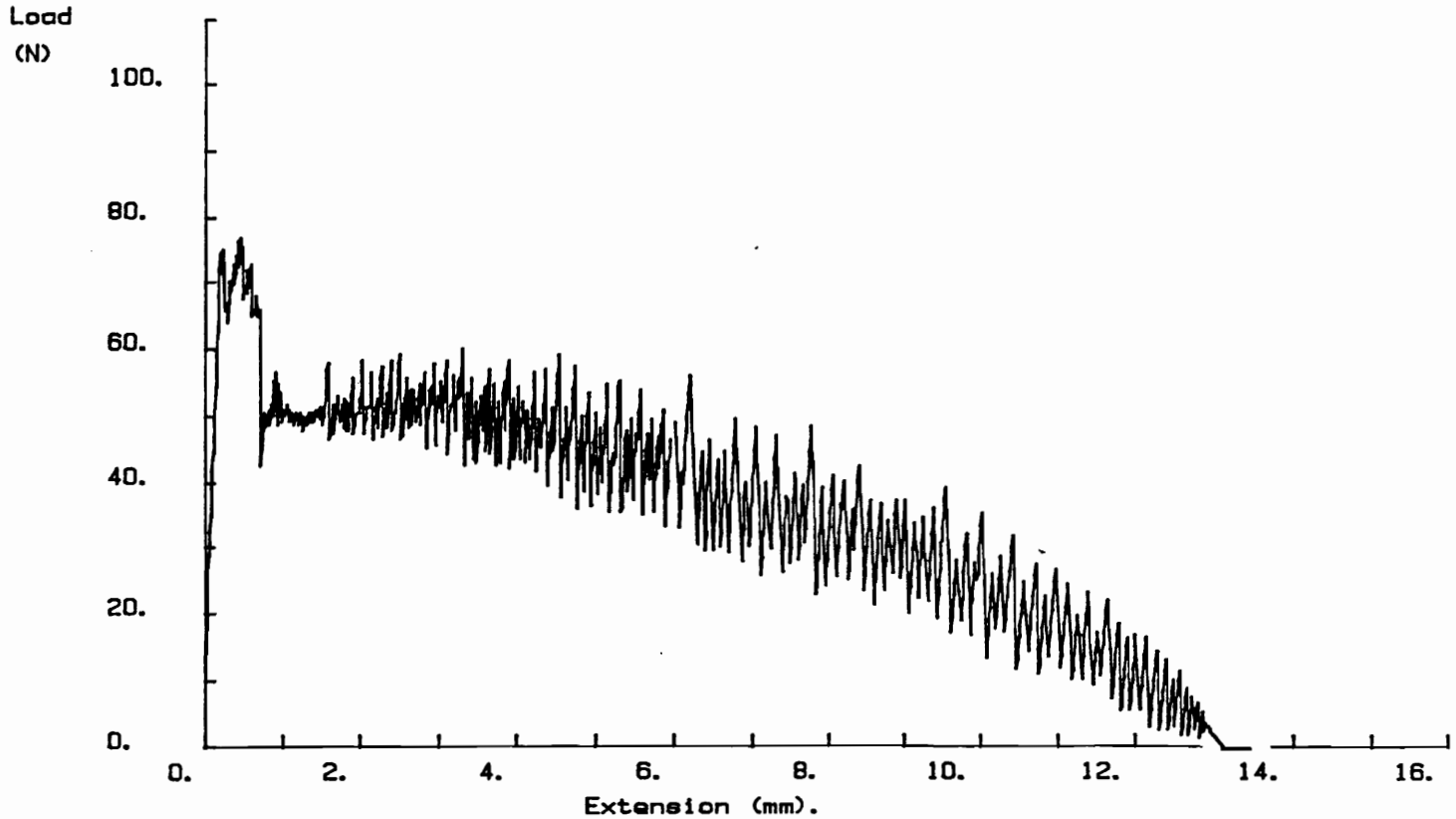

Date : 18MAR92 Max. Ext.: 16.00 Load beam: 200 Speed: 2.00

Operator: DiFrancia Max. Load: 110.0 Sample Length 37.6 CSA 3.5

Filename: cd177ba

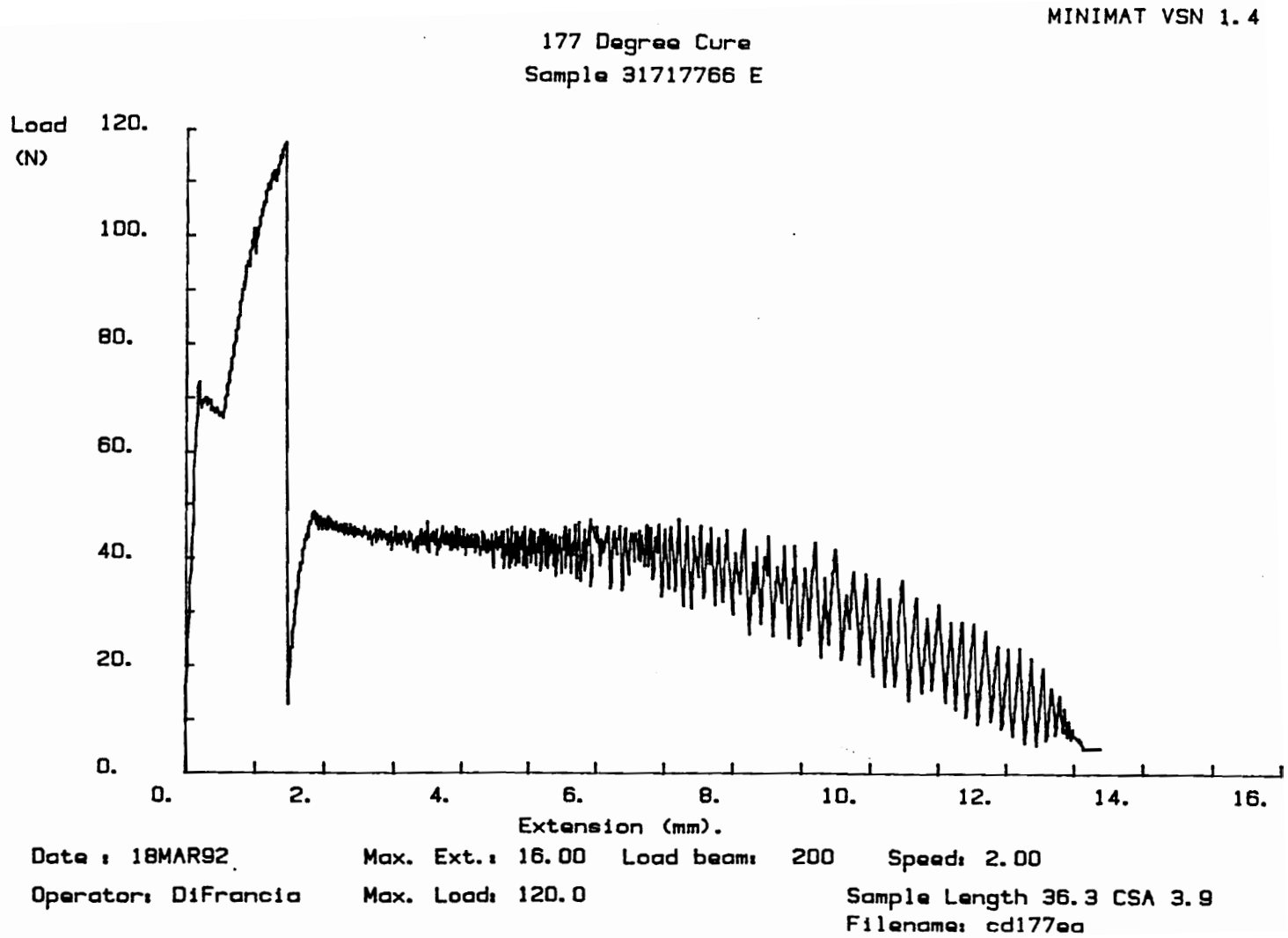
MINIMAT VSN 1.4
177 Degree Cure
Sample 31717766 E
Load
(N)
120.
100.
80.
60.
40.
20.
0.
0.
2.
4.
6.
8.
10.
12.
14.
16.
Extension (mm).
Date : 18MAR92
Max. Ext.: 16.00
Load beam: 200
Speed: 2.00
Operator: DiFrancia
Max. Load: 120.0
Sample Length 36.3 CSA 3.9
Filename: cd177ea

MINIMAT VSN 1.4

177 Degree Cure
Sample 40417768 I

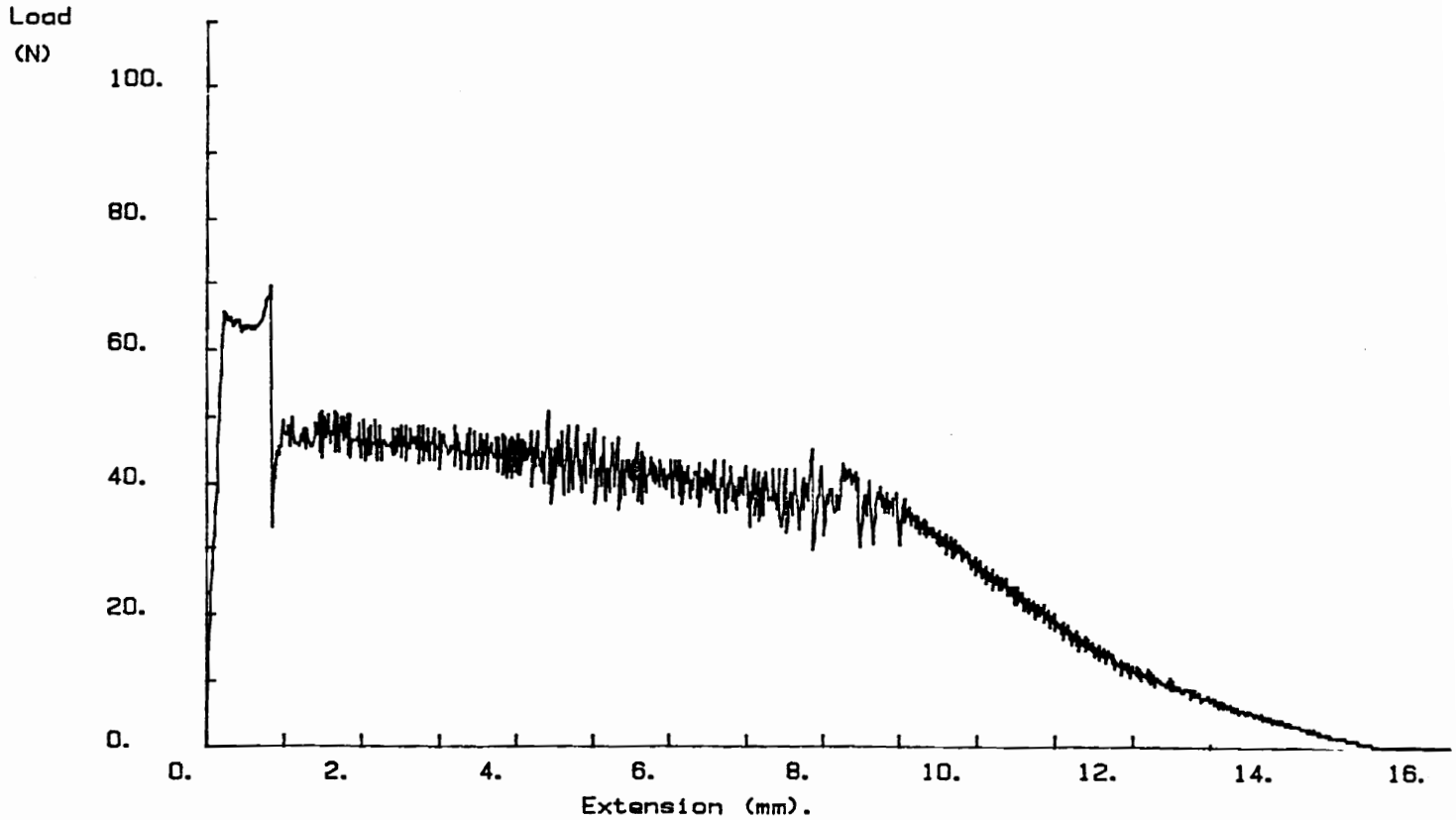

Date : 05APR92 Max. Ext.: 16.00 Load beam: 200 Speed: 2.00

Operator: DiFrancia Max. Load: 110.0 Sample Length 36.7 CSA 4.5

Filename: cd177ia

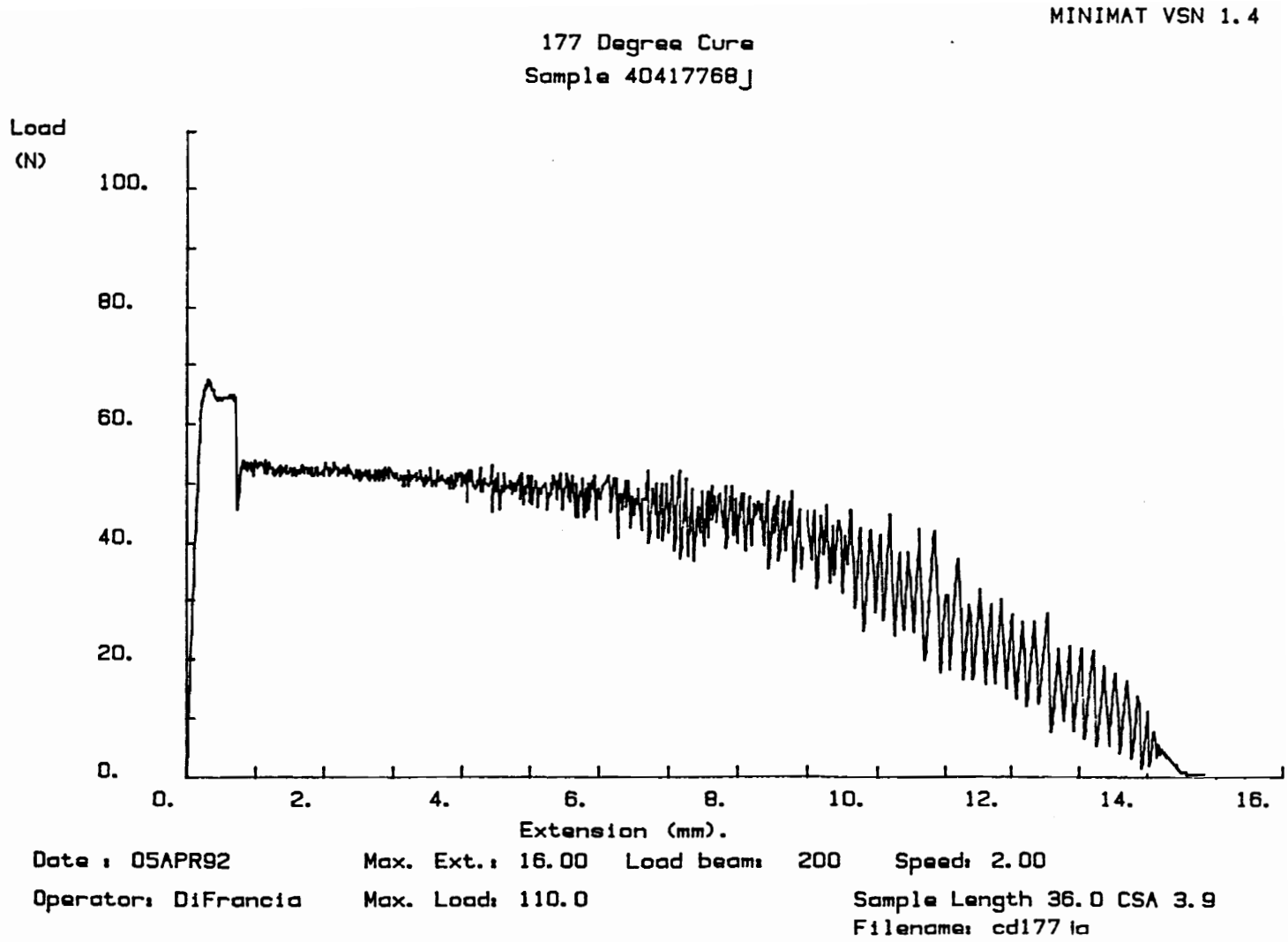
MINIMAT VSN 1.4
177 Degree Cure
Sample 40417768J
Load
(N)
100.
80.
60.
40.
20.
0.
0.
2.
4.
6.
8.
10.
12.
14.
16.
Extension (mm).
Date : 05APR92
Max. Ext.: 16.00
Load beam: 200
Speed: 2.00
Operator: DiFrancia
Max. Load: 110.0
Sample Length 36.0 CSA 3.9
Filename: cd177 ia

MINIMAT VSN 1.4

230 Degree Cure
Sample 31823066 A

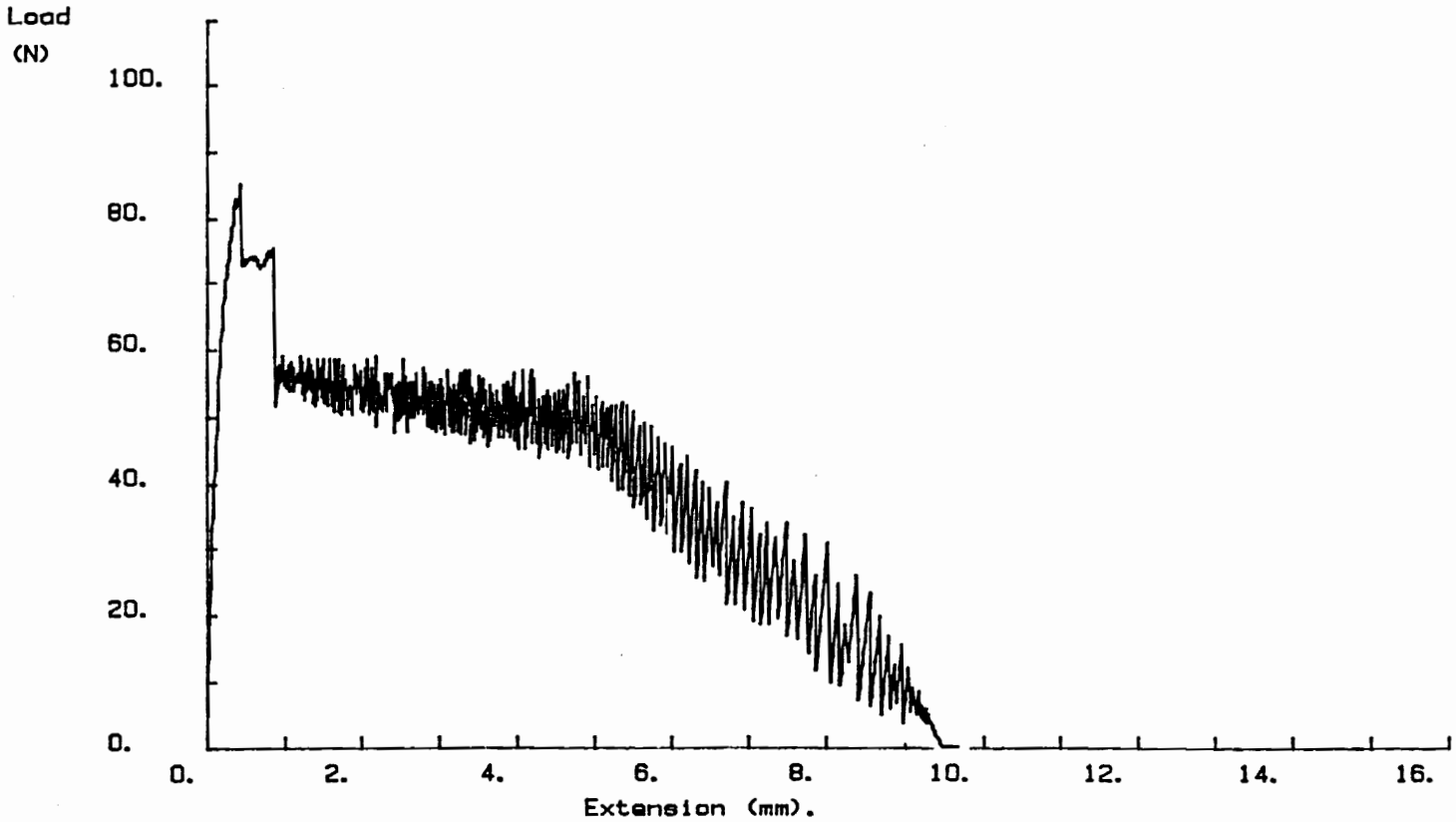

Date : 18MAR92 Max. Ext.: 16.00 Load beam: 200 Speed: 2.00

Operator: DiFrancia Max. Load: 110.0 Sample Length 36.7 CSA 3.4

Filename: cd230aa

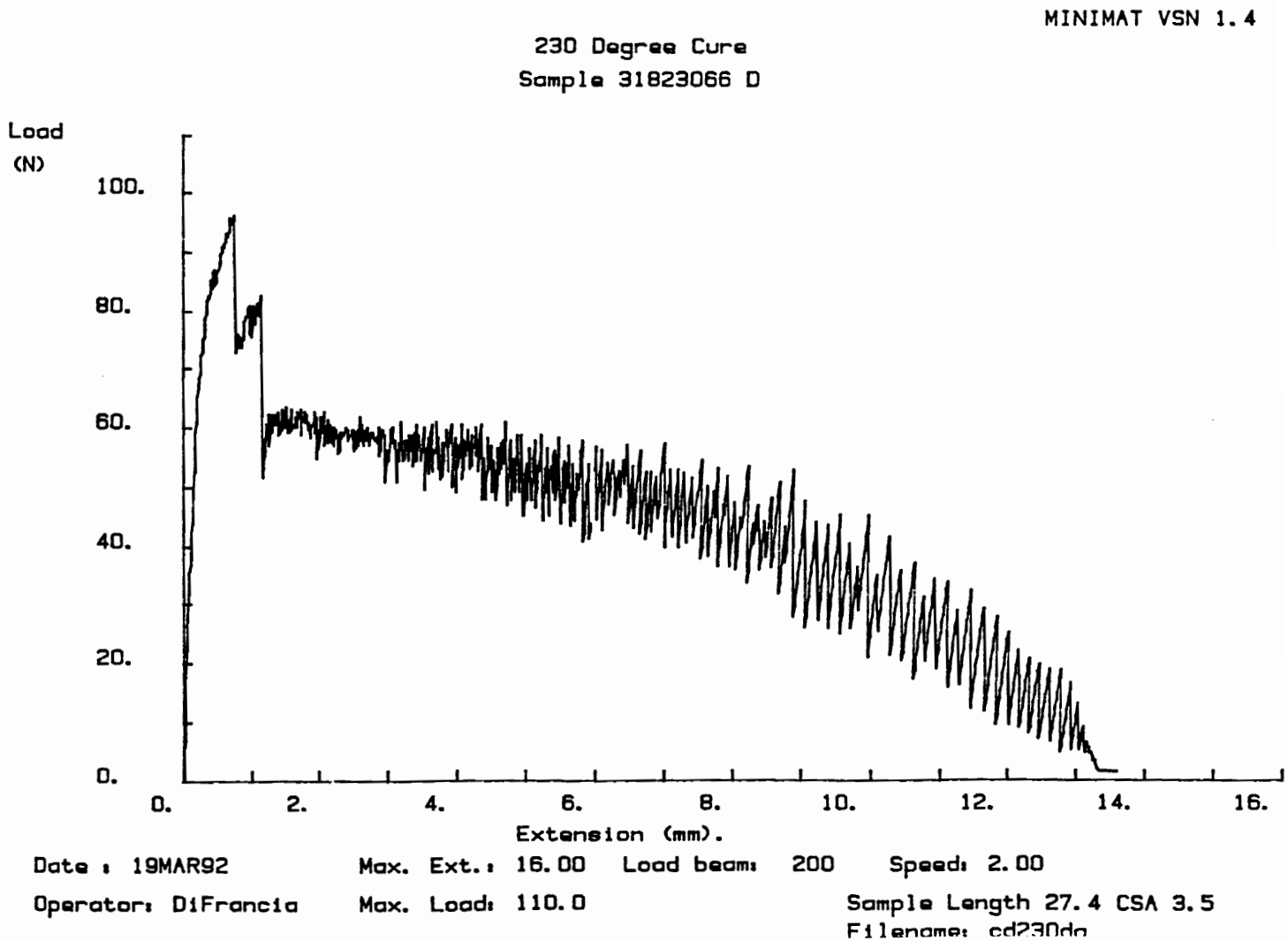
MINIMAT VSN 1.4
230 Degree Cure
Sample 31823066 D
Load
(N)
100.
80.
60.
40.
20.
0.
0.
2.
4.
6.
8.
10.
12.
14.
16.
Extension (mm).
Date : 19MAR92
Max. Ext.: 16.00
Load beam: 200
Speed: 2.00
Operator: DiFrancia
Max. Load: 110.0
Sample Length 27.4 CSA 3.5
Filename: cd230da

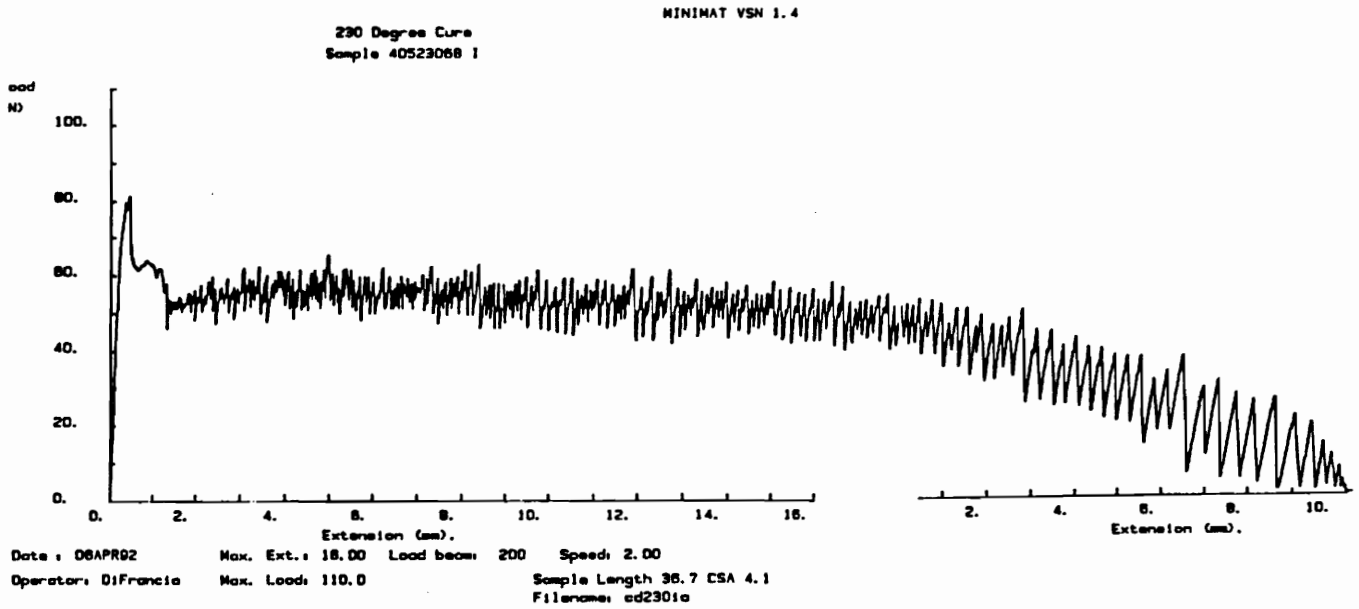
MINIMAT VSN 1.4
230 Degree Cure
Sample 40523068 I
oad
N)
100.
80.
60.
40.
20.
0.
0.
2.
4.
6.
8.
10.
12.
14.
16.
Extension (mm).
2.
4.
6.
8.
10.
Extension (mm).
Date : 08APR92
Max. Ext.: 18.00
Load beam: 200
Speed: 2.00
Operator: DiFrancia
Max. Load: 110.0
Sample Length 36.7 CSA 4.1
Filename: cd230ia

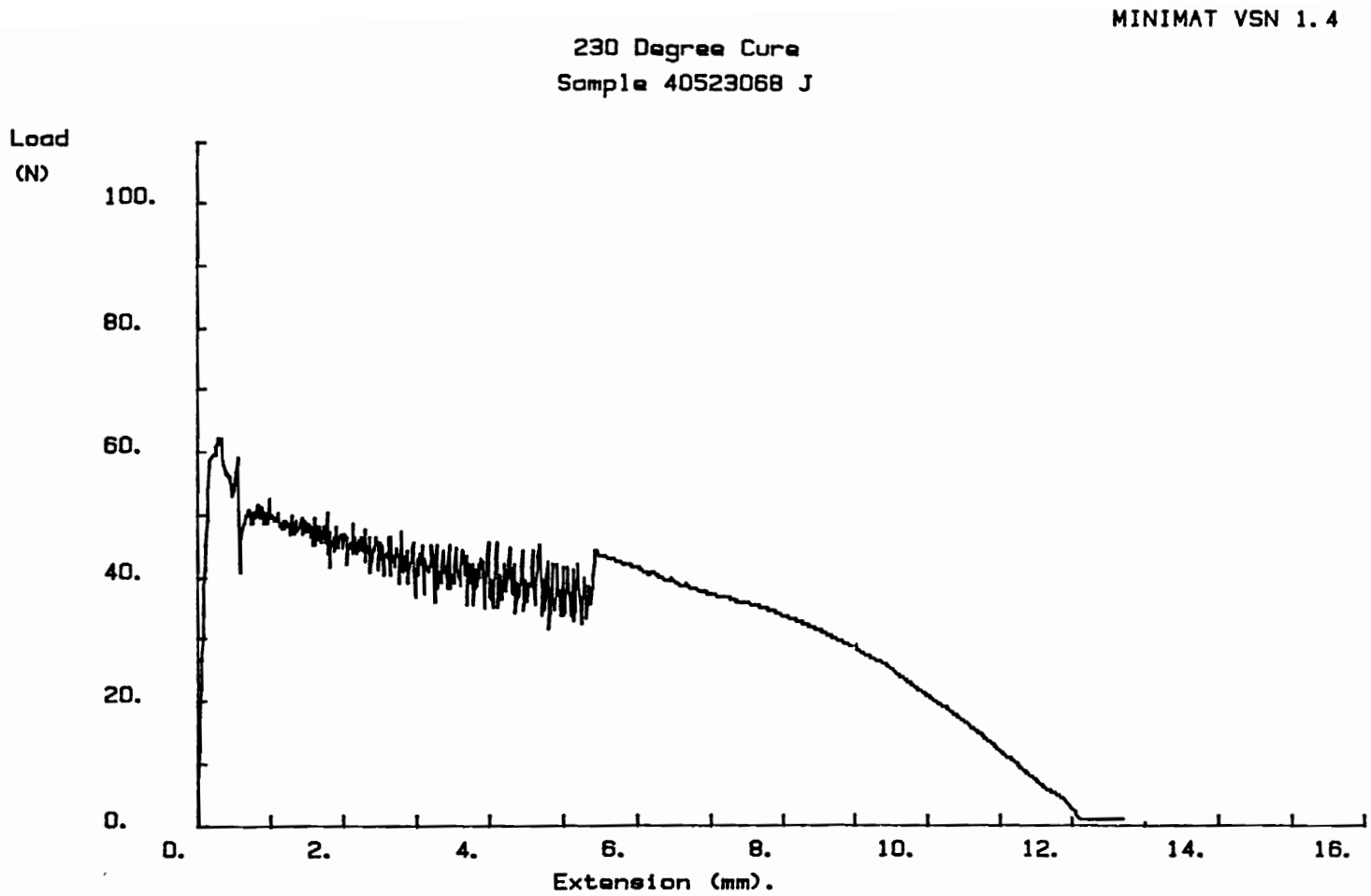

Date : 06APR92 Max. Ext.: 16.00 Load beam: 200 Speed: 2.00

Operator: DiFrancia Max. Load: 110.0 Sample Length 36.1 CSA 4.2

Filename: cd230 lo

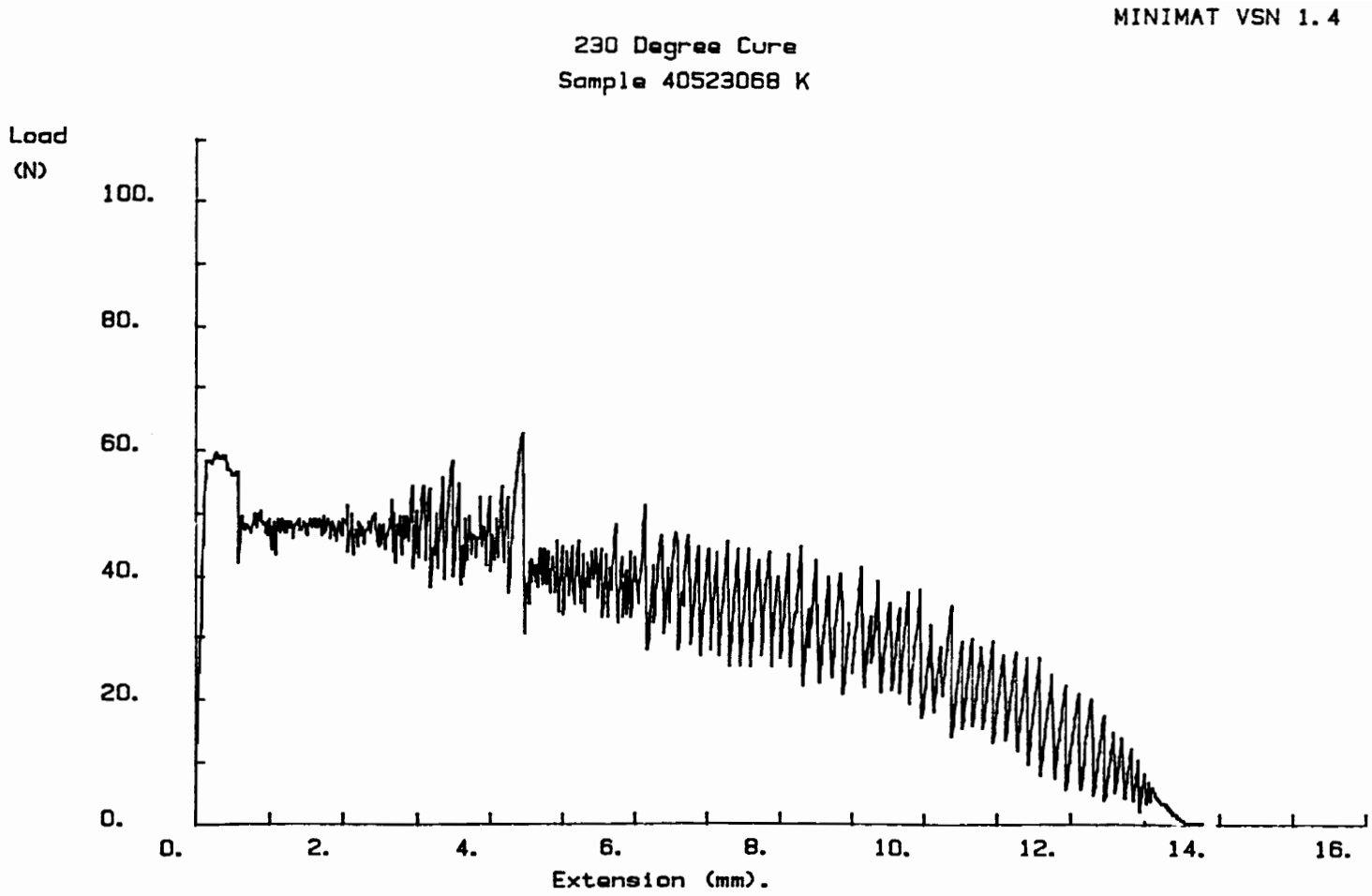
MINIMAT VSN 1.4
230 Degree Cure
Sample 40523068 K
Load
(N)
100.
80.
60.
40.
20.
0.
0.
2.
4.
6.
8.
10.
12.
14.
16.
Extension (mm).
Date : 06APR92
Max. Ext.: 16.00
Load beam: 200
Speed: 2.00
Operator: DiFrancia
Max. Load: 110.0
Sample Length 36.3 CSA 4.1

MINIMAT VSN 1.4

230 Degree Cure
Sample 40523068 L

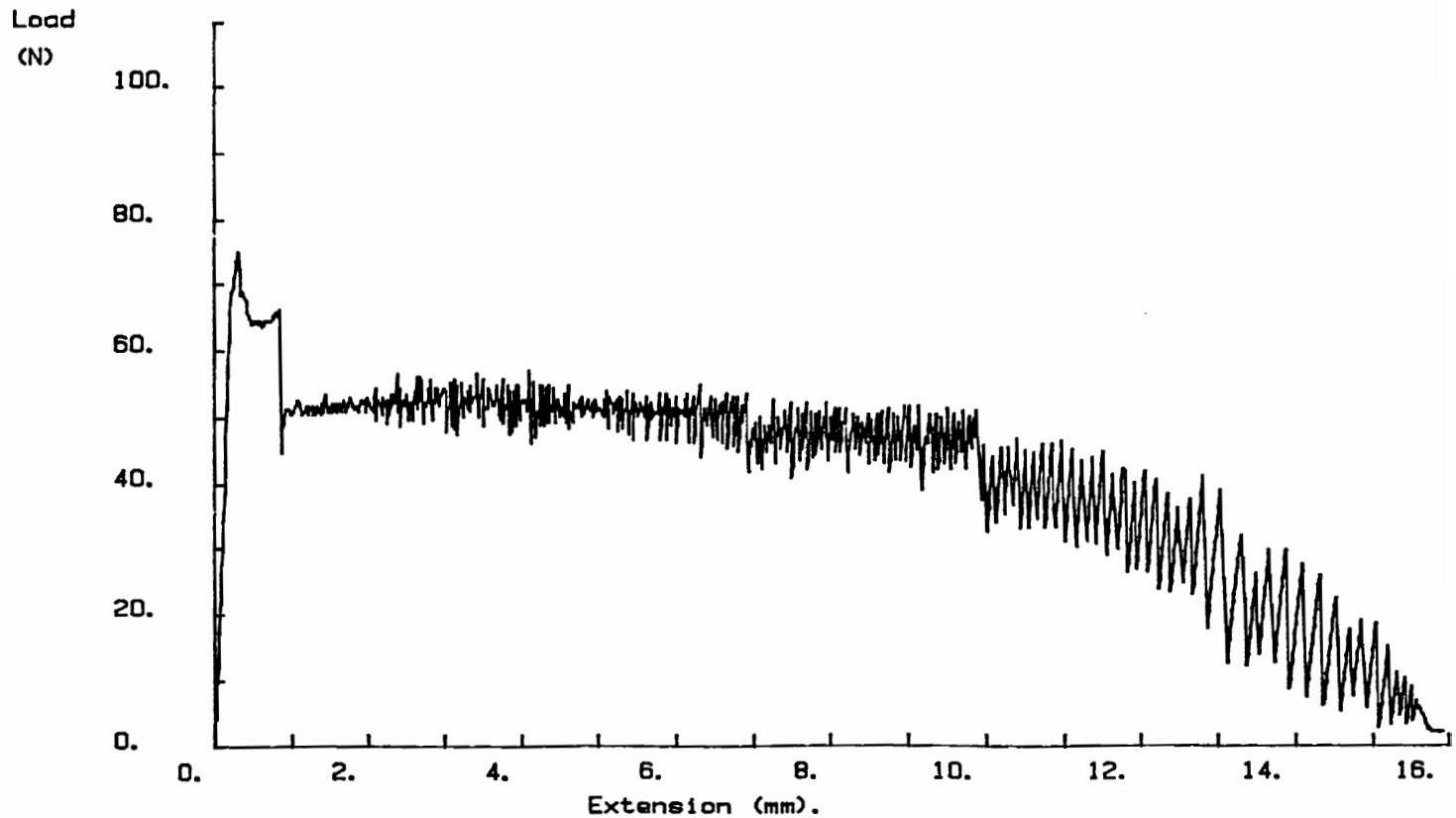

Date : 06APR92 Max. Ext.: 16.00 Load beam: 200 Speed: 2.00

Operator: DiFrancia Max. Load: 110.0 Sample Length 25.2 CSA 4.0

Filename: cd2301n

MINIMAT VSN 1.4

250 Degree Cure
Sample 32035067 E

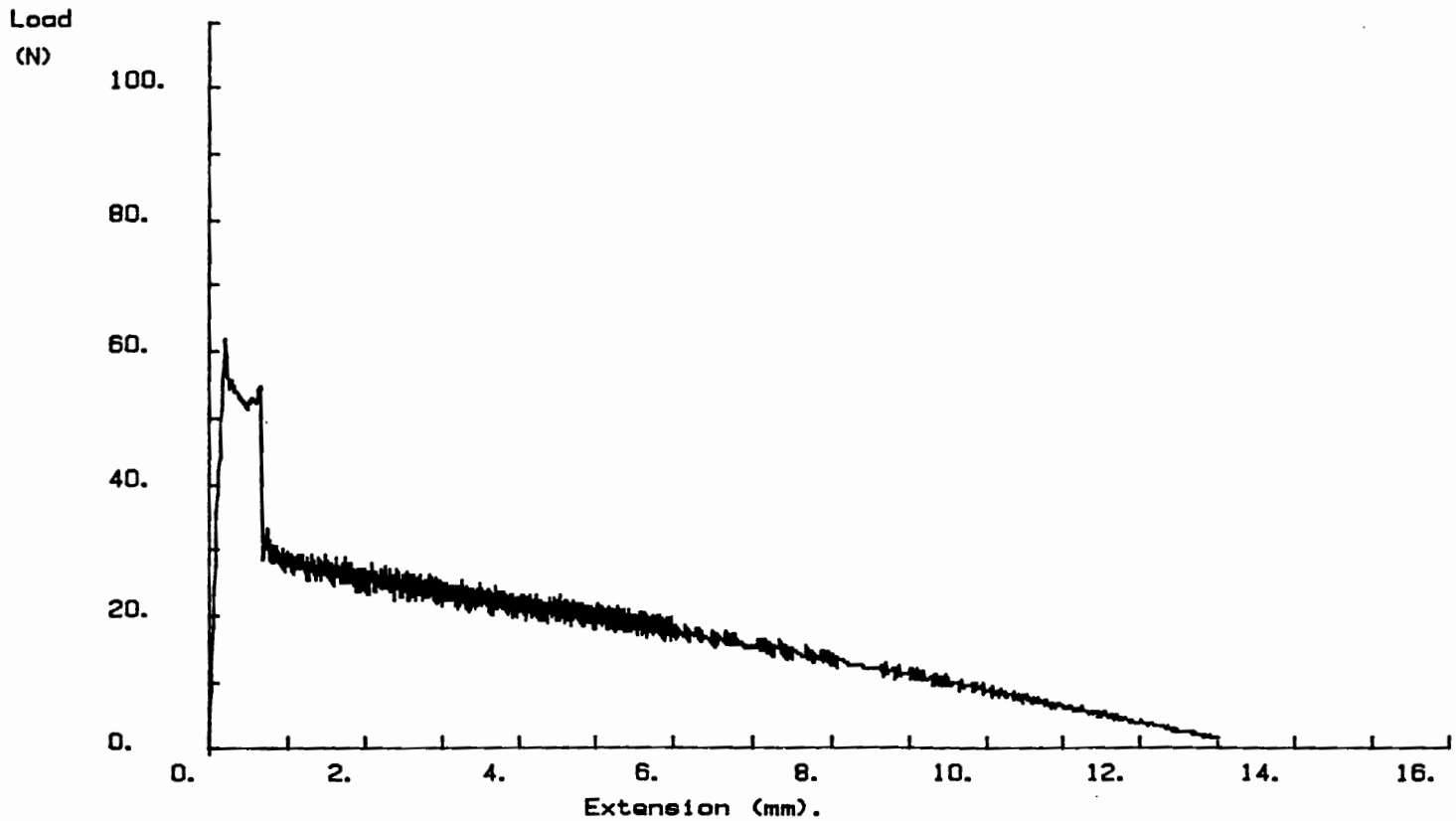

Date : 21MAR92 Max. Ext.: 16.00 . Load beam: 200 Speed: 2.00

Operator: DiFrancia Max. Load: 110.0 Sample Length 37.4 CSA 3.5

Filename: cd250en

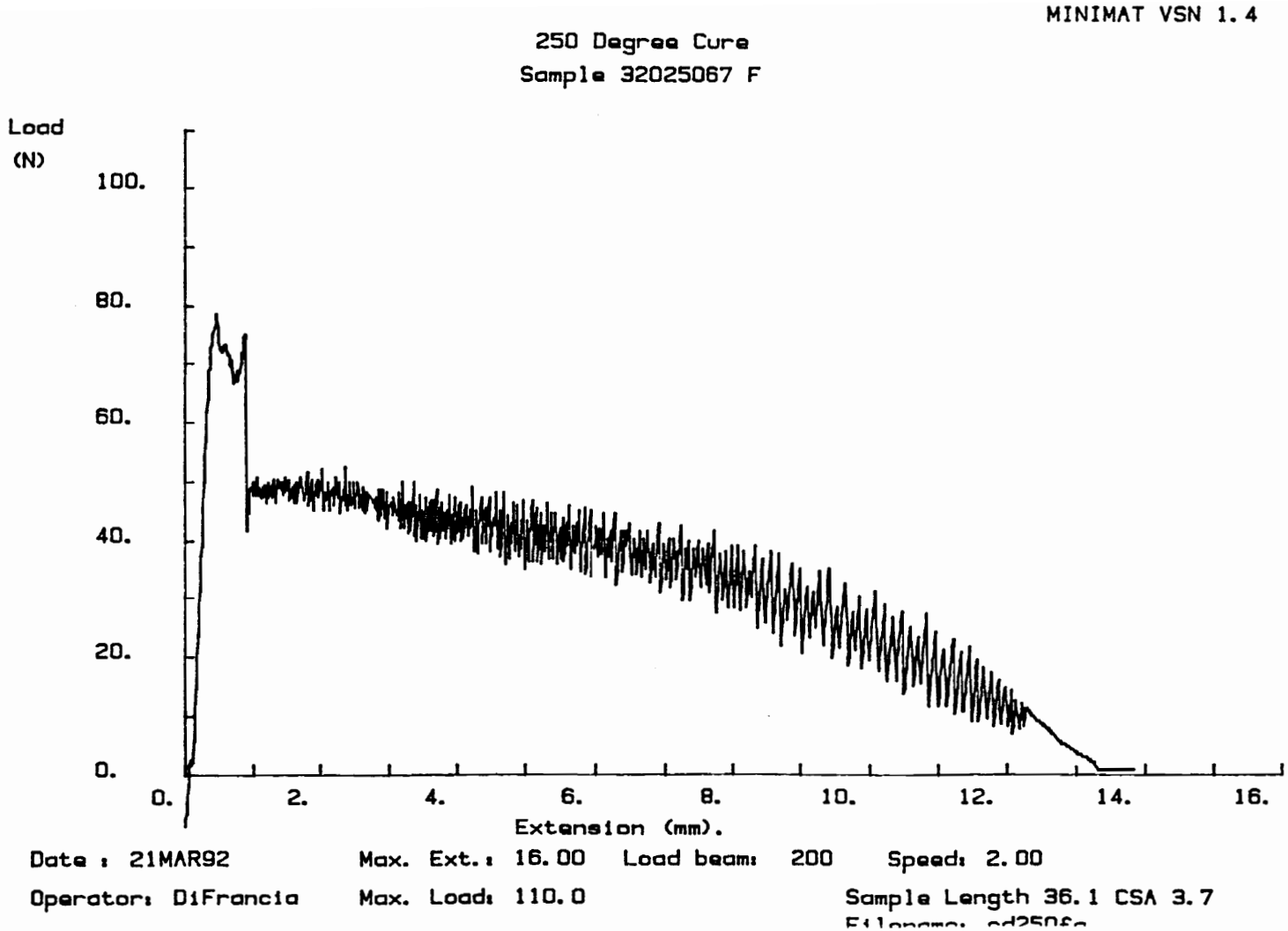
MINIMAT VSN 1.4
250 Degree Cure
Sample 32025067 F
Load
(N)
100.
80.
60.
40.
20.
0.
0.
2.
4.
6.
8.
10.
12.
14.
16.
Extension (mm).
Date : 21MAR92
Max. Ext.: 16.00
Load beam: 200
Speed: 2.00
Operator: DiFrancia
Max. Load: 110.0
Sample Length 36.1 CSA 3.7

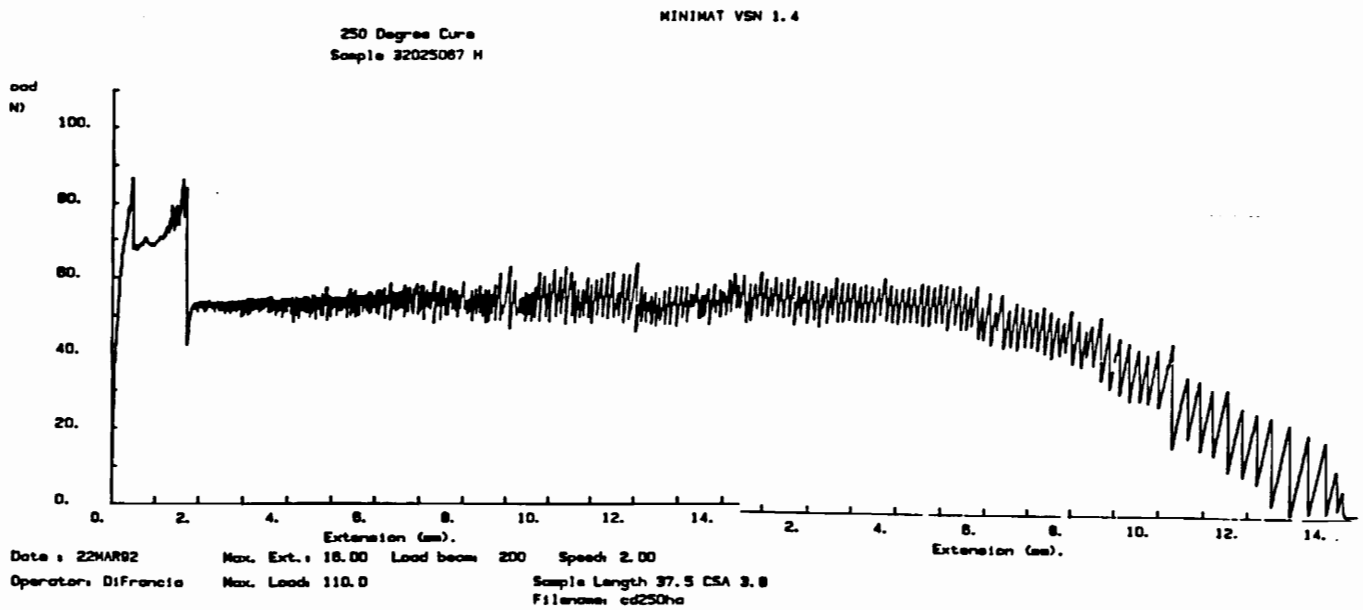
MINIMAT VSN 1.4
250 Degree Cure
Sample 32025087 H
oad
N)
100.
80.
60.
40.
20.
0.
0.
2.
4.
6.
8.
10.
12.
14.
Extension (mm).
2.
4.
6.
8.
10.
12.
14.
Extension (mm).
Date : 22MAR92
Max. Ext.: 16.00
Load beam: 200
Speed: 2.00
Operator: DiFrancia
Max. Load: 110.0
Sample Length 37.5 CSA 3.8
Filename: cd250ha

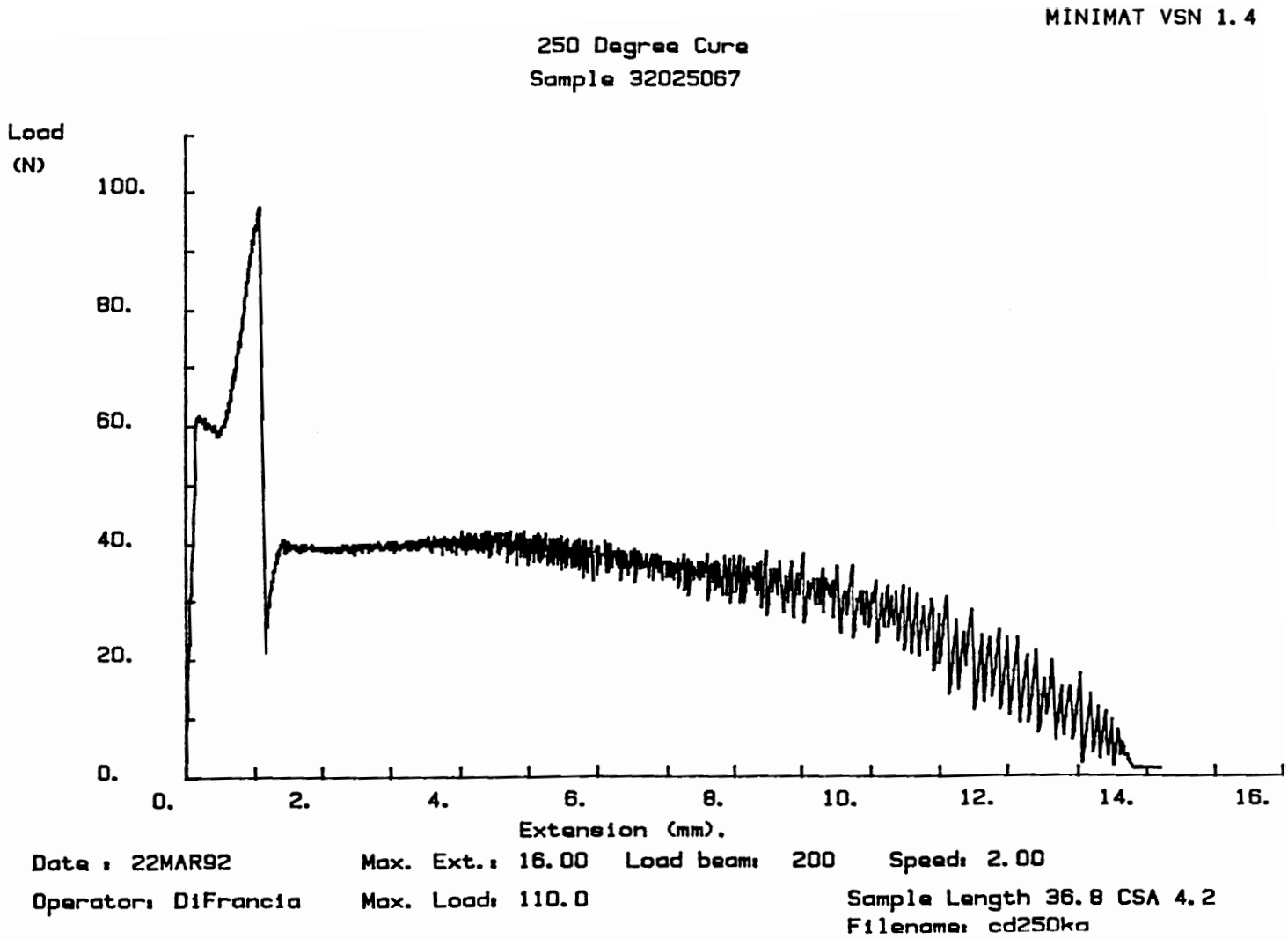
MINIMAT VSN 1.4
250 Degree Cure
Sample 32025067
Load
(N)
100.
80.
60.
40.
20.
0.
0.
2.
4.
6.
8.
10.
12.
14.
16.
Extension (mm).
Date : 22MAR92
Max. Ext.: 16.00
Load beam: 200
Speed: 2.00
Operator: DiFrancia
Max. Load: 110.0
Sample Length 36.8 CSA 4.2
Filename: cd250ka

Appendix B

```
text font "New Century Schlbk"
text size 12
text style "B"
text color Magenta()
select range A1..J50
format Scientific
Align Center

Put "= 7.25E-5" Into A1
Put "= 71E9" Into A2
Put "= 4.12E9" Into A3
Put "= .14" Into A4
Put "= .33" Into A5
Put "= 4.5869E-3" Into A6
Put "= A3/A2" Into A7
Put "= 14.95E6" Into A8

Put "=54.3" Into B1
Put "=81.84" Into B2
Put "=7.5E-3" Into B3
Put "=5449" Into B4
Put "=B4/(pi()*2*A1)" Into B5
Put "=B5/A8" Into B6
Put "=(B2-B1)/2+ B1" Into B7


Put "= ((pi()*A1^2*A8)/(A7*A4))*(A7*(1-A4)+1+A5+(2*A6))" Into C1
Put "= ((2*B6)/A1)*(((A7*A4)+(A6*A5))/(A7*(1-A4)+1+A5+(2*A6)))" Into C2
Put "= ((A7*A4)/((A7*A4)+(A6*A5)))*(C1-B7)*(exp(C2*B3)-1)" Into C3
Put "= (B7-C3)" Into C4
Put "= ((A7*A4)+(A6*A5))/(A7*(1-A4)+1+A5+(2*A6))" Into C5
Put "= (A6*(1-2*C5*A5))/(A7*(1-2*C5*A4))" Into C6
Put "= ((A7*A4)/((A7*A4)+(A6*A5)))*(B2-B7)*(exp(C2*B3)-1)" Into C7
Put "= (B7-C7)" Into C8

Put "= (B1/(2*pi()*A1^1.5))^2*(1-2*C5*A4)*(A2*(1+C6))^(-1)" Into D1
Put "= ((1-2*C5*A4)*((B2-(1+C6)*C3)^2))/(4*pi()^2*(A1)^3*A2*(1+C6))" Into D2
Put "= ((1-2*C5*A4)*((B2-(1+C6)*C7)^2))/(4*pi()^2*(A1)^3*A2*(1+C6))" Into D3
```

Vita

The author was born in Yorktown Heights, New York on August 8, 1963 to Mr. and Mrs. James S. DiFrancia. She graduated from Franciscan High School in Mohegan Lake, New York, in 1981 and obtained a Bachelor of Science degree in Chemistry from the State University College at Oneonta, Oneonta, New York, in 1985. As an undergraduate she pursued an evaluative study of computer software under Professor Harry Pence and research in rhodium catalysis under Professor Jack Kotz.

She began graduate studies at Virginia Polytechnic Institute and State University in September of 1985 and received her Master of Science in Chemistry in October, 1987. The masters work was on the Development of Fiber Optic Sensors Using an Active Polymeric Cladding.

The author has been a member of the Center for Adhesive and Sealant Science, the Center for Composite Materials Science, the Fiber and Electro-Optics Research Center and the National Science Foundation Science and Technology Center for High Performance Polymeric Adhesives and Composites. She is a member of the Adhesion Society and the American Chemical Society and was awarded graduate student Fellowships from the Adhesive and Sealant Council, Inc. for both 1991 and 1992.